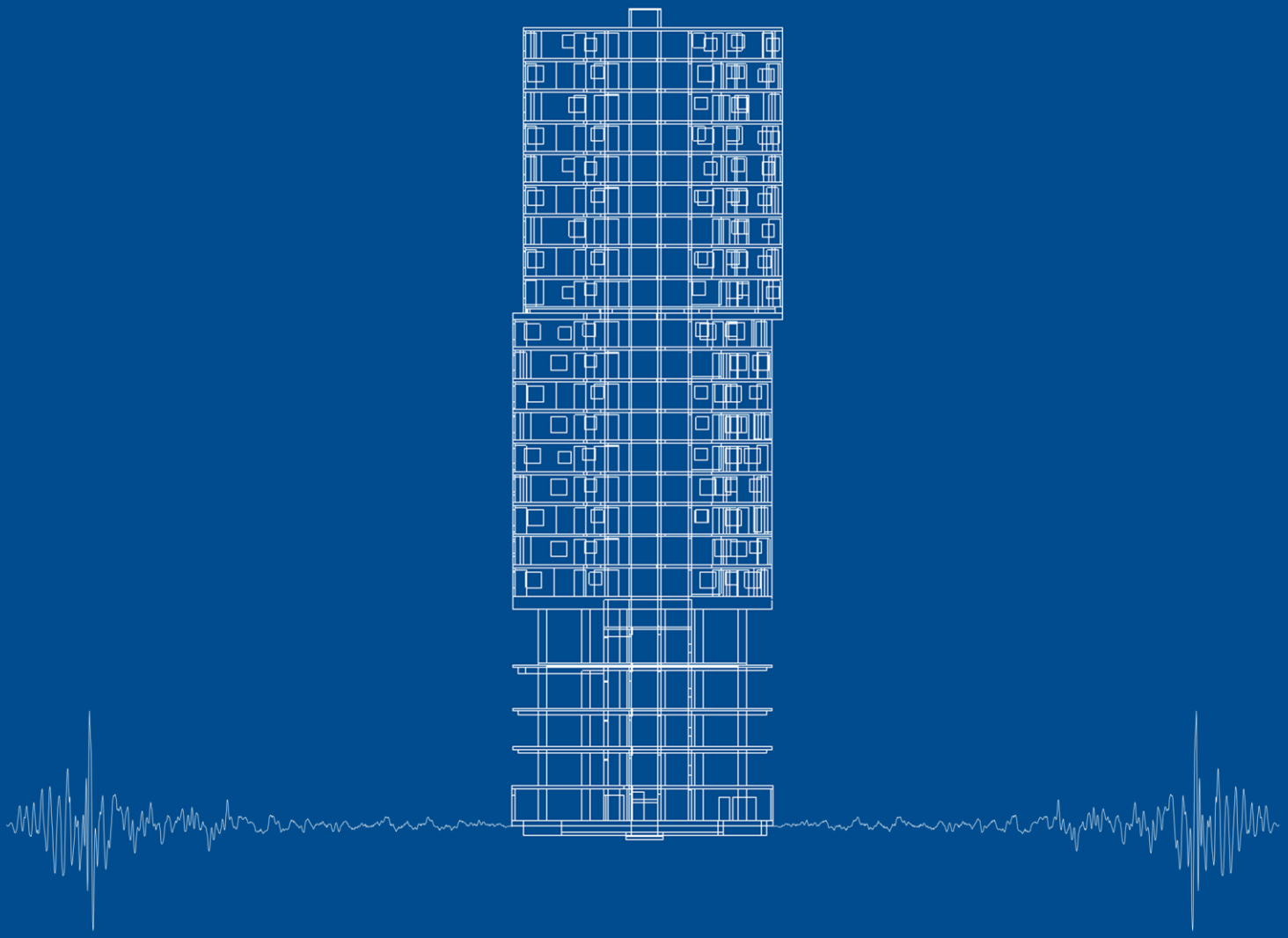

Development of a reliable and efficient 3D calculation model of a high-rise building under seismic loading

Delft University of Technology Zonneveld ingenieurs Henk Mussche MSc Thesis

Development of a reliable and efficient 3D calculation model of a high-rise building under seismic loading

Master of Science Thesis

By

H. Mussche

For the degree of Master of Science In Civil Engineering
at the Delft University of Technology

To be defended publicly on Friday, the first of June 2018 at 3:00 PM

Thesis committee:

Prof. dr. ir. J.G. Rots	TU Delft, Chairman
Dr. ir. M.A.N. Hendriks	TU Delft
Dr. ir. K.C. Terwel	TU Delft
Ing. H.J. Hoorn	Zonneveld ingenieurs b.v.

Student number: 4311302

Abstract

Since the 80's of the previous century the buildings in the northern province of the Netherlands are under seismic loading due to gas extraction induced earthquakes. Seismic assessment of existing structures is of importance in order to obtain insight in the impact of the earthquakes and in the dynamic behaviour of these existing structures. Based on these assessments, strengthening measures can be developed and analysed.

This thesis research focusses on the development of a reliable and efficient calculation model of an existing high-rise, reinforced concrete building in the Groningen area, in order to analyse the dynamic behaviour of the existing and subsequently retrofitted main bearing structure of this high-rise building.

By means of a 'Non-Linear Time History' (NLTH) analysis, consisting of a direct integration of the equation of motion, the assessment of the existing building is executed, according to the rules of the Nederlandse PraktijkRichtlijn (NPR 9998:2015). This type of analysis takes into account the dynamic effects and non-linear behaviour, like cracking of concrete and yielding of reinforcement. To this end, a full scale 3D model of the high-rise building 'La Liberté', situated in the city of Groningen, is created with Simulia Abaqus. With this model in Abaqus, multiple NLTH analyses are performed for optimisation of the 3D model in order to obtain correct results with a minimum amount of calculation costs. Through this process of optimisation of the model, a clear understanding of the dynamic behaviour of the building is developed. Also, the main sensitivities of the Abaqus model are determined; these sensitivities are: 'second order accuracy', 'beta damping', 'mesh dimension' and 'hourglassing control'.

The 3D model is verified by means of a simplified 1D beam type model, developed and analysed with the software package Matlab. This 1D model consists of three beam elements, corresponding to the three main structural parts of the building. The 1D model is analysed with an elastic, linear time history analysis; which means that the model is analysed over time without taking nonlinearities into account.

Next to this, a 'modal response spectrum analysis' is performed for verification of the 3D model results. With this analysis the maximum base shear force, based on the response spectrum of the earthquake and the natural frequencies of the building, is calculated.

The assessment of the building is performed with the 3D model in Abaqus according to the Near Collapse criterion of the NPR 9998:2015. The results show that the building meets this criterion of the NPR, based on the analysis with only one record of the NPR. Since at least seven various records should be applied, it is possible that the building does not meet the Near Collapse criterion for one of these records. Also from a structural point of view, it is interesting to develop and analyse strengthening possibilities for this specific building. Therefore, three strengthening proposals are developed and initially analysed with the 1D model in Matlab.

Acknowledgements

For their valuable support, feedback and advice during my research, I would like to express my gratitude to the members of my assessment committee: Jan Rots, Max Hendriks and Karel Terwel from TU Delft, and Harm Hoorn from Zonneveld ingenieurs.

I am also genuinely grateful to the people of Zonneveld Ingenieurs, whose expertise and knowledge were always a helpful guidance. Being given a position in their company honours me and I look forward to working together in future projects.

I also want to thank my family and friends for their unfailing support and encouragement during my study and research.

And last but not least, I would like to give special thanks to my wife, Irma, who supported me continually.

Table of Contents

1. Introduction

1.1. Background

Since the 60's of the previous century, gas has been extracted in several areas in The Netherlands. One of these areas is Groningen, a northern province of the Netherlands. To this day, the Groningen gas field is one of the largest gas fields in the world. But what started as a true goldmine, has now produced negative side-effects: In the 80's earthquakes started to occur in the Netherlands, mainly with the epicentre being in the province of Groningen. These earthquakes are human induced; the extraction of gas leads to compaction of the rock which then may become unstable, involving seismic events.

Since earthquakes (of these proportions) never occurred in the Netherlands until recently, it is not clear if and which of the existing buildings are able to withstand the earthquake loading. Therefore, seismic assessment is required in order to understand the impact of an earthquake on a structure and to consider possible strengthening measures.

Zonneveld ingenieurs designed several new high-rise buildings according to the design rules of the Nederlandse PraktijkRichtlijn (NPR 9998:2015); this NPR contains design rules for the specific situation in Groningen. These design calculations demonstrate that the earthquake loading results in rather large base shear forces. For new buildings, it is usually well possible to adjust the design and implement strengthening measures, with a minimum amount of extra costs. However, for existing buildings, specific measures need to be developed and examined in order to implement them in the existing design. Therefore, it is required to investigate the dynamic behaviour of a building and the impact of an earthquake in order to assess whether strengthening is required and if so, to develop specific applicable strengthening measures.

Several analysis methods are available in order to calculate the impact of an earthquake; each with its advantages, disadvantages, restrictions and capabilities. Linear calculation methods require a small amount of calculation time and effort, but will usually give less accurate results and also less insight in the dynamic behaviour of the structure. On the other hand, advanced, non-linear analysis methods require a thorough understanding of the theory and more verification and validation of the results; yet, these advanced analyses usually result in more insight in the behaviour of the structure and in the impact of an earthquake.

One of the non-linear analysis methods is the 'Non-Linear Time History' (NLTH) analysis, in which the response of a structure on an earthquake is calculated over a certain time domain. This basically consists of the direct integration of the equation of motion of the system of the building, taking into account nonlinear behaviour of the material such as cracking of concrete and yielding of reinforcement. This method is usually performed with the aid of a Finite Element (FE) software package.

This research contains an investigation of the NLTH analysis of an existing high-rise building, performed with the software package Abaqus. The building is a cast in place, reinforced concrete building of 21 storeys, approximately 72 meters high, and an area of 25 x 25 meter. The research shows how such a building can be represented in a spatial model and what parameters are sensitivities for the analysis and the results. With this model, the impact of an earthquake on an existing high-rise building can be determined and strengthening measures can be developed for this specific building. Next to this, the results of the spatial 3D model are validated and verified with a simplified 1D model, developed and analysed with the aid of Matlab.

1.2. Objective and scope

The objective of this thesis is defined as follows:

"Develop a reliable and efficient (3D) calculation model of an existing high-rise building under seismic loading in order to analyse the dynamic behaviour of the existing and seismic retrofitted main bearing structure"

To achieve this objective, the research is limited to a case study of an existing high-rise, reinforced concrete building situated in the city of Groningen and analyses according to the seismic assessment rules of the NPR9998:2015.
The study is carried out with the aid of a 3D model, created with the finite element software package Abaqus, version 2016. This model is developed with solid elements for the concrete parts and surface (shell) elements for the reinforcement parts and the existing main bearing structure is analysed through plastic, non-linear time history analyses.
The reliability of the 3D model is ensured through verification by means of a simplified 1D Matlab model and a 'modal response spectrum analysis'. This 1D model in Matlab consists of three Euler Bernoulli beam elements. Based on the NLTH analyses in Abaqus, strengthening measures are developed and analysed with the 1D model in Matlab.
Through a process of multiple NLTH analyses of the 3D model in Abaqus, in which the model is improved and optimised, the efficiency of the model is improved. Through the verification and optimisation, a reliable and efficient calculation model is developed.

1.3. Outline of the thesis

Chapter 2 describes the high-rise building of the case study "La Liberté" in Groningen and the earthquake loading as defined by the NPR. *Chapter 3* discusses the development of the 1D model in Matlab and the results of the analysis with high, initial stiffness and low, cracked stiffness of the concrete. In *chapter 4* an overview of the input in Abaqus is given, together with the properties and modelling choices. The verification of the 3D model and the results of the process of analyses with several varying parameters and sensitivities are discussed in *chapter 5*, and the analysis of the seismic behaviour of the building is elaborated in *chapter 6*. In *chapter 7*, some basic suggestions of strengthening measures are discussed and implemented in the 1D model of the structure for initial analysis of the effect of these measures on the structure. In *chapter 8* the conclusion of the research is discussed together with recommendations for further research.

2. ‘La Liberté’ and Earthquakes in Groningen

For this research the high-rise building ‘La Liberté’ in the city of Groningen is considered as case study. In this chapter, a description of the building and its structural design is given; next to this, the seismic assessment rules of the NPR are discussed and elaborated.

2.1. Residential tower La Liberté

The project La Liberté, situated at the south-west side of the city of Groningen, consists of two towers of respectively 38 and 72 meters high. The design is made by the French architect Dominique Perrault, known for the National Library in Paris. The name of the building refers to the French architect and the street name, Laan van de Vrijheid (avenue of freedom). Both towers are used for offices, apartments and a hotel (Hoogendoorn, 2011).

Figure 2.1: View of the two towers of La Liberté in Groningen.

For this research only the high tower is used as a case study. Since a dilatation is applied in the connection, the effects of the low tower on the high tower are expected to be minimal and the low tower is therefore neglected.

2.1.1.Structure

The foundation consists of a concrete slab with a thickness of 1200-1500 millimeters and 125 auger piles with a diameter of 700 millimeters and a length of approximately 30 meters. The design value of the bearing capacity of these piles is in the range of 4000 to 5000 kilonewton (kN).

The bearing structure from the basement till the 4th floor consists of a square of 20 columns (750 x 750 mm) with a stiff core located in the middle of each storey. This core goes up to the top floor and has a dimension of approximately 8 x 10 meters. From the 4th floor, the bearing structure is ensured through concrete shear walls with a thickness of 250 and 300 millimetres. Two floor plans are shown in the figures below; the first figure shows a floor plan of the first floor with the columns and core as bearing structure and the second figure shows the floor plan of the fourth floor with the shear walls as bearing structure. The concrete of the bearing structure consists of cast in place concrete.

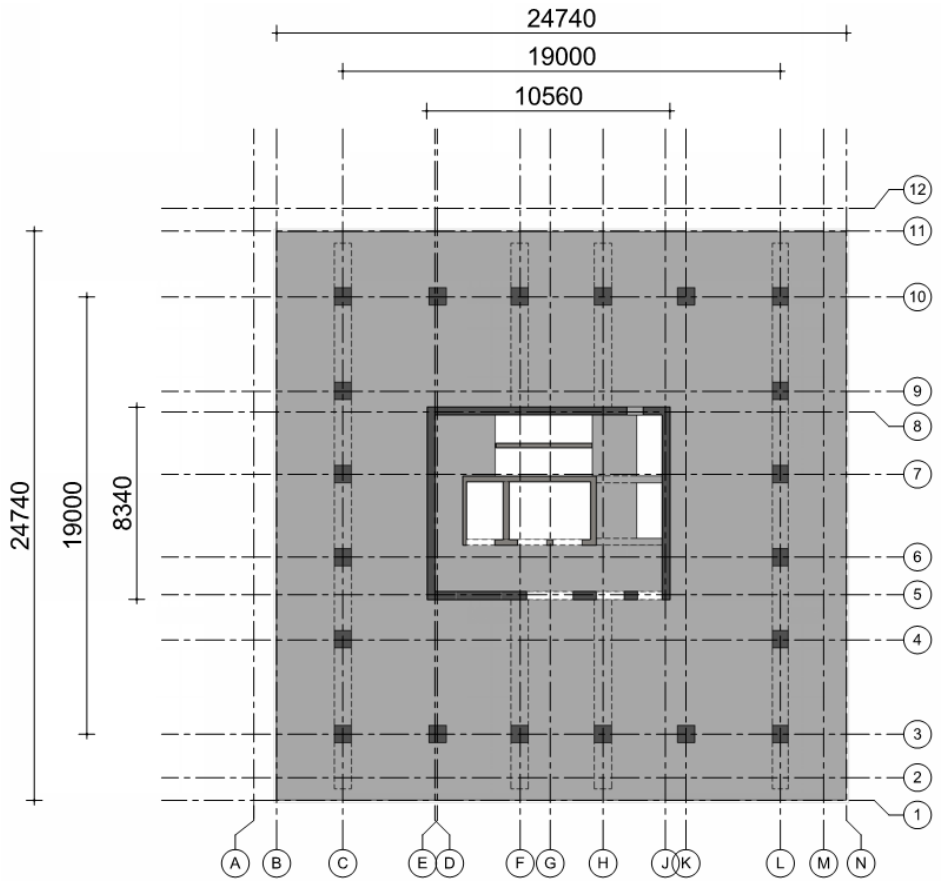

Figure 2.2: Floor plan of the first floor with columns and core as bearing structure.

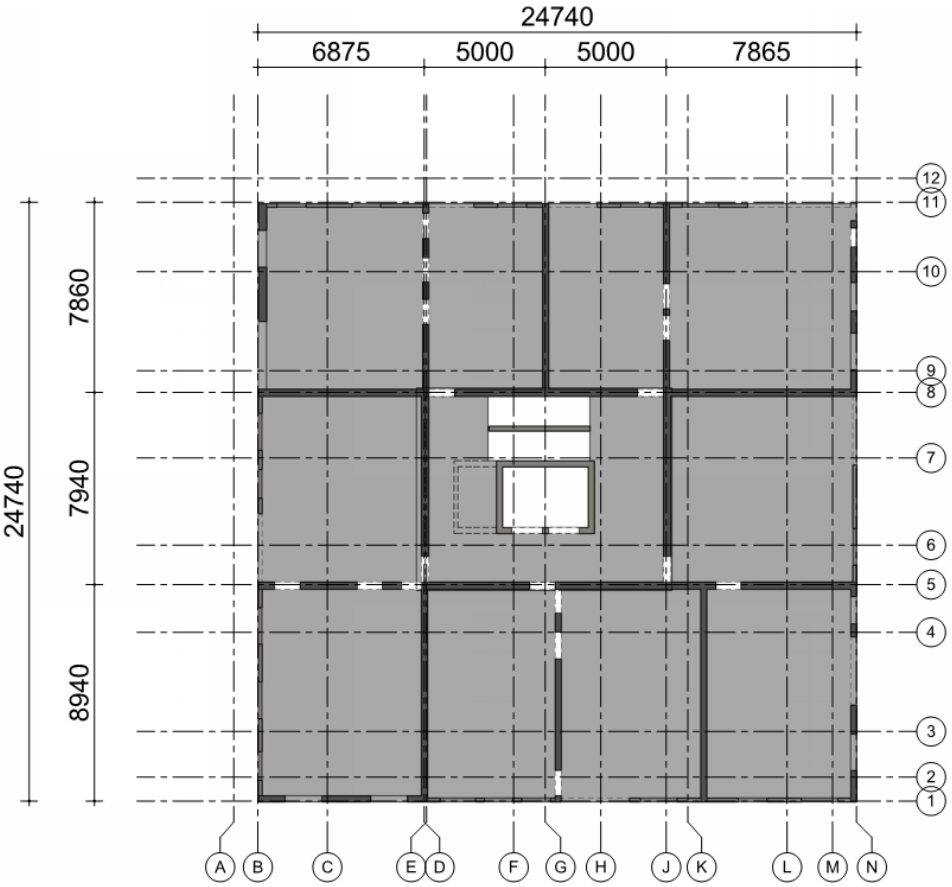

Figure 2.3: Floor plan of the fourth floor with the shear walls as bearing structure.

Another detail of the design is the shift of the top part of the building. The top 9 storeys are shifted approximately one meter relative to the lower part of the building in two directions. This is clearly shown in the two figures below.

Figure 2.4: View of the shifted part of the top of the building (left) and a cross section of the tower (right).

2.1.2. Model of structure

The structural design of the building has been created by the engineering company Ingenieursbureau Dijkhuis. For the calculations of the displacements of the building due to wind loading, they simplified the building to a 1D model. In this model, the building is divided in three parts, with varying area, moment of inertia and concrete class.
In order to verify the 3D model of Abaqus and to perform an initial dynamic analysis, a 1D model has been developed in Matlab; this model is based on the 1D model of Dijkhuis and is also used for the initial assessment of the strengthening measures.
Some of the parameters of Dijkhuis are adjusted to the load and material factors of a seismic analysis, since these factors differ from a Serviceability Limit State (SLS) calculation.

The applied parameters of the 1D model are shown in the table below.

Table 2-1: Overview of the parameters of the 1D model.

Floor	Length [m]	Area [m^2]	Inertia I_{xx} [m^4]	Inertia I_{yy} [m^4]	Concrete class	Mass [kg]
-1 till 3A	21.36	22.76	815	878	C35/45	46.69E5
4 till 12	29.44	32.23	1391	1718	C28/35	100.5E5
13 till 21	29.5	32.23	1391	1718	C20/25	98.45E5

The following figures show the considered structural elements for the calculation of the moments of inertia in X- and Y-direction and for the area.

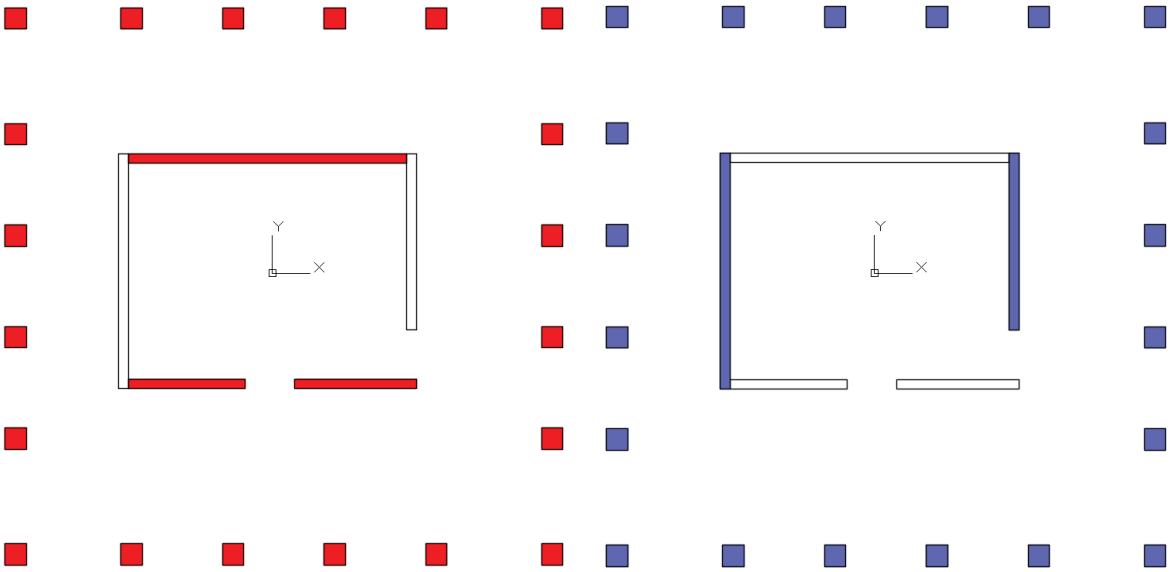

Figure 2.5: Cross section of the first floor; the red elements are considered for the X-direction and the blue elements for the Y-direction, see also Table 2-1.

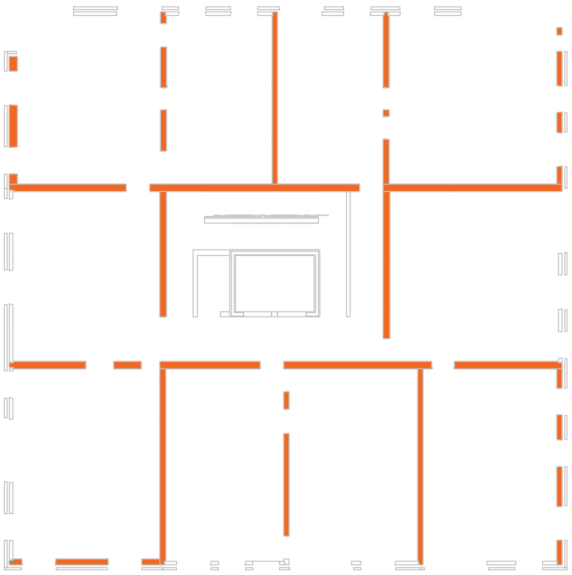

Figure 2.6: Cross section of the top part of the building; the orange elements are considered for both X- and Y-direction, see also Table 2-1.

In chapter 3, a more detailed description of the 1D model is given.

The implementation of the coordinate system, which is applied both in the 1D and 3D model is shown in the figure below, together with the representation of the building by the two models.

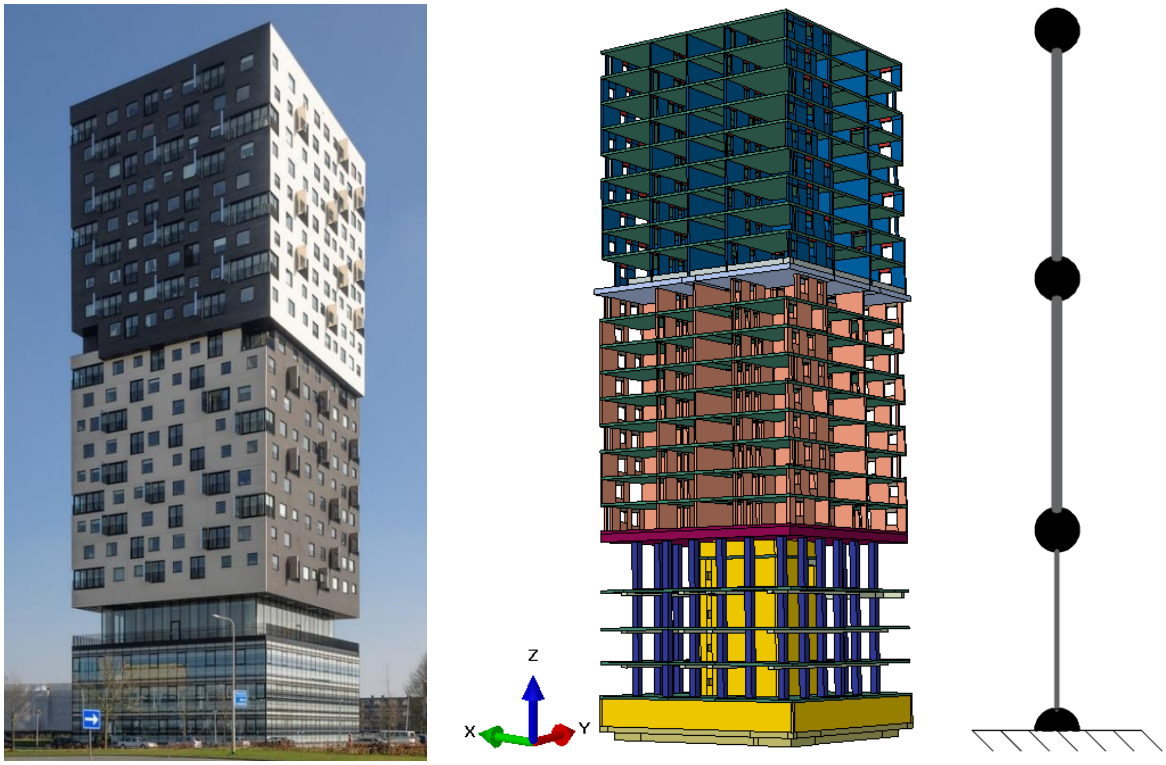

Figure 2.7: Representation of the building through the 3D and 1D model.

2.2. Groningen Earthquakes

The earthquakes in the province of Groningen are so-called 'human induced' earthquakes, which means they are caused by human activity. Due to this activity, the stresses and strains on the earth's crust are disrupted. In the case of Groningen, these earthquakes are a direct result of the gas extraction from the soil in this area. The main difference between these particular human induced earthquakes and the common tectonic earthquakes is the depth at which they occur. Since these human induced earthquakes occur at a smaller depth, a 'gas-quake' has a larger impact than a tectonic earthquake with the same magnitude on Richter's scale (Dwarshuis, 2017).

2.2.1. NPR 9998 Design Rules

Since Eurocode 8, which contains design rules for earthquake resistance design, is not mandatory by law in the Netherlands, the buildings and structures in the Netherlands are not designed to withstand earthquake loading. Also, national annexes for this Eurocode are not drafted, which could have captured the specific situation in Groningen. Therefore, it was decided to set up the Nederlandse Praktijkrichtlijn (NPR 9998:2015) which is based on Eurocode 8 and meant to provide an initial guidance for the concerned parties (Nederlands Normalisatie-Instituut, 2015).

In the NPR three different 'limit states' are elaborated for new buildings and for existing buildings only one limit state is considered, namely 'Near Collapse'. The magnitude of the earthquake and the design values of the materials are related to the applied limit state in the seismic assessment.

The Near Collapse limit state is defined through the following criterion:

"The structure is heavily damaged and the remaining strength and stiffness in horizontal direction is small; the structural members are still able to sustain the vertical loads. Most of the non-structural elements have collapsed and large permanent drifts are present. Progressive collapse does not occur; however, the structure is not able to withstand another earthquake or load, regardless the intensity."

Chapter 3 of the NPR describes multiple methods for determining the magnitude of the earthquake, depending on the type of analysis; the general method for a NLTH analysis is described and elaborated below.

The first step is to determine the peak ground acceleration. This value is related to the location of the structure of interest and can be determined with the map in Figure 2.8.

Figure 2.8: Reference peak ground accelerations according to the NPR.

The next step is to determine two elastic response spectra; one spectrum at depth (-30 [m]) and one at ground surface level.

An elastic response spectrum shows the peak responses of a series of single degree of freedom systems with varying natural frequency on a base acceleration applied to these systems

The use and application of the response spectrum depends on the type of analysis. In this research, the spectrum is applied for the scaling procedure of the accelerograms, which is further elaborated below. Yet, the spectrum can also be applied for the calculation of the (base) shear forces through the 'lateral force method' and the 'modal response spectrum analysis'.

For a NLTH analysis both spectra are used for the scaling procedure of the accelerograms. The Netherlands Standardization Institute (NEN) made 11 signals available which meet the response spectrum at depth (-30 [m]) for the scope of the NPR 9998:2015. The ratio between these two spectra determines the scaling factor for the signals (accelerograms), depending on how the signals are applied in the model. The signals of the NEN correspond to the elastic response spectrum at depth (-30 m.); however, if the signals are applied at ground surface level, these signals need to be scaled, corresponding to the ratio between the two spectra. The two spectra are shown in Figure 2.9.

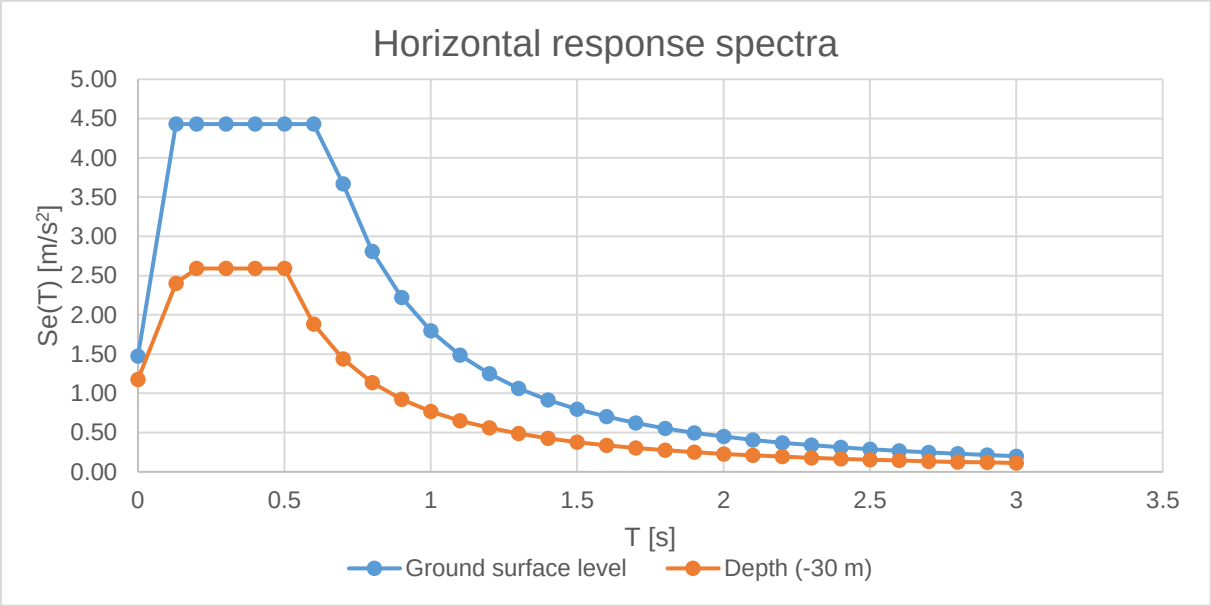

Figure 2.9: Response spectra at ground surface level (blue) and at depth of 30 meter (orange) according to the NPR.

The scaling procedure mainly consists of two steps:

- Vertical (amplitude) scaling;
- Horizontal (frequency) scaling.

The vertical scaling factor is determined with the following formula:

$$f_{sc,v} = \frac{S_{a,su}(T_B)}{S_{a,-30}(T_B)} * S_{a,-30}(0) * 1.05 = \frac{0.451475}{0.264} * 1.177 * 1.05 = 2.114\ [\mathrm{m/s^2}]$$

In which:

- $f_{sc,v}$ is the vertical scaling factor;
- $S_{a,su}(T_B)$ is the value of the plateau of the response spectrum at ground surface level;
- $S_{a,-30}(T_B)$ is the value of the plateau of the response spectrum at depth (-30 m.);
- $S_{a,-30}(0)$ is the value at $T = 0$ of the response spectrum at depth (-30 m.);
- Factor 1.05 is a scaling factor to meet the requirement of NPR 3.2.3.1c.

The horizontal scaling procedure is executed with the aid of software, called Seismomatch of Seismosoft. The original and scaled sixth signal in X-direction are shown in Figure 2.10. The direction of these signals on the structure is arbitrary and each signal should be applied in several directions of the structure, in order to find the maximum impact of the earthquake on the structure.

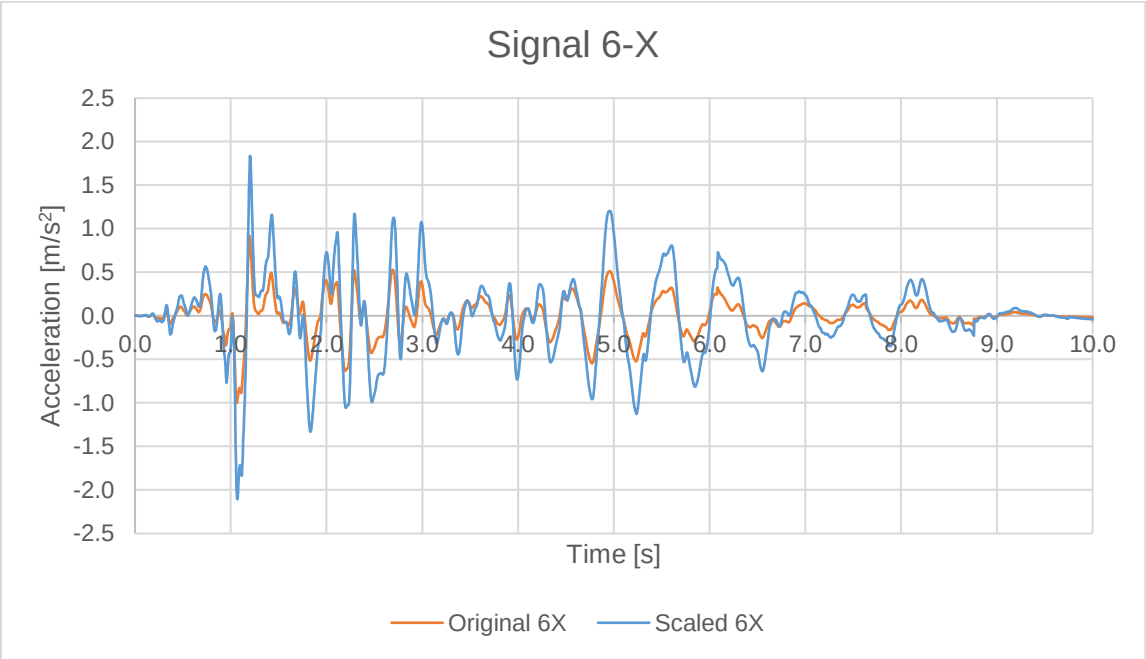

Figure 2.10: The original NEN accelerogram and the 'spectrally matched' accelerogram.

The procedure is equal for each horizontal accelerogram. For the accelerograms in vertical direction, the scaling procedure is a bit different. In this case, only the horizontal or frequency scaling is applied, since the amplitude of the vertical acceleration does not vary much over the depth. This scaling procedure is fully executed with the software Seismomatch.

The duration of each accelerogram is ten seconds; in the 3D model the accelerograms are applied in three directions, two horizontal and one vertical direction. In the 1D model only two signals are used: one in the horizontal and one in the vertical direction.
For the 1D model in Matlab, the displacements corresponding to the accelerograms, are applied as earthquake loading. The applied displacements are shown in the graph below.

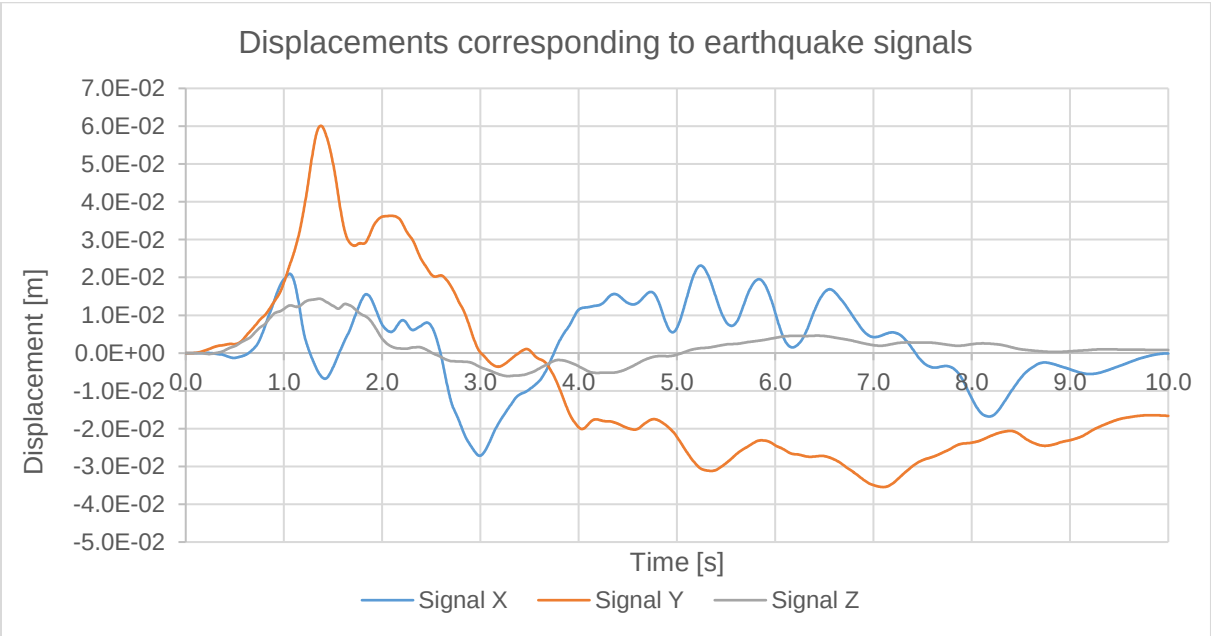

Figure 2.11: Accelerogram related displacements in X, Y and Z direction.

2.3. Summary chapter 2

This chapter discussed the main bearing structure of the high-rise building ‘La Liberté’ which is used as case study for this research. It was shown that the building can be divided into three parts, for the development of the 1D model. Next to this, the rules for seismic assessment according to the near collapse criterion of the NPR were discussed. Also the accelerograms, developed by the NEN, are scaled to the response spectrum of the ground surface level.

In the following chapter, the assembling and results of the 1D Matlab model are discussed and elaborated.

3. 1D Model in Matlab

As discussed in chapter 2, the structure can be simplified to a 1D beam model based on the calculations of Ingenieursbureau Dijkhuis. For an initial analysis of the structure and the strengthening measures, the 1D model is developed. Also the 3D model in Abaqus is validated with the results of this model. The model is developed with the software Matlab, which is able to numerically integrate the differential equation of motion.
In this chapter, the theory and input of the 1D model is elaborated. Also the basic principles of the Matlab solver are discussed and finally the results of the analyses of the 1D model are reviewed and summarized.

3.1. Matlab input

The differential equation of motion for a system with multiple degrees of freedom is given by:

$$\underline{F} = \boldsymbol{M}\underline{\ddot{x}} + \boldsymbol{C}\underline{\dot{x}} + \boldsymbol{K}\underline{x}$$

In which

- $\underline{F}$ is the 'general' force vector;
- $\boldsymbol{M}, \boldsymbol{C}, \boldsymbol{K}$ are the mass, damping and stiffness matrices respectively;
- $\underline{\ddot{x}}, \underline{\dot{x}}, \underline{x}$ are the 'general' acceleration, velocity and displacement vectors respectively.

The goal is to define these matrices and vectors and supply them to the solver of Matlab; this process is discussed in this paragraph.
The first step is to define the matrices with the parameters of the structure, as mass, moment of inertia and stiffness; these properties form the mass and stiffness matrices. The construction of these matrices is based on the theory of Carlos A. Felippa (Felippa, 1986).
In this process, first the matrices of each element is determined separately and then combined to create the matrices of the whole system, consisting of three elements. Once the mass and stiffness matrices of the whole system are created, the damping matrix is defined according to the theory of Rayleigh damping ($\boldsymbol{C} = \alpha * \boldsymbol{M} + \beta * \boldsymbol{K}$).
The next step is to apply a solver to solve the numerical problem. And finally, the boundary conditions and the earthquake load are defined and applied to the system of equations. The earthquake load is applied through a displacement vector.

3.1.1. Beam elements and parameters

The mass and stiffness matrices are based on the theory of Carlos A. Felippa, elaborated in his book: “Introduction to Finite Element Methods” (Felippa, 1986). The applied beam elements are so-called Euler Bernoulli bending beams. In the figure below an example of a beam element is shown with the general degrees of freedom $u_{x,1}, u_{y,1}, \theta_{z,1}, u_{x,2}, u_{y,2}, \theta_{z,2}$.

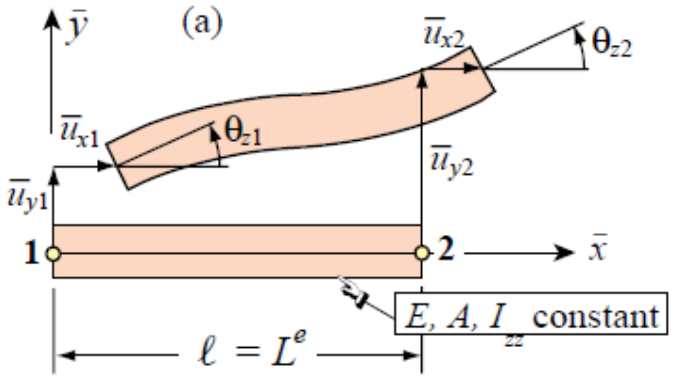

Figure 3.1: 1D beam element with six degrees of freedom

In this approach, a beam element has six degrees of freedom: two translational and one rotational degree of freedom per node. The dimension of the matrices of a beam is therefore six by six.

The local mass and stiffness matrices for one element are shown below.

$$M = \frac{\rho A l}{420}\begin{bmatrix} 140 & 0 & 0 & 70 & 0 & 0 \\ 0 & 156 & 22l & 0 & 54 & -13l \\ 0 & 22l & 4l^2 & 0 & 13l & -3l^2 \\ 70 & 0 & 0 & 140 & 0 & 0 \\ 0 & 54 & 13l & 0 & 156 & -22l \\ 0 & -13l & -3l^2 & 0 & -22l & 4l^2 \end{bmatrix}$$

$$K = \frac{EA}{l}\begin{bmatrix} 1 & 0 & 0 & -1 & 0 & 0 \\ 0 & 0 & 0 & 0 & 0 & 0 \\ 0 & 0 & 0 & 0 & 0 & 0 \\ -1 & 0 & 0 & 1 & 0 & 0 \\ 0 & 0 & 0 & 0 & 0 & 0 \\ 0 & 0 & 0 & 0 & 0 & 0 \end{bmatrix} + \frac{EI}{l^3}\begin{bmatrix} 0 & 0 & 0 & 0 & 0 & 0 \\ 0 & 12 & 6l & 0 & -12 & 6l \\ 0 & 6l & 4l^2 & 0 & -6l & 2l^2 \\ 0 & 0 & 0 & 0 & 0 & 0 \\ 0 & -12 & -6l & 0 & 12 & -6l \\ 0 & 6l & 2l^2 & 0 & -6l & 4l^2 \end{bmatrix}$$

Figure 3.2: The mass and stiffness matrices of a single beam element according to the theory of C.A. Felippa.

The input parameters for the matrices of the 1D model are shown in Table 3-1. The length of the first element of the building includes the height of the basement, in order to match with the Abaqus model. The two Young's moduli, E_0 and E_{cr}, correspond to the non-cracked and cracked concrete respectively, which are used for comparison purposes.

Table 3-1: Input parameters for the 1D model in Matlab based on the calculations of Ingenieursbureau Dijkhuis.

Element	ρ [kg/m^3]	A [m^2]	E_0 [N/m^2]	E_{cr} [N/m^2]	I_{xx} [m^4]	I_{yy} [m^4]	l [m]
1	9604.29	22.76	$3.41 * 10^{10}$	$1.2 * 10^{10}$	815	878	21.36
2	12831.94	32.23	$3.231 * 10^{10}$	$1.1 * 10^{10}$	1391	1718	29.44
3	12535.56	32.23	$3.0 * 10^{10}$	$1.0 * 10^{10}$	1391	1718	29.5
Total	**24569510 kg**						**80.3**

The matrices are created for each separate element and then joined together into one matrix, to create the matrix of the system of three elements. In the system with three elements, certain nodes of the separate elements overlap and have therefore the same displacements and rotations. For example, the displacements of node two of the first element ($N_{1,2}$) are equal to the displacements of node one of the second element ($N_{2,1}$).
The same process holds for both the mass and stiffness matrix. The concatenating process is shown in the figure below and the dimension of the matrices for the total system is 12 by 12.

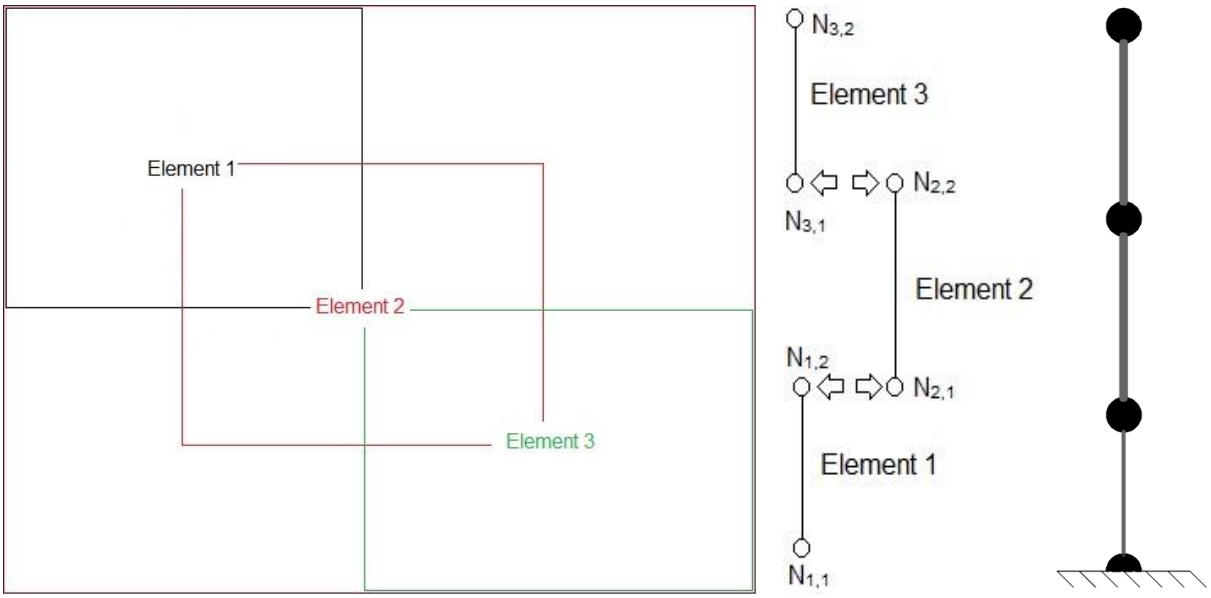

Figure 3.3: Principle of joining matrices into one matrix of the system consisting of three elements.

The final 1D model consists of four nodes; the first node corresponds to the foundation of the building. The other nodes correspond to the 4th, 12th and 22nd floor (roof) of the building, respectively. This composition is based on the fact that the stiffness or moment of inertia changes significantly at these floors, as shown in table Table 2-1.

3.1.2.Rayleigh damping

The damping is implemented by Rayleigh damping, which is defined by the parameters α and β, corresponding to the damping of the lower and higher frequencies respectively.
The parameters and damping matrix are calculated with the following formulas:

$$\alpha = \frac{2 * \omega_1 * \omega_2(\xi_1 * \omega_2 - \xi_2 * \omega_1)}{\omega_2^2 - \omega_1^2}; \qquad \beta = \frac{2(\xi_2\omega_2 - \xi_1\omega_1)}{\omega_2^2 - \omega_1^2}$$

$$\boldsymbol{C} = \alpha * \boldsymbol{M} + \beta * \boldsymbol{K}$$

In which:

- ω_1 is the lowest frequency of the model;
- ω_2 is the higher frequency of interest;
- ξ_1 and ξ_2 are the first and second damping ratio (for example 2% or 5%);
- $\boldsymbol{C}, \boldsymbol{M}, \boldsymbol{K}$ are the damping, mass and stiffness matrices respectively;

The frequencies (ω_1, ω_2) can be determined through a free vibration of the system, which is obtained by applying an initial displacement at one of the nodes. From the displacement graph, the period of the system can be measured and so the frequency can be calculated with the following relation:

$$T = \frac{1}{f} = \frac{2\pi}{\omega}$$

The free vibration of node 4 of the system in the X-direction is shown in the following figures. Figure 3.4 shows an overview of the displacement of the node over time. The slow oscillation is the first, lowest, eigenfrequency. Figure 3.5 shows a close-up of the free vibration, in which two other frequencies are clearly visible. The plot shows three frequencies, which correspond to the three free vibrating nodes of the system in X-direction, while the foundation is clamped.

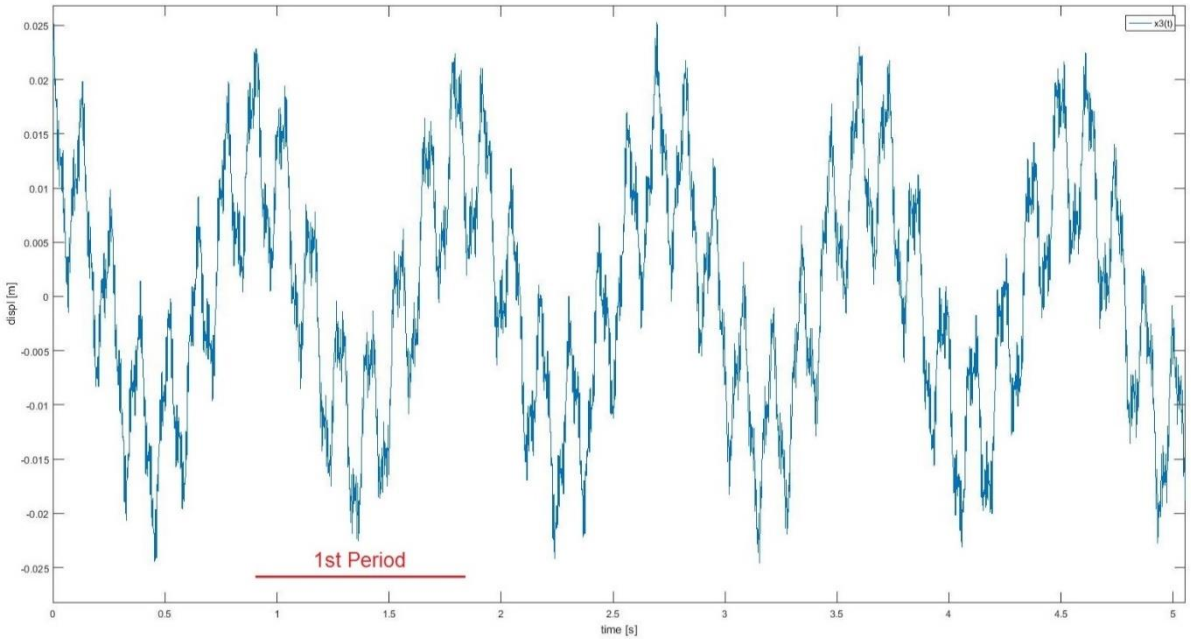

Figure 3.4: Free vibration in X-direction of the 4th node of the system.

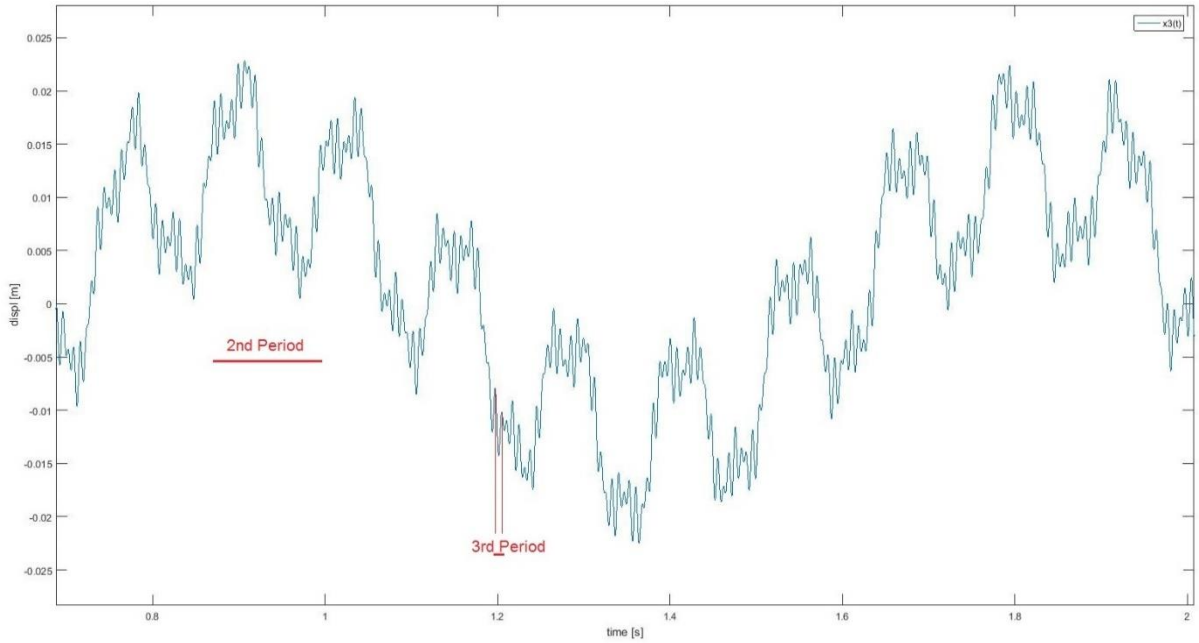

Figure 3.5: Close-up of the free vibration in X-direction of the 4th node of the system.

The measured values for the X direction are the following:
$T_{1,x} = 0.898$ [s] → $f_{1,x} = 1.11$ [Hz] → $\omega_{1,x} = 6.97$ [rad/ s]
$T_{2,x} = 0.123$ [s] → $f_{2,x} = 8.13$ [Hz] → $\omega_{2,x} = 51.08$ [rad/ s]
$T_{3,x} = 0.009$ [s] → $f_{3,x} = 111.1$ [Hz] → $\omega_{3,x} = 698.1$ [rad/ s]

For the Y direction, the same method is applied and the measured values are the following:
$T_{1,y} = 0.964$ [s] → $f_{1,y} = 1.037$ [Hz] → $\omega_{1,y} = 6.515$ [rad/ s]
$T_{2,y} = 0.142$ [s] → $f_{2,y} = 7.042$ [Hz] → $\omega_{2,y} = 44.25$ [rad/ s]
$T_{3,y} = 0.011$ [s] → $f_{3,y} = 90.90$ [Hz] → $\omega_{3,y} = 571.14$ [rad/ s]

The α and β factors for the damping matrix are calculated, based on two frequencies of the model. The lowest frequency is determining for the α-factor and one of the higher frequencies determines the β-factor; according to the equations given on the previous page.
The calculated α and β factors are given below, the factors are calculated for T_1 & T_2 and for T_1 & T_3:

X-Direction
$\alpha_{x,1\&2} = 0.307$; $\beta_{x,2} = 0.00086$ (2.5%); (damping for ***third*** frequency: 30%)
$\alpha_{x,1\&3} = 0.345$; $\beta_{x,3} = 0.000071$ (2.5%); (damping for ***second*** frequency: 0.48%)

Y-Direction
$\alpha_{y,1\&2} = 0.284$; $\beta_{y,2} = 0.00098$ (2.5%) (damping for ***third*** frequency: 28%)
$\alpha_{y,1\&3} = 0.322$; $\beta_{y,3} = 0.000087$ (2.5%) (damping for ***second*** frequency: 0.51%)

Both damping ratios are applied to the system with a free vibration in X-direction; the results are shown in Figure 3.6 and Figure 3.8.

Figure 3.6 shows the result of the $\alpha_{x1,3}$ and $\beta_{x,3}$ factors, corresponding to the first and third frequency of the system (ω_1 & ω_3). This figure clearly shows that the third frequency is damped out over time in the first two seconds. However, the effect of the beta damping on the second frequency is relatively small.

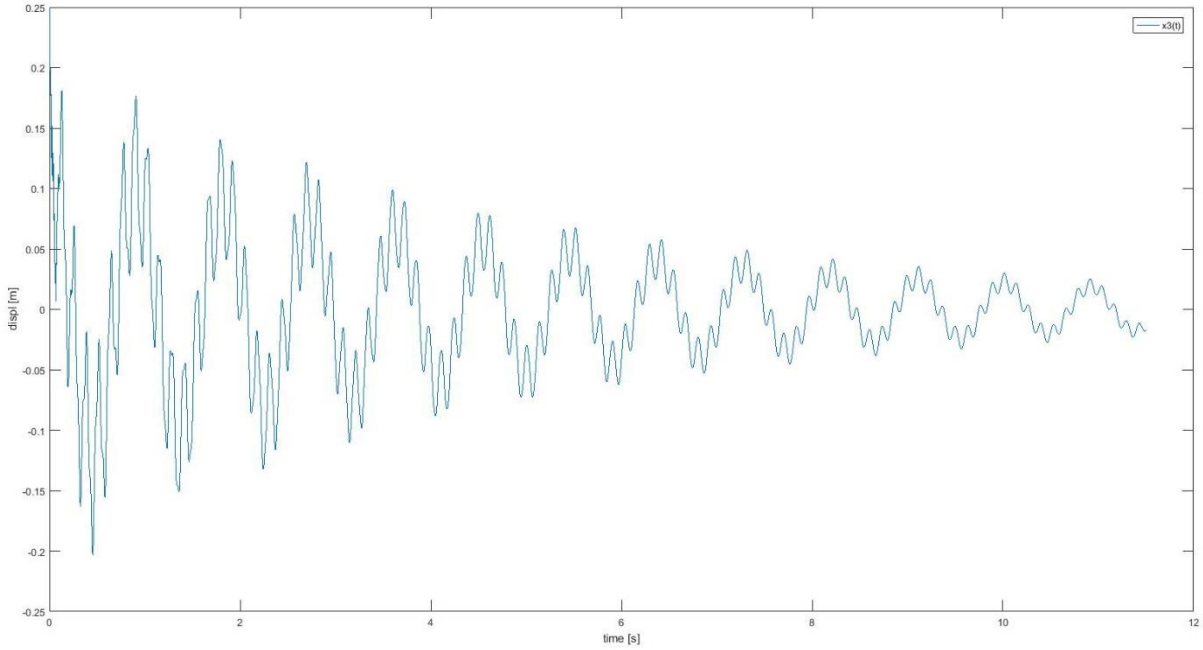

Figure 3.6: Damped free vibration in X-direction with low 'beta damping'.

If the damping ratio is determined with the ***first*** and ***third*** frequency, the damping ratio for the ***second*** frequency is then equal to approximately 0.48%; the corresponding Rayleigh damping for the three frequencies is shown in the graph below.

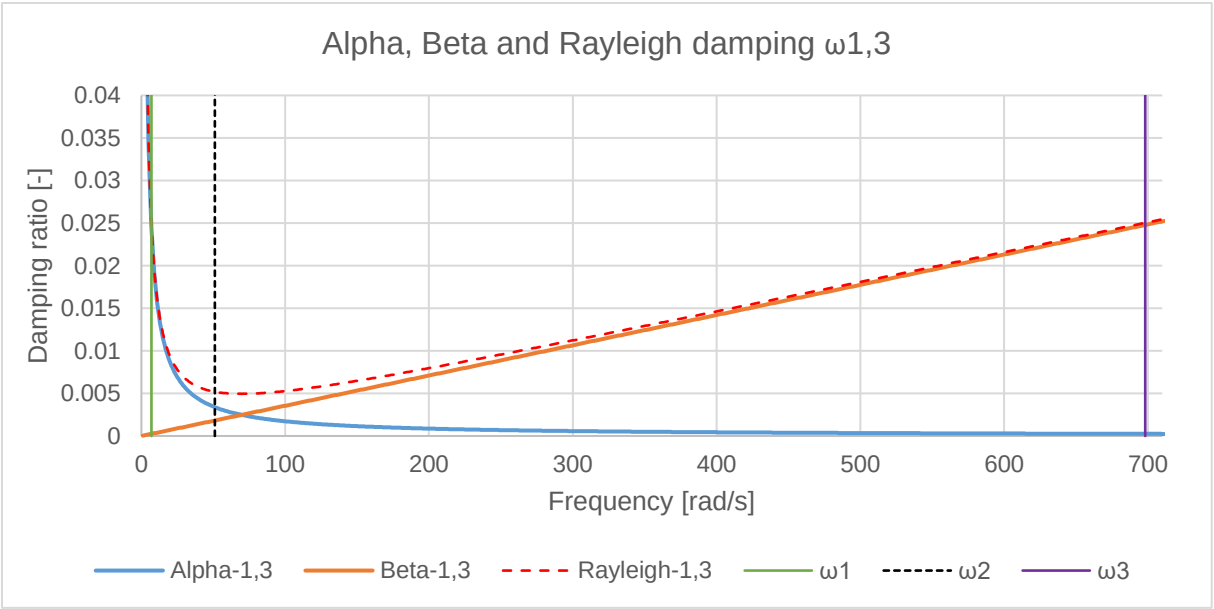

Figure 3.7: Damping ratio with Rayleigh damping for frequency 1 and 3 of X-direction.

The graph shows that the damping ratio for ω_1 and for ω_3 is equal to 0.025, which corresponds to 2.5% damping; however, the damping ratio for ω_2 is about 0.0048, which corresponds to a damping of 0.48%.

Figure 3.8 shows the result of a higher β-factor, corresponding to the first and second frequency of the system (T_1 & T_2). From this figure, it can be seen that all the frequencies are damped out over time.

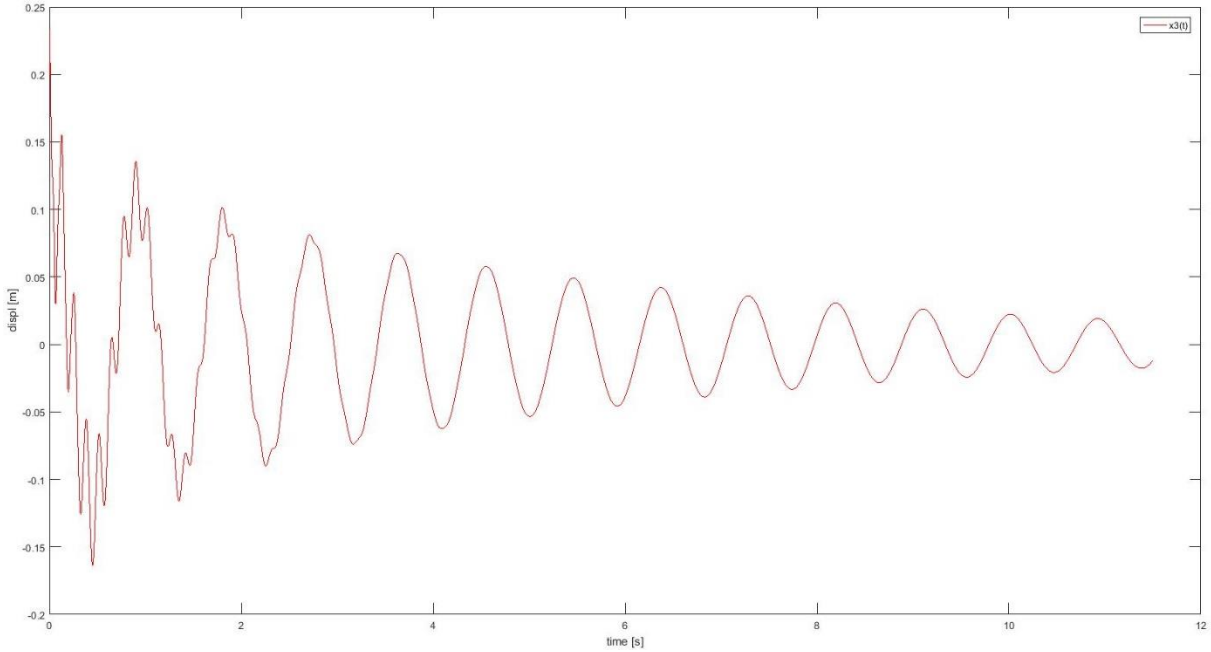

Figure 3.8: Damped free vibration in X-direction with high 'beta damping'.

If the damping ratio is determined with the ***first*** and ***second*** frequency, the damping ratio for the ***third*** frequency is then equal to approximately 30%.

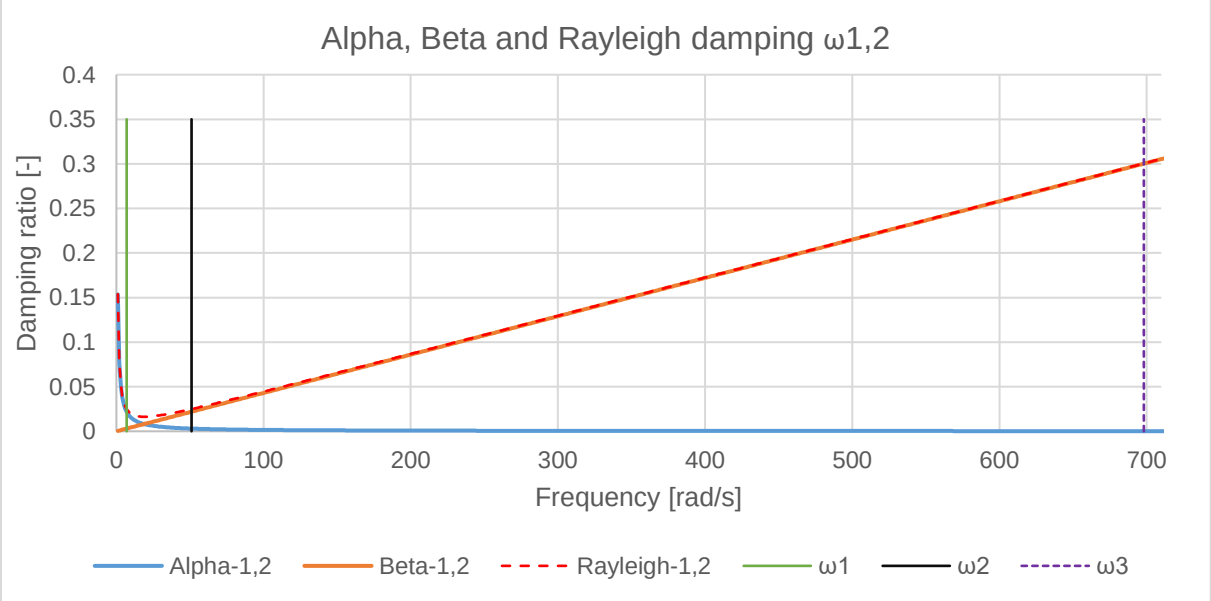

Figure 3.9: Damping ratio with Rayleigh damping for frequency 1 and 2 of X-direction.

The graph shows that the damping ratio for ω_1 and for ω_2 is equal to 0.025, which corresponds to 2.5% damping; however, the damping ratio for ω_3 is about 0.3, which corresponds to a damping of 30%.

The figures Figure 3.6 and Figure 3.8 show that the damping is rather small for the second frequency or quite high for the third frequency. In order to use a reasonable amount of damping, the response spectrum of the earthquake accelerograms can be used to determine the two frequencies for calculation of the Rayleigh damping factors. The response spectrum shows the peak response corresponding to the accelerograms of the earthquake. This spectrum can therefore be used for determining a range for which a maximum amount of damping is beneficial. In Figure 3.10, the response spectrum is shown with two periods which mark a range in which the damping of 2.5% is applied.

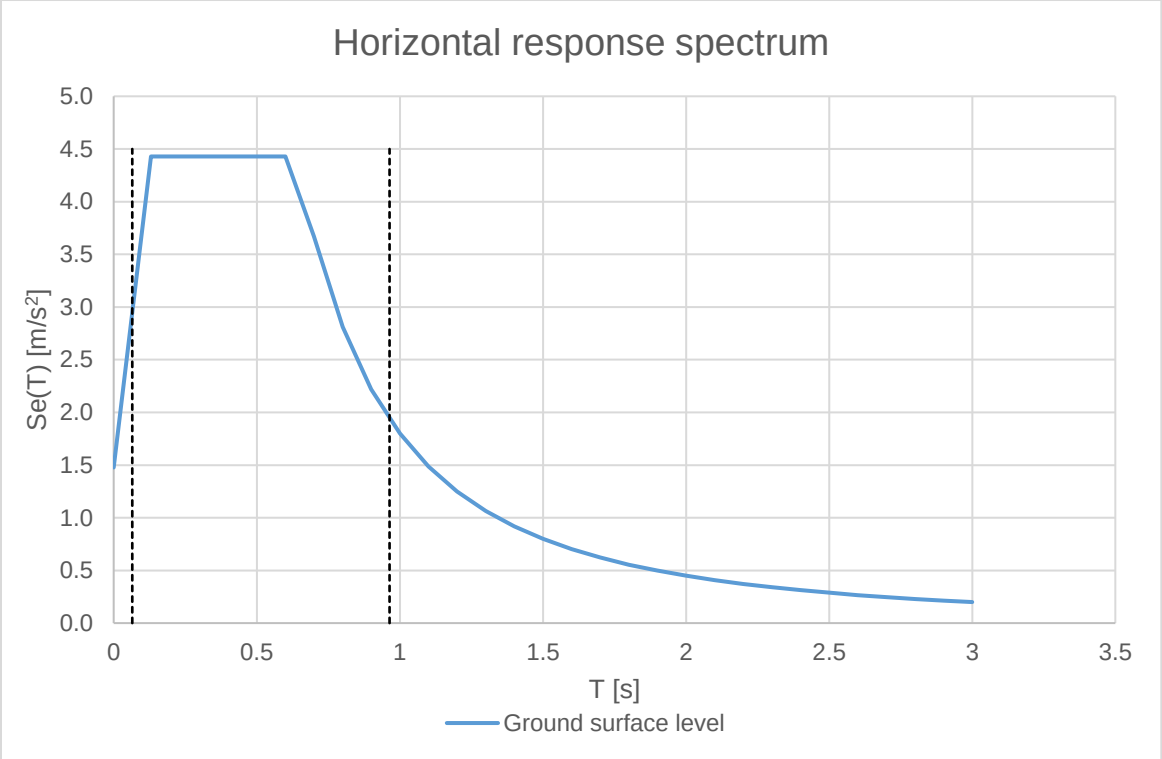

Figure 3.10: Response spectrum of the NPR with range for which periods damping is beneficial.

Range:
$T_1 = 0.964\ [\text{s}] \rightarrow f_1 = 1.037\ [\text{Hz}] \rightarrow \omega_1 = 6.515\ [\text{rad/ s}]$
$T_2 = 0.065\ [\text{s}] \rightarrow f_2 = 15.38\ [\text{Hz}] \rightarrow \omega_2 = 96.66\ [\text{rad/ s}]$

Damping factors:
$\alpha = 0.3052;\ \beta = 0.00048\ (2.5\%)$

3.1.3.Matlab solver

Solvers for ordinary differential equations are standardized in Matlab and are based on the Backward Euler or Forward Euler method or an expansion of these methods. A basic elaboration of the Forward Euler method is given in this paragraph.
The equation of a dynamic problem is given by:

$$\underline{F} = \boldsymbol{M}\underline{\ddot{x}} + \boldsymbol{C}\underline{\dot{x}} + \boldsymbol{K}\underline{x}$$

In which

- $\underline{F}$ is the 'general' force vector;
- $\boldsymbol{M}, \boldsymbol{C}, \boldsymbol{K}$ are the mass, damping and stiffness matrices respectively;
- $\underline{\ddot{x}}, \underline{\dot{x}}, \underline{x}$ are the 'general' acceleration, velocity and displacement vectors respectively.

In this problem, x depends on time, and the initial conditions (IC's) are defined through $x(0)$ and $\dot{x}(0)$ (displacement and velocity at time is zero). In order to investigate how the system behaves in time, the solver has to advance time, from the starting time t_0 at $t = 0$. The current time is defined as: $t_1 = t_0 + \Delta_t$.
Also, the state of the system needs to be defined, for example by the vector q; the state vector contains the displacements and velocities of the degrees of freedom of the system.
q_0 is the initial state, containing the initial conditions:

$$q_0 = \begin{bmatrix} x_0 \\ \dot{x}_0 \end{bmatrix}$$

And q_1 is the state at time step t_1:

$$q_1 = \begin{bmatrix} x_1 \\ \dot{x}_1 \end{bmatrix}$$

The goal of the solver is to obtain the values for q_1.

Using a Taylor series expansion (TSE), a relation between the state q_0 and the state q_1 can be found.
The TSE of a function $f(x)$ around the point a is given by:

$$f(a) = \sum_{n=0}^{\infty} \frac{f^n(a)}{n!}(x-a)^n = f(a) + (x-a)\frac{f'(a)}{1!} + (x-a)^2\frac{f''(a)}{2!} + \cdots$$

Expanding $x(t)$ around the point t_0 with a TSE up to quadratic terms and evaluating this expansion at $t_1 = t_0 + \Delta_t$ results in the following expression:

$$x(t_0 + \Delta_t) = x(t_0) + \frac{(t_0 + \Delta_t) - t_0}{1!}\frac{\delta x}{\delta t}\bigg|_{t=t_0} + \frac{\left((t_0 + \Delta_t) - t_0\right)^2}{2!}\frac{\delta^2 x}{\delta t^2}\bigg|_{t=t_0} + HOT$$

In which HOT stands for Higher Order Terms, which are neglected for the sake of simplicity.

Using the same expansion for $\dot{x}(t)$ and truncating the expression up to linear terms, the following relations are obtained:

$$x_1 = x_0 + \Delta_t \dot{x}_0 + O(\Delta_t^2)$$
$$\dot{x}_1 = \dot{x}_0 + \Delta_t \ddot{x}_0 + O(\Delta_t^2)$$

In which the term $O(\Delta_t^2)$ stands for the local truncation error, which occurs during a single iteration of the solver. The terms x_1 and $\dot{x}_1$ are the results, calculated by the solver and the terms x_0 and $\dot{x}_0$ are the input values supplied as initial conditions. The acceleration at $t = 0$ ($\ddot{x}_0$) can be calculated through the equation of motion:

$$\ddot{x}_0 = \frac{1}{m} * (-c\dot{x}_0 - kx_0 + F(0))$$

In which

- m, c, k are the mass, damping and stiffness respectively;
- $F(0)$ is the applied force at $t = 0$;
- $\dot{x}_0, x_0$ are the velocity and displacement at $t = 0$ respectively.

This relation between the two states at t_0 and t_1 is an explicit relation and known as Euler's method or Forward Euler. Another scheme can be obtained by using a TSE and is known as the Backward Euler, which is an implicit scheme. These schemes form the basis of the solvers in Matlab. The principle as elaborated above for a single degree of freedom also applies to a system of multiple degrees of freedom (Keijdener & Jarquin-Laguna, 2015).

The applied solver for the 1D model is the default ODE45 solver. This solver is based on an explicit Runge-Kutta (4,5) formula and in general it is the best function to apply for most problems; this Runge-Kutta method is an expansion of the Forward Euler method.

3.2. Results

In this paragraph, the results of the analyses are displayed in graphs of the displacements. Also a comparison between the analyses with the initial stiffness and reduced stiffness is provided.

3.2.1. Initial stiffness

First, the results of the analysis with the initial stiffness (E_0) are shown. The graphs show the displacements of each node of the system in X, Y, and Z-direction.

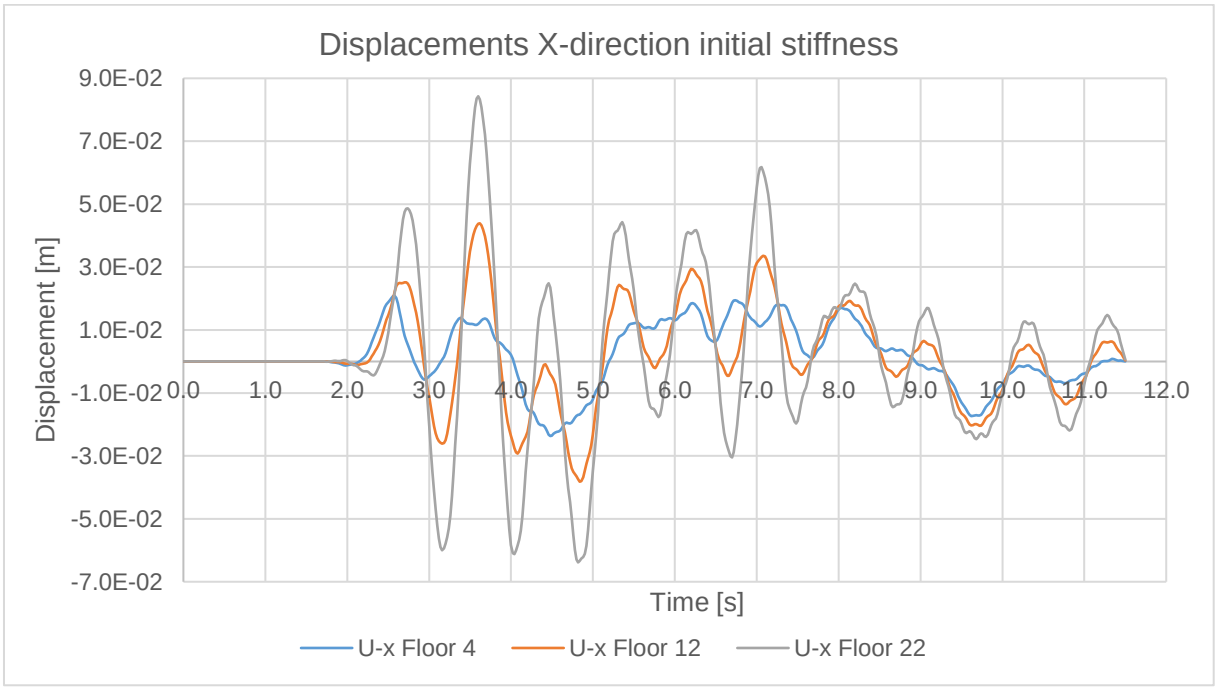

Figure 3.11: Displacements of 3 nodes in X-direction with initial stiffness.

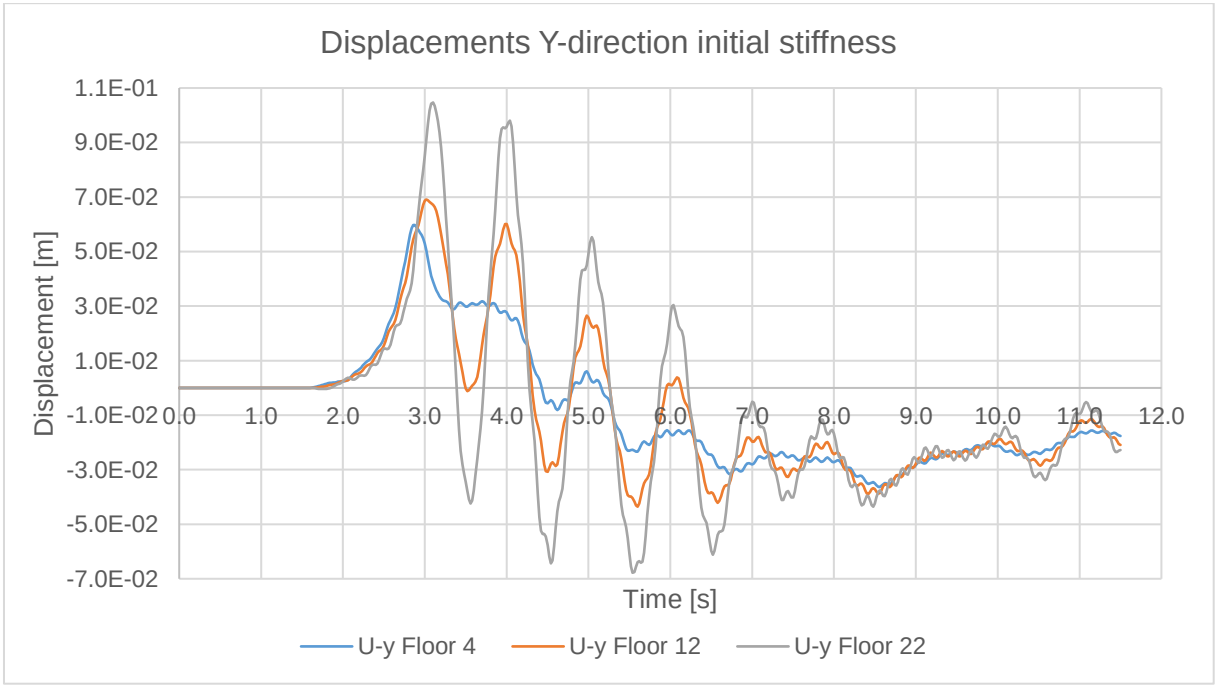

Figure 3.12: Displacements of 3 nodes in Y-direction with initial stiffness

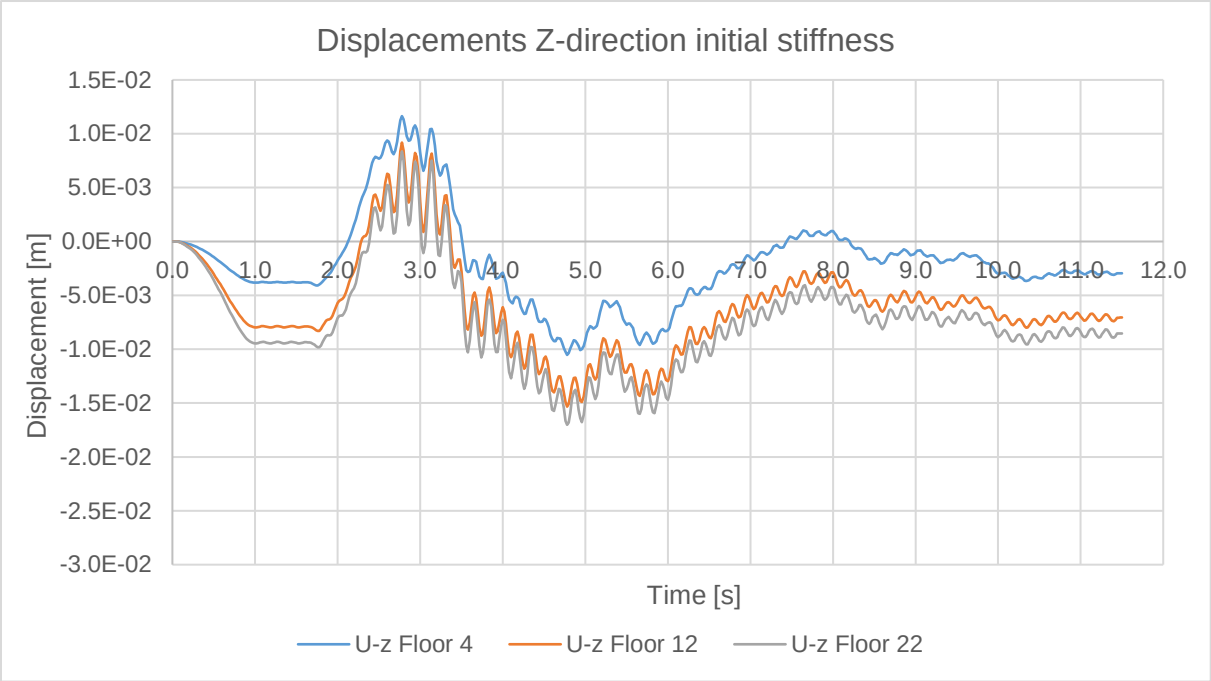

Figure 3.13: Displacements of 3 nodes in Z-direction with initial stiffness.

The maximum displacements of the analysis with the initial stiffness are summarized in Table 3-2

Table 3-2: Overview of the maximum displacements and drifts in X and Y-direction with initial stiffness.

Direction	Maximum displacement [m]		
	Floor 4	Floor 12	Floor 22
X	0.0238	0.0435	0.0834
Drift X	0.111%	0.108%	0.137%
Y	0.0578	0.0680	0.101
Drift Y	0.280%	0.110%	0.146%

The maximum drifts of the floors of the building are smaller than the drift limit, which is equal to 0.53%, according to Eurocode 8.

3.2.2. Reduced stiffness

In this paragraph, the results of the analysis with the reduced stiffness ($\frac{1}{3} * E_0$) are displayed.

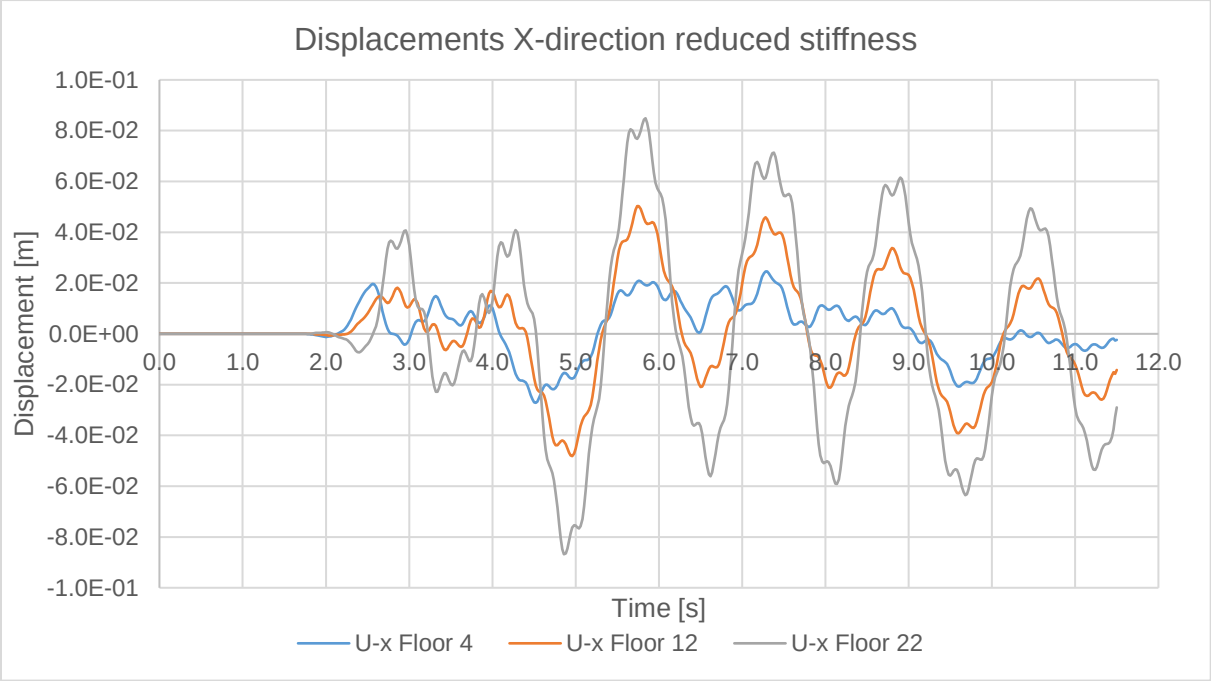

Figure 3.14: Displacements of 3 nodes in X-direction with reduced stiffness.

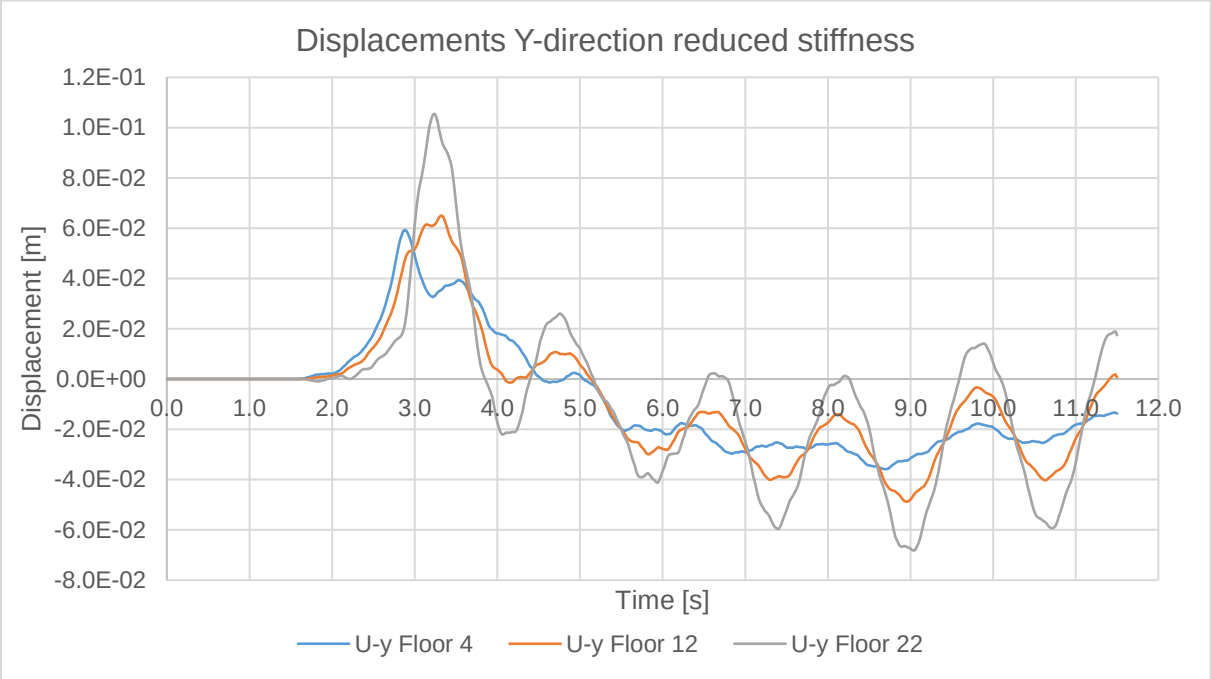

Figure 3.15: Displacements of 3 nodes in Y-direction with reduced stiffness.

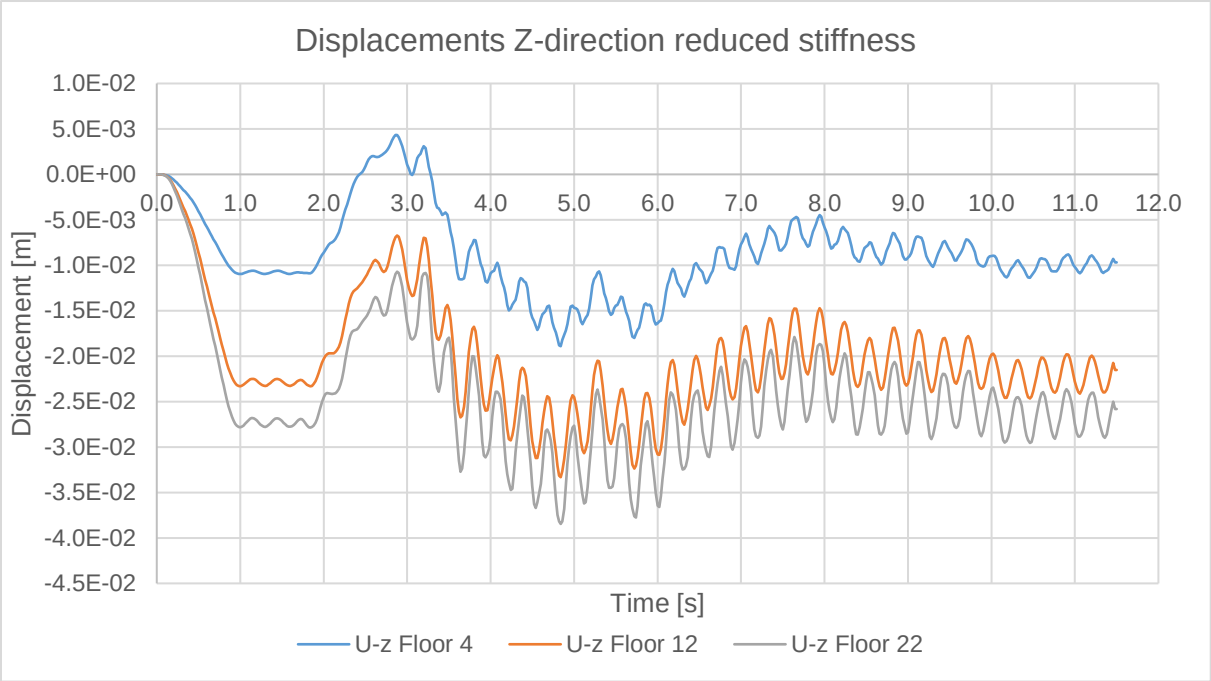

Figure 3.16: Displacements of 3 nodes in Z-direction with reduced stiffness.

The maximum displacements of the analysis with the reduced stiffness are shown in the table below.

Table 3-3: Overview of the maximum displacements and drifts in X and Y-direction with reduced stiffness.

Direction	Maximum displacement [m]		
	Floor 4	Floor 12	Floor 22
X	0.027	0.0546	0.0933
Drift X	0.127%	0.105%	0.151%
Y	0.0594	0.0691	0.108
Drift Y	0.278%	0.101%	0.150%

The maximum drifts of the building are smaller than the drift limit, which is equal to 0.53%, according to Eurocode 8.

3.2.3. Comparison of results

A comparison between the results of the analyses with the initial and reduced stiffness is given in the table below.

Table 3-4: Comparison of the results of the initial stiffness model and reduced stiffness model for X and Y-direction.

Direction	Maximum displacement [m]		
	Floor 4	Floor 12	Floor 22
X (E_0)	0.0238	0.0435	0.0834
X (E_{red})	0.027	0.0546	0.0933
Drift X (E_0)	0.111%	0.108%	0.137%
Drift X (E_{red})	0.127%	0.105%	0.151%
Y (E_0)	0.0578	0.0680	0.101
Y (E_{red})	0.0594	0.0691	0.108
Drift Y (E_0)	0.280%	0.110%	0.146%
Drift Y (E_{red})	0.278%	0.101%	0.150%

The results show that the displacements of the model with the reduced stiffness are larger than those of the initial stiffness model. This makes sense, since a smaller stiffness also results in less resistance against deformation. However, for the Y-direction the difference between the maximum displacements is rather small; though, the graphs show that the period of the vibrations of the reduced stiffness model is larger, as expected with a smaller stiffness.
The occurring drifts are smaller than the limits, even for the analyses with the reduced stiffness.
In chapter 5 the results of the Matlab analyses are used for verification of the elastic analyses with the 3D model.

3.3. Summary chapter 3

In this chapter the parameters of the 1D model of the building were discussed and elaborated. The 1D model was constructed from Euler-Bernoulli beams, according to the theory of C.A. Felippa.
Next to this, the numerical parameters of the Rayleigh damping were investigated and determined, according to the maximum expected response based on the response spectrum.
The 1D model was developed in the software package Matlab, which is able to solve the equations of motions of the system. A brief description of the basic solvers, standardized in Matlab, was presented.
Finally, the results of the analyses with initial stiffness (Young's modulus) and reduced stiffness, corresponding to cracked concrete, were discussed.

The following chapter discusses the development of the 3D model in Abaqus.

4. 3D Model in Abaqus

In this chapter the 3D model as created in Abaqus is discussed and elaborated. The model in Abaqus consists of many different components and modelling steps; each step in this process of modelling is discussed in this chapter.
The input in Abaqus can be divided into the following modules. Each module is elaborated in this chapter and a brief overview of the process is given below.

- Part
- Property
- Step
- Interaction
- Load
- Mesh

A complete 3D model of the building has been made in Autodesk Revit and is exported to Abaqus. In Abaqus the first step is to create parts, from which the model can be assembled. For example, each wall, floor and column is created as a part and by assembling these separate parts, the model is made, assembled. Next, the properties, as material and section, are assigned to these parts. Once the model is assembled, the analysis procedure (step), the loading and the boundary conditions are defined. Finally, the constraints, which determine the interaction between the parts, and the mesh size and mesh properties are defined.

4.1. Part

As described above, a 3D model of the building has been imported in Abaqus as separated parts. The total number of parts can be rather high, since each piece of wall, floor and column is imported separately. To make a more workable model, multiple parts can be merged together as one new part; for example, the walls of multiple floors are merged together as one part, Figure 4.1. This reduces the number of parts in the model and increases the speed of modelling. Also less interactions and constraints between separate parts need to be defined. However, parts with sharp angles and small edges are more difficult to mesh and result in a fine mesh with many small elements, which reduces the stable time. Therefore, it is not always preferable to merge many parts into one big part. A balance between the number of parts, their shape and the mesh size of the parts need to be found.

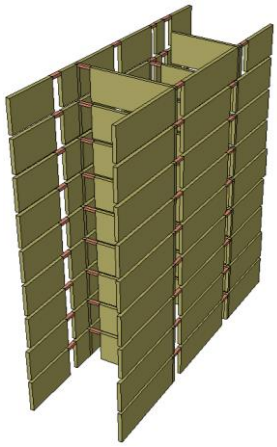

Figure 4.1: Walls of multiple floors merged into one part.

4.1.1. Concrete solids

Different types of parts are available in Abaqus, namely: solids, shells and wires. This division of parts corresponds to 3D, 2D and 1D elements respectively. For this research the concrete parts of the building are modelled with solid elements. The properties of the elements are discussed in chapter 4.6.

4.1.2. Reinforcement shells

The reinforcement is modelled with shell parts. Abaqus offers a simplified method for modelling reinforcement which can be useful for large models, since it is rather time consuming to model each reinforcement bar separately. With this simplified method, the reinforcement is modelled as a shell with a certain thickness t which depends on the area and the center to center distance of the rebars. For example, a wall has two reinforcement nets, one on each side, with vertical and horizontal rebars. In Abaqus, both nets are modelled as a shell with a certain offset from the outside of the wall, corresponding to the cover on the reinforcement. The area and the center to center distance are defined as well as the angle of the rebars, for the horizontal or vertical orientation. Multiple layers of reinforcement with different dimensions and angles can be defined for each shell. Figure 4.2 and Figure 4.3 show the principle of the reinforcement shell and the input in Abaqus.

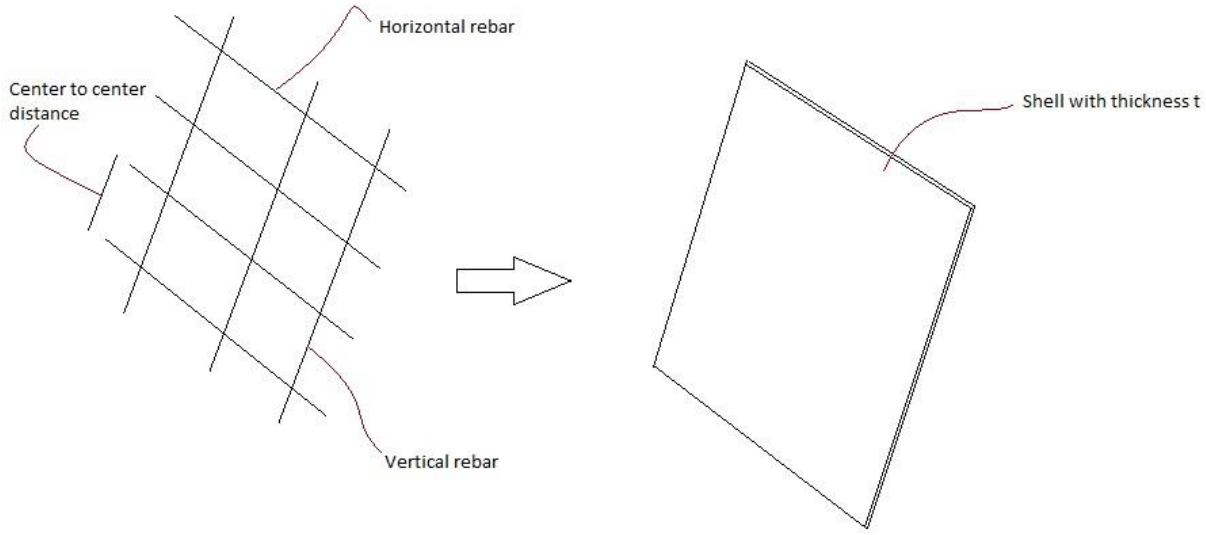

Figure 4.2: Principle of a reinforcement shell in Abaqus.

Rebar Layers

Rebar geometry: (•) Constant ( ) Angular ( ) Lift equation-based

Layer Name	Material	Area per Bar	Spacing	Orientation Angle
Horizontal-12	B500	0.000113	0.15	0
Vertical-10	B500	7.85E-005	0.125	90

Figure 4.3: Table with input of the reinforcement parameters in Abaqus.

Abaqus calculates the thickness of the reinforcement shell with the following formula: $t = \frac{A}{s}$, in which A is the area of the rebar and s is the spacing of the rebars, corresponding to Figure 4.3 above.

Figure 4.4 shows an example of a concrete wall (yellow) with reinforcement nets modelled as shells (green). In order to create a proper connection between the reinforcement of separate

parts, the reinforcement shells are extended above and below the concrete wall. Then, the extended part is embedded in the floor, above or below the wall, and a tie constraint between the floor reinforcement and the extended wall reinforcement is defined. The interaction between the concrete and the reinforcement is defined by the interaction property 'embedded region'. Both interaction types, embedded region and tie constraint, are further explained in chapter 4.4 about interactions and constraints.

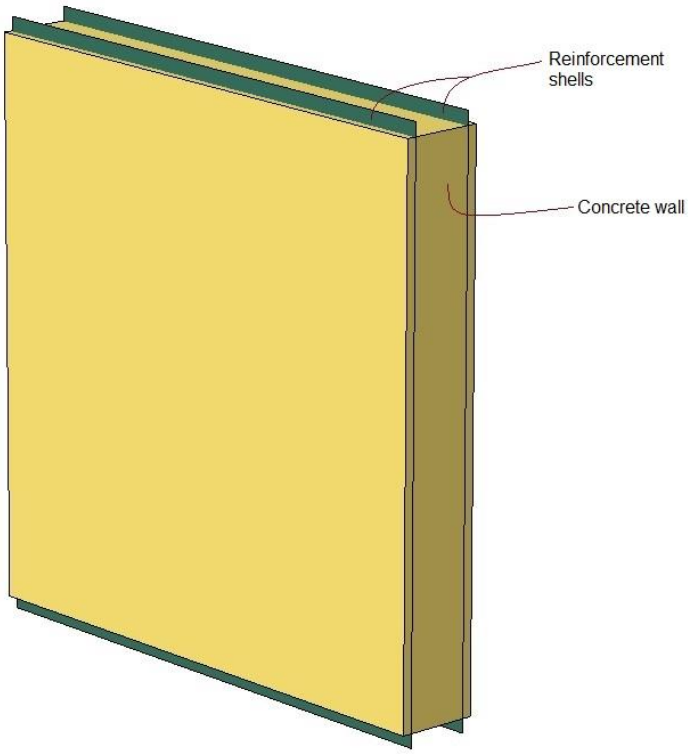

Figure 4.4: Example of a wall with embedded reinforcement shells.

4.2. Property

Once all parts are created, properties can be determined and assigned to the parts. This contains the definition of the material parameters, the sections (solid, shell, beam) and the orientation of profiles and materials.

The first step in the property module is to define the material properties. The material properties which are used for this model are described below. Two different materials are applied: concrete and reinforcement steel; for concrete, several strength classes are used.
The first two analyses with the 3D model in Abaqus are executed with elastic material properties, for verification of the 3D model with the 1D model in Matlab.

4.2.1. Elastic material properties

The elastic material properties are defined in Abaqus by means of the elasticity moduli of the materials. The first elastic analysis is performed with the initial stiffness (E_0) of concrete and reinforcement steel. The second elastic analysis is executed with the cracked or reduced stiffness ($E_{red} \approx \frac{1}{3} * E_0$) of concrete and the initial stiffness (E_0) of the reinforcement steel. The input parameters are given in Table 4-1.

Table 4-1: Overview of elastic material parameters for concrete and reinforcement.

Material	E_0 [N/m^2]	E_{red} [N/m^2]	ν [-]
C20/25	$2.99 * 10^{10}$	$1.0 * 10^{10}$	0.2
C28/35	$3.23 * 10^{10}$	$1.1 * 10^{10}$	0.2
C35/45	$3.41 * 10^{10}$	$1.2 * 10^{10}$	0.2
B500	$21.0 * 10^{10}$	$21.0 * 10^{10}$	0.3

4.2.2. Plastic material properties

For the plastic analyses, additional and different material properties are required. These parameters are discussed in this paragraph.
The partial factors are used to determine the design values of the strength of the material. Next to the common material factors also an additional seismic factor is defined in chapter 3 of the NPR; the factors are shown in Table 4-2.

Table 4-2: Partial factors for design values and seismic loading.

Material	Concrete	Reinforcement steel	All
Factor	γ_c	γ_s	$\gamma_{m\ (seismic)}$
Value	1.5	1.15	1.2

The design values of the materials are shown in the table below.

Table 4-3: Design values of the materials.

Material	E_0 [N/m^2]	ν [-]	$\sigma_{c,d}$ [N/m^2]	$\sigma_{t,d}$ [N/m^2]
C20/25	$2.99 * 10^{10}$	0.2	$11.1 * 10^{6}$	$0.86 * 10^{6}$
C28/35	$3.23 * 10^{10}$	0.2	$15.5 * 10^{6}$	$1.08 * 10^{6}$
C35/45	$3.41 * 10^{10}$	0.2	$19.4 * 10^{6}$	$1.25 * 10^{6}$
B500	$21.0 * 10^{10}$	0.3	$365 * 10^{6}$	$365 * 10^{6}$

4.2.2.1. Concrete

For concrete, the material model Concrete Damage Plasticity (CDP) of Abaqus is applied; this material model is suitable for concrete under cyclic loading and is based on two failure criteria: cracking in tension and crushing in compression. The model is defined through the following input parameters:

- Plasticity;
  - Dilation angle (ψ);
  - Eccentricity of plastic potential surface (ϵ);
  - Ratio of initial biaxial yield stress to initial uniaxial yield stress (compressive);
  - Ratio of second stress invariant tensile meridian to compressive meridian (K_c).
- Compressive/tensile behaviour;
  - Stress-strain data;
  - Compression/tension damage.

The plasticity input basically determines the yield condition of the material model. For this research, the default, recommended values of Abaqus are applied ($\psi = 10°$; $\epsilon = 0.1$; $\frac{f_{b0}}{f_{c0}} = 1.16$; $K_c = \frac{2}{3}$) (Abaqus, 2017).

Stress-strain data

The tensile and compressive behaviour input is determined through the stress-strain curves for tension and compression. For this research the stress-strain curves are based on the formulas of Hordijk et al. (Hordijk, 1986) and Thorenfeldt et al. (Thorenfeldt, 1987) respectively.

The formula of Hordijk et al. is given by:

$$\sigma_{tension} = \sigma_{t,d}\left\{\left[1 + \left(3\frac{\varepsilon}{\varepsilon_{tu}}\right)^3\right]\exp\left(-6.93\left(\frac{\varepsilon}{\varepsilon_{tu}}\right)\right) - 0.027\frac{\varepsilon}{\varepsilon_{tu}}\right\} \qquad \varepsilon_{tu} = 5.136 * \frac{G_f}{\sigma_{c,t,d}}$$

In which:

$\sigma_{tension}$	is the tensions stress corresponding to the strain (ε);
$\sigma_{t,d}$	is the design value for the 5% fractile tension stress (according to Table 4-3);
ε	is the strain value for which the stress ($\sigma_{tension}$) is calculated;
G_f	is the fracture energy of the concrete in tension.

The formula of Thorenfeldt et al. is given by:

$$\sigma_{compression} = \sigma_{c,d}\left(\frac{\varepsilon}{\varepsilon_p}\right)\left(\frac{n}{n - \left(1 - \left(\frac{\varepsilon}{\varepsilon_p}\right)^{nk}\right)}\right) \qquad n = 0.8 * \frac{\sigma_c}{17};\ k = \begin{cases} 1 & \varepsilon_p < \varepsilon < 0 \\ 0.67 + \frac{\sigma_c}{62} & \varepsilon < \varepsilon_p \end{cases}$$

In which:

$\sigma_{compression}$	is the compression stress corresponding to the strain (ε);
$\sigma_{c,d}$	is the design value for the compression stress (according to Table 4-3);
σ_c	is the characteristic value for the compression stress; ($\sigma_{c,d}$ without safety factors);
ε	is the strain value for which the stress ($\sigma_{compression}$) is calculated;
ε_p	is the strain at which first plasticity occurs.

In the figures Figure 4.5 and Figure 4.6, the basic principles of the CDP material model according to the Abaqus manual are shown (Abaqus, 2017).

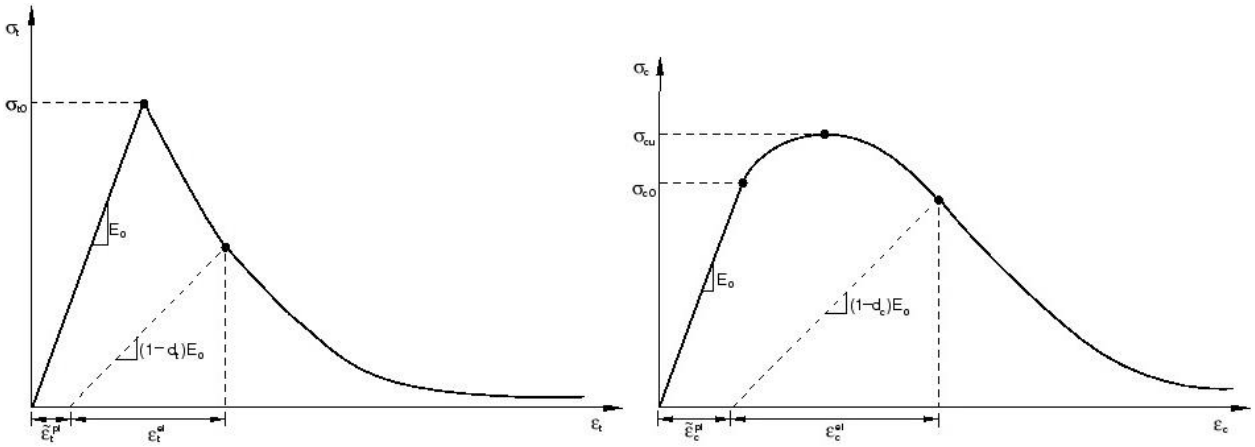

Figure 4.5: Tensile behaviour (left) and compressive behaviour (right) of CDP material model (Abaqus documentation 2016).

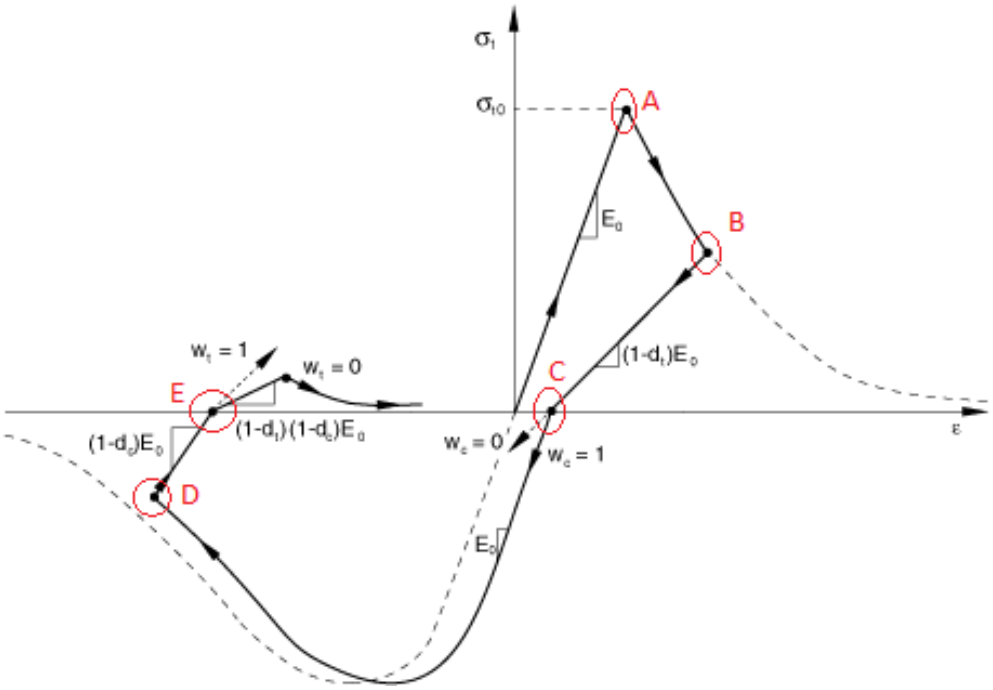

Figure 4.6: Cyclic behaviour of CDP material model with stiffness recovery (w_c,w_t).

Figure 4.6 shows the behaviour of the CDP model under cyclic loading; the marked regions are discussed below:

A. The maximum tensile stress is reached, plasticity occurs;
B. The loading changes from tension to compression, the stiffness is: $E_t = E_0 * (1 - d_t)$;
C. The stress becomes zero, remaining strain is plastic strain
   The stiffness in compression depends on the value of stiffness recovery (w_c);
D. The loading changes from compression to tension, the stiffness is: $E_c = E_0 * (1 - d_c)$ if the stiffness recover (w_C) is set to 1;
E. The stress becomes zero, remaining strain is plastic strain; the remaining stiffness is equal to: $E_0 * (1 - d_t) * (1 - d_C)$.

Damage and stiffness recovery

As discussed previously, the material model is based on the failure criteria of cracking in tension and crushing in compression. The material model, as shown in Figure 4.6, reduces the

stiffness of the material as plasticity occurs. The amount of stiffness reduction is defined through the damage parameters of tension (d_t) and compression (d_c); the value of the damage parameters is related to the amount of plasticity in the material. For example, if only a small amount of plasticity occurs, the material is hardly damaged; however, if the amount of plasticity becomes rather high, the damage increases as well.
The parameters stiffness recovery w_c and w_t determine the extent to which the stiffness is recovered once the load changes from tension to compression or from compression to tension. The default settings are based on the theory that if concrete is cracked in tension and the crack closes, the compressive stiffness is recovered ($w_c = 1$), since cracked concrete still can resist compressive loading. However, if concrete is crushed in compression, the tensile stiffness is not recovered ($w_t = 0$), since crushed concrete is not able to resist tensile loading.

Calculation of the input parameters
The input of the material properties is related to the dimension of the mesh in order to get the correct material behaviour. The following parameters are used to define the stress strain behaviour for compression and tension:

- Initial Young's modulus (E_0);
- Compressive/tensile strength;
- Fracture energy (only for tension);
- Target residual crack width;
- Mesh size;
- Displacement at 1% compressive/tensile strength stress.

When the stress goes to zero from tension or compression, the cracks will not close completely. The residual crack width is the plastic strain, equal to $\tilde{\varepsilon}_{c,t}^{pl}$ in Figure 4.5. If the strain becomes really large, the stress decreases according to the softening curve but it may not become smaller than 1% of the strength due to requirements of Abaqus. Therefore, a target residual crack width is required for the calculation of the damage parameters. This will prevent that the residual crack width, or plastic strain, becomes unrealistic high.
The calculation of the input parameters for the stress-strain curves is based on the description of the Abaqus manual and is given below (Abaqus, 2017).

Mesh dependent total strain (ε_{total})
The total strain is calculated as the elastic strain from the elastic branch plus the strain following from stress-strain curve formula (Thorenfeldt, Hordijk) divided by the mesh size in order to get a correct value for the fracture energy per element.

$$\varepsilon_{total} = \varepsilon_{el,0} + \frac{\varepsilon_{m1}}{L_m}$$

In which:

- $\varepsilon_{el,0}$ is the strain from the elastic branch $\left(\frac{\sigma_u}{E_0}\right)$;
- ε_{m1} is the *plastic* strain of the stress-strain curve formula corresponding to σ; this value corresponds to a mesh size of one meter;
- L_m is the dimension of the mesh.

Mesh dependent plastic strain (ε_{pl})

The plastic strain is determined based on the target residual crack width.

$$\varepsilon_{pl,n} = \varepsilon_{pl,n-1} + \frac{\varepsilon_{total,max} * d_{max}}{n_{input}}$$

In which:

- d_{max} is the maximum damage parameter (usually about 0.99, 1% strength remaining);
- $\varepsilon_{total,max}$ is the target residual crack width;
- n_{input} is the number of input points used for this calculation (arbitrary).

Mesh dependent elastic strain (ε_{el})

Finally, the elastic strain is the total strain subtracted with the defined plastic strain.

$$\varepsilon_{el} = \varepsilon_{total} - \varepsilon_{pl}$$

The corresponding damage parameter for each stress-strain point is determined by the following formula:

$$d = -\left(\frac{\sigma}{\varepsilon_{el} * E_0} - 1\right)$$

Inelastic strain for Abaqus input (ε_{ck})

With these parameters, the inelastic strain can be calculated with the formula:

$$\varepsilon_{ck} = \varepsilon_{pl} + \frac{d}{1-d} * \frac{\sigma_y}{E_0}$$

This formula is used by Abaqus to calculate the plastic strains from the inelastic strain input. This calculation is performed by Abaqus to check whether the input is correct. Since the plastic strains (ε_{pl}) are already calculated, the equation is rewritten to calculate the inelastic strains. The yield stress, inelastic strain and damage parameter are calculated and can be used as input for Abaqus. The parameters which are used for the calculation are shown in the figure below.

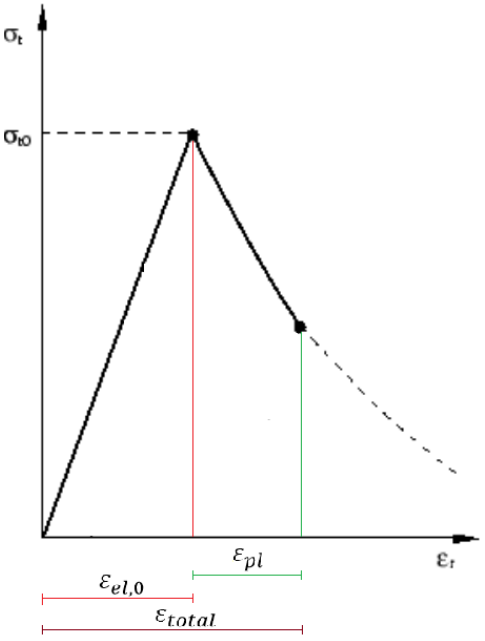

Figure 4.7: Parameters for calculation of Abaqus input.

4.2.2.2. Reinforcement steel

For the reinforcement steel, a plastic material model is applied. In this model the material is defined as *elastic-perfectly plastic*. The design values used for this material are given in Table 4-3. In the graph below, the stress-strain diagram for the reinforcement steel is shown.

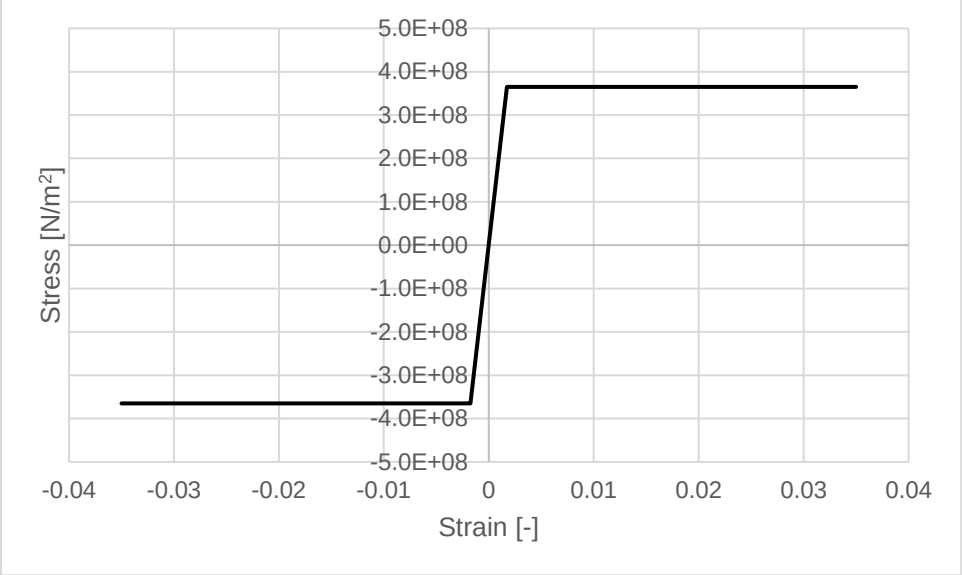

Figure 4.8: Stress-strain diagram of reinforcement steel B500.

4.2.2.3. Element deletion

An additional material parameter for both concrete and reinforcement is a factor for element deletion (Zonneveld ingenieurs b.v., 2016). This property is useful for the stability of the analysis, since it prevents a large drop of the stable time or an excessive increase of the mass scaling, by deleting the critical elements. Besides, it makes progressive collapse of the structure possible.

The element deletion is determined through the following parameters:

- dV_C if the volume change due to compression is larger than 3%;
- dV_t if the volume change due to tension is larger than 30%;
- $PEEQ$ if the equivalent plastic strain in compression becomes larger than the determined threshold, which deviates per mesh dimension.

The threshold for the plastic equivalent strain is related to the size of the mesh and is therefore different for several parts.

4.2.2.4. Small scale material test

A small scale test is performed to check whether the material properties are defined correct and the material models behave as expected. The input parameters for both material models are tested with a small cube test in Abaqus. A cube element is used for this test and the model is shown in Figure 4.9.

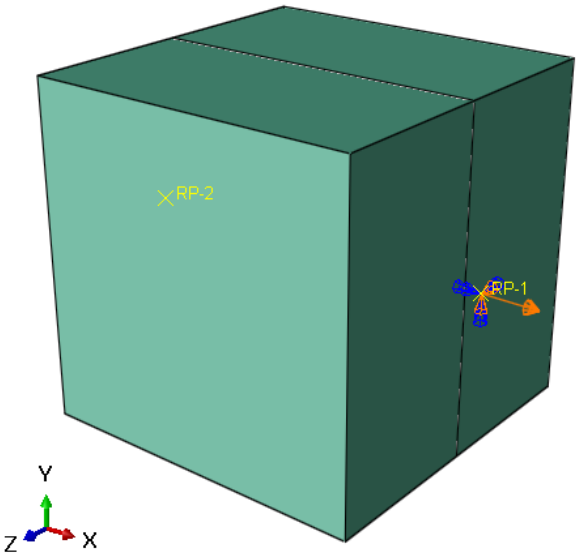

Figure 4.9: Model of a cube with 1 element and rebar layer

The cube is modelled as 1 element with a dimension of 0.1 meter. The test is performed with an imposed deformation in X-direction at one side of the cube, while the other side of the cube is constrained in X-direction; the remaining degrees of freedom are not constrained. The material parameters are shown in the table below.

Table 4-4: Overview of applied material properties in material test

Material	E_0 [N/m^2]	ν [-]	$\sigma_{c,d}$ [N/m^2]	$\sigma_{c,t,d}$ [N/m^2]	$\varepsilon_{plastic}$
C20/25	$2.99 * 10^{10}$	0.2	$11.1 * 10^{6}$	$0.86 * 10^{6}$	$\sim 2.9 * 10^{-5}$
B500	$21.0 * 10^{10}$	0.3	$365 * 10^{6}$	$365 * 10^{6}$	$\sim 1.7 * 10^{-3}$

The imposed deformation is equal to $5.5 * 10^{-4}$ meter, which is equal to a strain of $5.5 * 10^{-3}$, so plasticity is expected. In the graphs below, the results of the test are shown by the stress-strain diagrams of the concrete and reinforcement element.

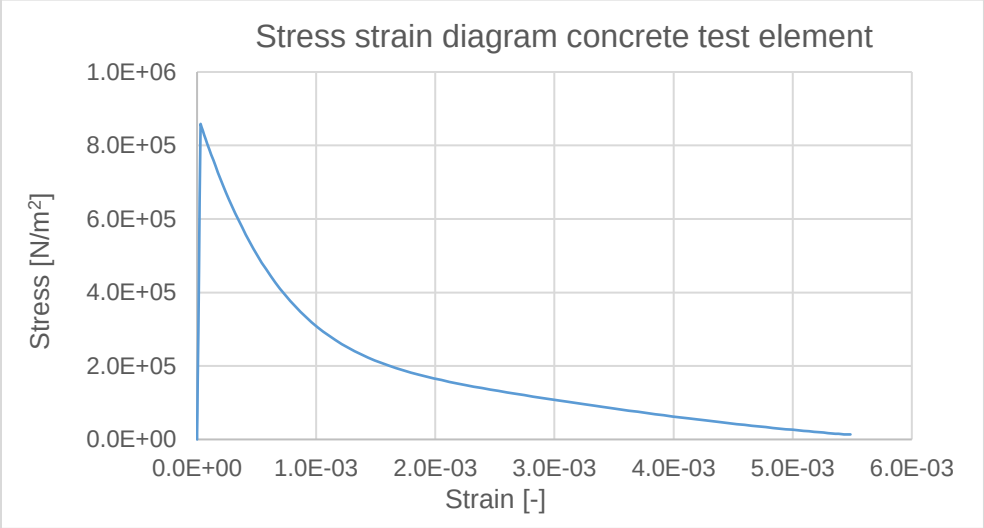

Figure 4.10: Stress-strain diagram of the concrete test element.

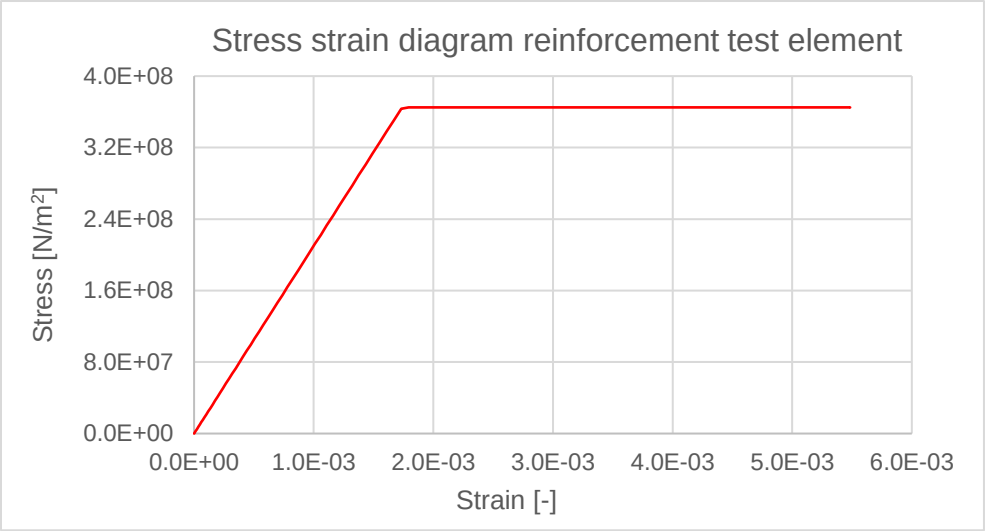

Figure 4.11: Stress-strain diagram of the reinforcement test element.

The following test is performed with a cyclic loading, in which first a positive imposed deformation and then a negative imposed deformation is applied. The stress-strain diagram in Figure 4.12 shows the cyclic behaviour of the CDP material model. First, the displacement increases in positive direction, which causes tensile stress; once the strain becomes larger than the plasticity limit, plasticity occurs and the stress in the element decreases. Next, the displacement changes from positive to negative direction, which causes compressive stress and therefore, the stress goes to zero and becomes negative. The slope of the part from positive stress to zero stress differs from the initial slope. This is caused by the stiffness degradation of the CDP material model. As soon as damage occurs, the stiffness is reduced by the following formula: $(1 - d) * E_0$. In this formula, d is the amount of damage with a range between 0 and 1.

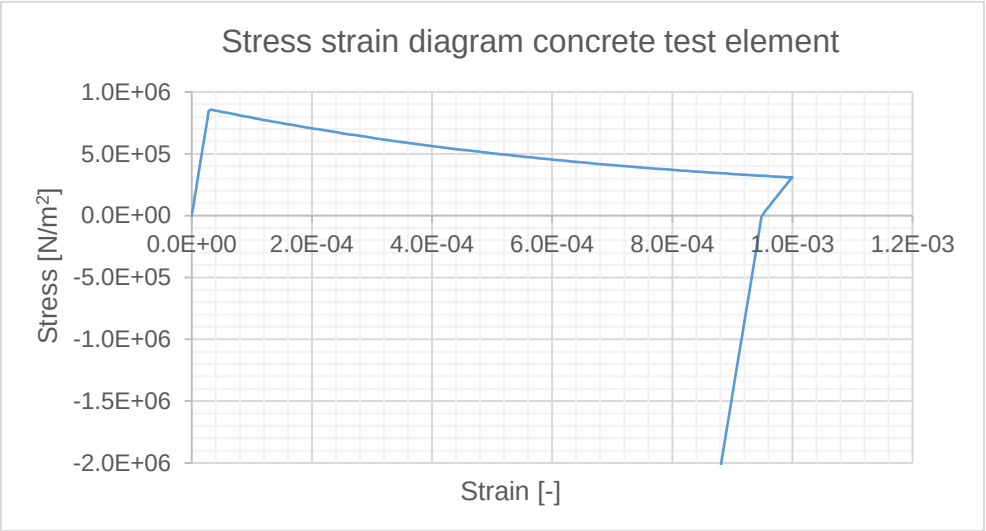

Figure 4.12: A part of the stress-strain diagram of the concrete test element under cyclic loading.

The results of both tests show that the material model performs as expected.

4.2.3. Material Damping

In Abaqus, damping is implemented through Rayleigh damping. This damping is defined through the parameters α and β, which correspond to the damping of the lower and higher frequencies respectively.
The parameters are calculated with the following formulas:

$$\alpha = \frac{2 * \omega_1 * \omega_2(\xi_1 * \omega_2 - \xi_2 * \omega_1)}{\omega_2^2 - \omega_1^2}; \qquad \beta = \frac{2(\xi_2\omega_2 - \xi_1\omega_1)}{\omega_2^2 - \omega_1^2}$$

In which:

- ω_1 is the lowest frequency of the model;
- ω_2 is the higher frequency corresponding to one of the highest main modes;
- ξ_1 and ξ_2 are the first and second damping ratio (for example 2% or 5%).

The principle of the Rayleigh damping is shown in the graph below.

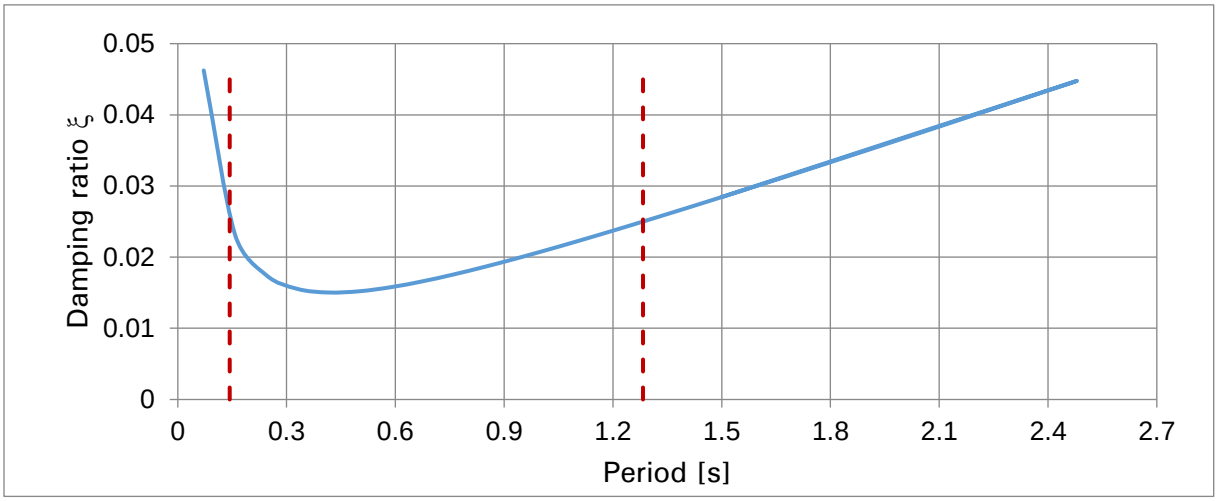

Figure 4.13: Principle of Rayleigh damping.

The damping is 'fitted' on two frequencies (red lines in Figure 4.13) of the model. According to the NPR, the frequencies 'should be chosen with care' taking into account the main modes of the model. The main modes are determined with a frequency analysis of the model in Abaqus and the results are shown in Table 4-5. For example the 1^{st} and 5^{th} mode are main modes, since a rather high percentage of the mass is activated in these specific modes. It is expected that these modes will contribute significantly to the seismic response.

Table 4-5: Results of the frequency analysis in Abaqus.

Mode	Eigenvalue	Frequency		Activated mass [kg]			Total activated [%]		
		Rad/s	Cycles/s	X	Y	Z	X	Y	Z
1	23.986	4.8976	0.77947	2.45E+06	1.36E+07	3.42E+00	11%	**59%**	0%
2	25.022	5.0022	0.79613	1.33E+07	2.36E+06	3.03E+01	**69%**	69%	0%
4	271.53	16.478	2.6226	1.02E+06	1.22E+05	5.33E+03	74%	70%	0%
5	362.95	19.051	3.0321	3.66E+04	3.89E+06	1.42E+04	74%	**87%**	0%
6	418.84	20.466	3.2572	2.83E+06	1.36E+03	9.14E+03	87%	87%	0%
8	1244.6	35.28	5.6149	7.24E+03	4.51E+03	1.90E+07	87%	87%	**83%**
10	1927	43.898	6.9865	8.19E+03	3.34E+05	3.22E+04	89%	89%	83%
300	40398	200.99	31.989	8.60E+03	5.06E+02	1.84E+03	97%	97%	91%
		Total:		**2.23E+07**	**2.24E+07**	**2.08E+07**			

For the calculation of the α and β factor of the Rayleigh damping, the frequencies of the 1^{st} and 10^{th} mode are used. The higher modes are expected to have a relative small contribution to the seismic response of the building and are therefore not used for determining the Rayleigh damping. The total activated mass in these higher modes, from mode 11 till mode 300, is equal to approximately 8%, compared to 89% in the first 10 modes.
Some of the main modes are shown in the figures below.

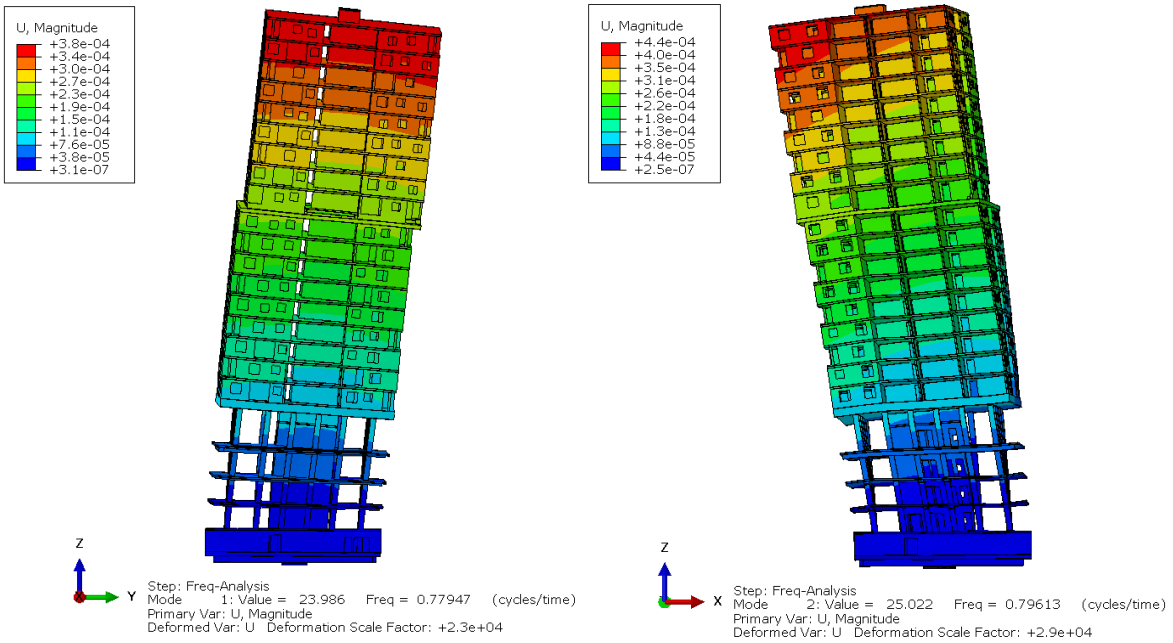

Figure 4.14: Eigenmode 1 and eigenmode 2 of the 3D model.

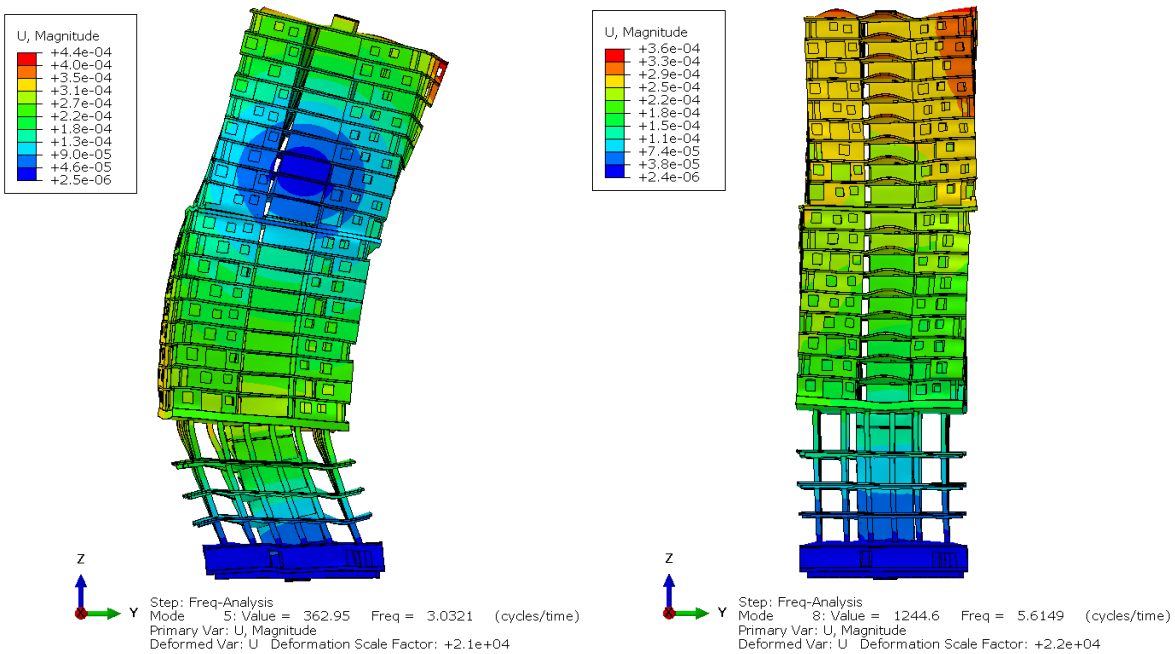

Figure 4.15: Eigenmode 5 and eigenmode 8 of the 3D model.

The α and β factors corresponding to the 1st and 10th mode are calculated for a damping ratio of 2.5% in both modes:

$$\alpha = \frac{2 * 4.9 * 43.9(0.025 * 43.9 - 0.025 * 4.9)}{43.9^2 - 4.9^2} = 0.22031$$

$$\beta = \frac{2(0.025 * 43.9 - 0.025 * 4.9)}{43.9^2 - 4.9^2} = 0.00102$$

Next to the Rayleigh damping, the plastic definition of the materials also contributes to the damping of the system.

4.2.4. Sections

Once all material properties are defined, the sections can be created. The function of a section is to assign certain properties to the parts. The section of a part determines its properties, function and possibilities for the remaining part of the modelling process and the analyses. Multiple sections can be assigned to a part, in order to make distinction between several properties within a part.
In this research, two different types of sections are applied, namely solid 3D sections and shell surface sections. All the concrete parts are modelled as solid 3D elements and all reinforcement is modelled as shell elements.

4.3. Step

In the step module the type of analysis and some related properties are defined. The type of step is directly related to the purpose and loading of the analysis. If the goal of the analysis is to investigate the impact of an earthquake on a certain structure, a dynamic analysis, and thus a dynamic type of step, is required. However, a static load can be applied through more than one type of step: a static step and a dynamic step.

For this research, two different types are applicable: static and dynamic. The static analysis can be used for applying the gravity loading on the model. The dynamic analysis is used for applying the earthquake loading.
In advance of the earthquake load, the gravity needs to be applied to the model with a static or dynamic analysis. The advantage of a static analysis is the duration of that type of analysis. However, a static analysis is only applicable if the analysis is linear, since nonlinearity usually results in convergence problems (a static analysis uses the implicit scheme, see 4.3.1). Therefore, the gravity analysis should be performed with linear material properties in a static analysis, in order to prevent nonlinearity. Since multiple analyses are performed in the process with different models and parameters, it is beneficial to use the static analysis for the gravity loading in order to save time.
The duration of the accelerograms is 10 seconds and the gravity load is applied in 1 or 1.5 seconds. Therefore, the total duration of the steps in this research is 11 or 11.5 seconds, respectively.

4.3.1. Dynamic analysis

Two dynamic analysis procedures are available in Abaqus: implicit and explicit. The main difference between these procedures is that the explicit scheme obtains values for dynamic quantities at $t + \Delta t$ based entirely on available values at time t while the implicit scheme solves for dynamic quantities at time $t + \Delta t$ based not only on values at t, but also on these same quantities at $t + \Delta t$. Since they are implicit, nonlinear equations need to be solved. In combination with expected plasticity, and therefore nonlinearity, the implicit solver might not converge or would take a large amount of small steps for solving the equations. Therefore, the explicit solver is preferable.

The analysis time of the explicit solver depends on the stable time of the model. This stable time is calculated with the highest eigenvalue of the model. Therefore, it depends on the stiffness, density and size of the element. The smallest element in the model determines the stable time of the analysis, which means that the mesh size affects the stable time and thus the total time of the analysis. A coarse mesh will result in less accurate results but a shorter analysis time and a fine mesh gives more accurate results but a longer analysis time. Hence, it is important to find an optimal balance between the mesh size and the analysis time. Also the beta factor of the Rayleigh damping influences the stable time of the explicit analysis.

A method to increase the stable time is by applying mass scaling in critical elements. The basic principle of mass scaling is increasing the mass of an element which has a stable time smaller than a certain, user defined, limit. By increasing the mass, the eigenvalue of the element decreases and so the stable time becomes higher. This method works properly as long as the mass scaling remains small enough throughout the analysis, since a high amount of mass scaling results in unrealistic results.

4.4. Interaction

Once all parts are assembled and the model is created, the connections between the separate parts need to be defined. Abaqus offers a broad variety of interactions, constraints and connectors for connection of the parts. The connection has to be a proper simulation of the reality in order to obtain reliable and realistic results. In this model three different constraints are applied: tie constraint, coupling and embedded region; these types are described below.

4.4.1. Tie constraint

As described in chapter 2.1.1, the building mainly consists of cast in place, reinforced concrete and the connection between the walls and floors can therefore be modelled as rigid or fixed. In Abaqus, this can be modelled with a tie constraint. A tie constraint can be applied between two surfaces and makes all active degrees of freedom equal for the element nodes on both surfaces. The tie constraint is used for the connection between walls and floors and their reinforcement. In the figure below, the basic principle of a tie constraint between two parts is shown. The red lines represents the tie between the two surfaces.

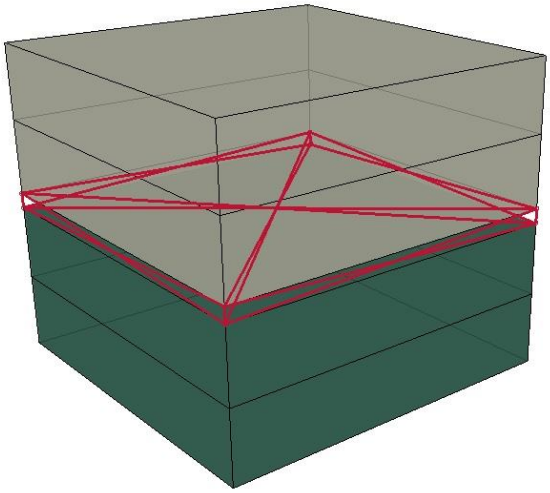

Figure 4.16: Principle of a tie between two surfaces; the degrees of freedom of the tied nodes are equal.

4.4.2. Coupling

The coupling constraint can be applied between a reference point and a surface or nodes. The coupling makes the desired degrees of freedom of the surface or nodes equal to the degrees of freedom of the reference point. The coupling constraint is applied on the piles of the building in order to efficiently apply the earthquake loading and extract results; this is further described in chapter 4.5. Figure 4.17 shows an example of a coupling between a reference point and a part.

Figure 4.17: Example of a coupling between a reference point (red) and a section of a part (pink).

4.4.3. Embedded region

The embedded constraint can be applied to elements that lie within host elements, like reinforcement in concrete. The principle of the constraint is that the translational degrees of freedom of the embedded nodes are constrained to the corresponding degrees of freedom of the host element; the rotational degrees of freedom are not constrained. This type of constraint is applied to the reinforcement, which lies within the concrete elements. The basic principle of an embedded constraint is shown in Figure 4.18.

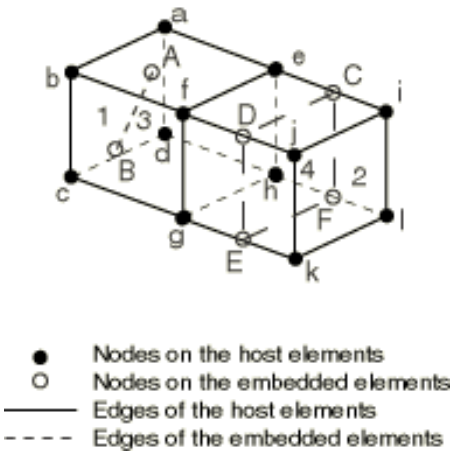

Figure 4.18: Principle of the embedded constraint according to the Abaqus manual.

The status of the modelling process is shown in Figure 4.19. The materials are defined, the model is assembled and the constraints are applied to the intersections of the parts.

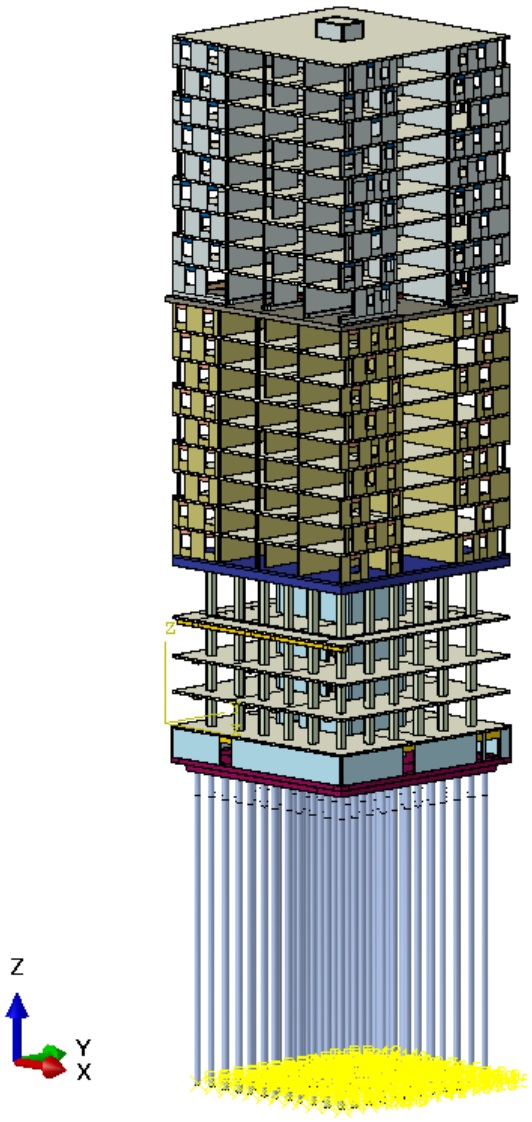

Figure 4.19: Assembled model of La Liberté.

4.5. Load

In the load module the boundary conditions of the model and the loads are defined. In this model, the gravity is applied as a load, while the earthquake is applied through the boundary conditions.

4.5.1. Boundary conditions

As mentioned above, the loading of the earthquake is applied through the boundary conditions of the model. These boundary conditions are applied on the reference points beneath the piles (Figure 4.19), which enables direct extraction of the reaction forces. The reference points are coupled to the piles with a kinematic coupling for all three translational degrees of freedom.
The upper part of the piles, approximately 2 meter, is not coupled to the reference points, considering the weak layers of the soil in the first 7 till 10 meter from ground level. Besides, this method also ensures a more realistic transfer of the accelerations to the building compared to a coupling over the total height of the pile. In that case, the earthquake signal is directly applied at the foundation which results in a unrealistic large peak accelerations of the building. Figure 4.20 shows a cone penetration test of the soil at the location of the building. It shows that the first 8~10 meter are weak soil layers. Since the top of the piles are at a depth of approximately 5 meter, the coupling of the reference points goes up to about 7 meter below the ground surface level.

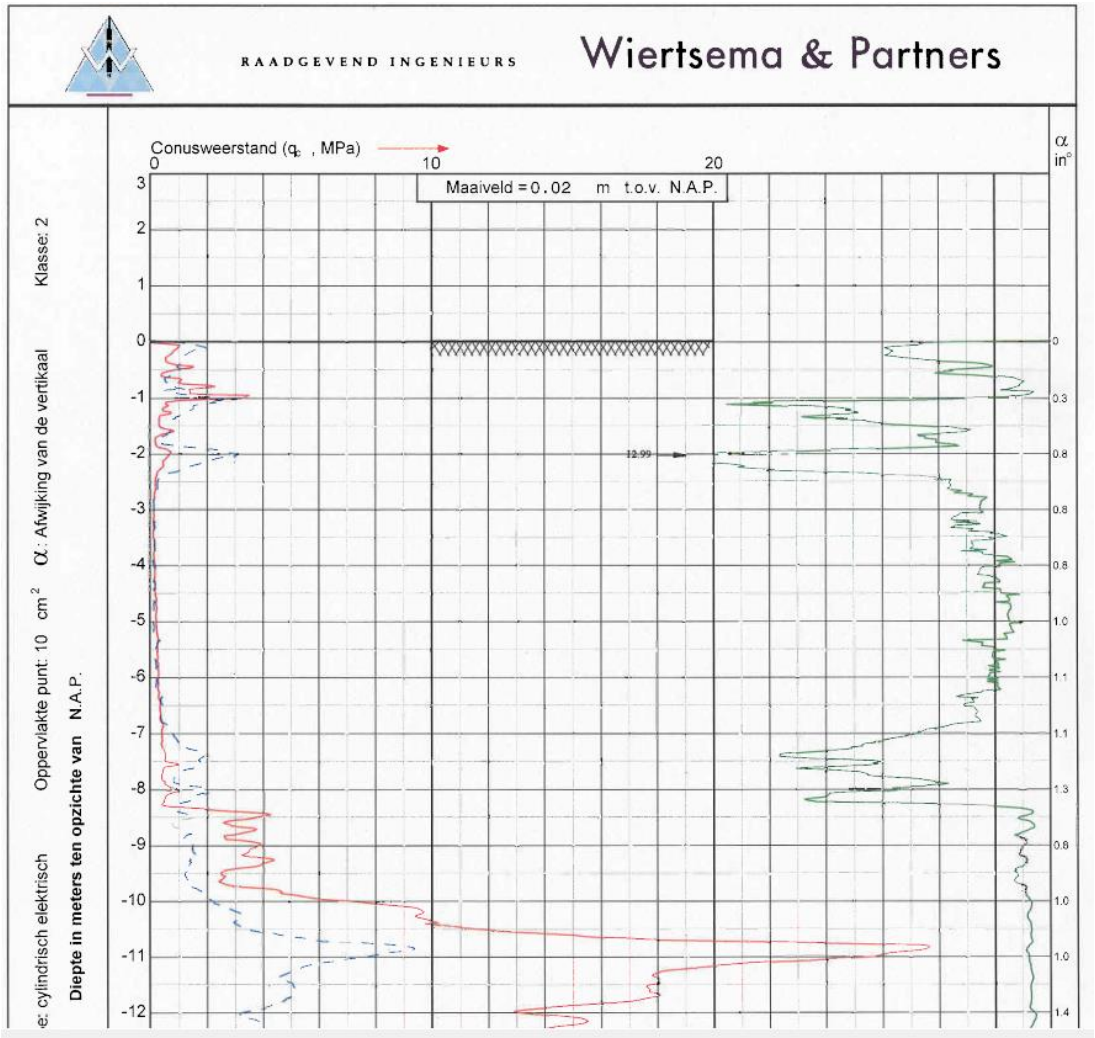

Figure 4.20: Cone penetration test at the location of La Liberté.

Four different boundary conditions are applied on the model; one for the rotational degrees of freedom and three for the translational degrees of freedom. The first boundary condition is only applied for modelling considerations and is created in the initial step and propagated throughout the analysis. The other boundary conditions are modified in the earthquake step, in which the acceleration is applied. The accelerograms of the earthquake are applied as accelerations on the reference points, shown in Figure 4.19. The application of the boundary conditions is shown in Figure 4.21.

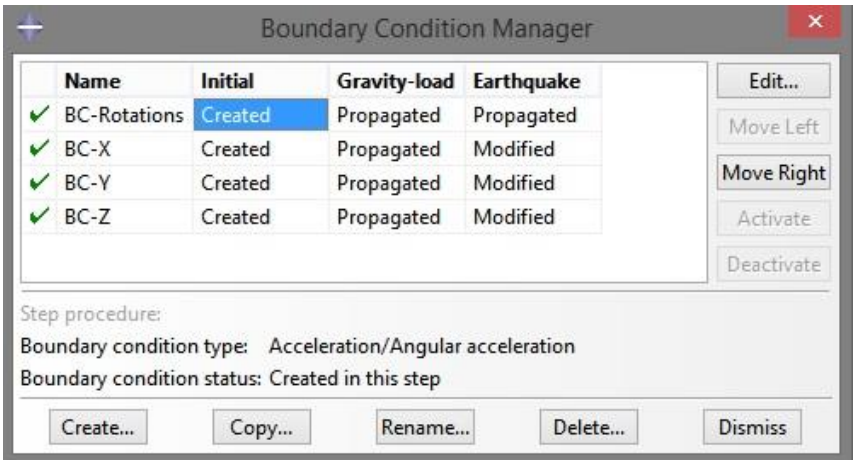

Figure 4.21: Application of the boundary conditions in the model.

In the graph below, the applied accelerograms as applied at the reference point are shown.

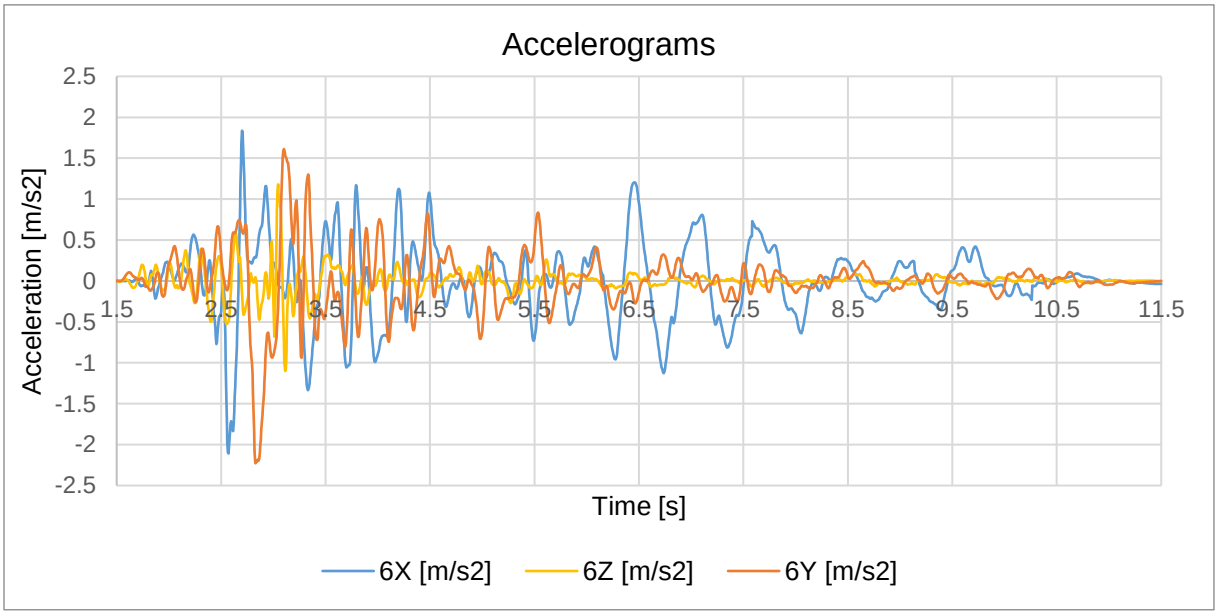

Figure 4.22: Applied accelerograms according to the NPR.

4.5.2. Gravity load

In Abaqus, a specific type of load is available for applying the gravity on a model. The gravity is applied on the whole model, or on a part of the model if desirable, by a factor equal to 9.81 m/s^2. The load can be applied with an amplitude over time or with a linear ramp, depending on the type of analysis. If a dynamic analysis is applied, a smooth amplitude is recommended in

order to minimize and damp out any dynamic effects. In case of a static analysis, a linear ramp can be used since the analysis does not account for dynamic effects.

4.6. Mesh

In the mesh module the dimension, properties and type of the elements is determined. As mentioned before, an optimal balance between the size of the mesh and the amount of elements should be found in order to keep the analysis time as minimal as possible. Therefore, several element dimensions are applied in the model, varying between 0.1 meter for small parts and 0.5 meter for bigger parts. The concrete properties are adjusted to the element size, since these are dependent on the mesh size.
Several properties and control mechanisms, as distortion control and hourglassing control, are element dependent and can be defined in the mesh module.
For this research, the default values of the mesh properties are applied in the initial model. During the process, several mesh controls are adjusted.
Also the type of element is defined, although the suitable types of element also depend on the properties of the part. In this model, two different element types are applied, namely solid and surface elements. The solid elements are applied on the concrete parts and the surface elements on the reinforcement parts.
The applied solid element is C3D8R, which is a Continuum, Three-dimensional element with eight nodes and one integration point (reduced integration), Figure 4.23.

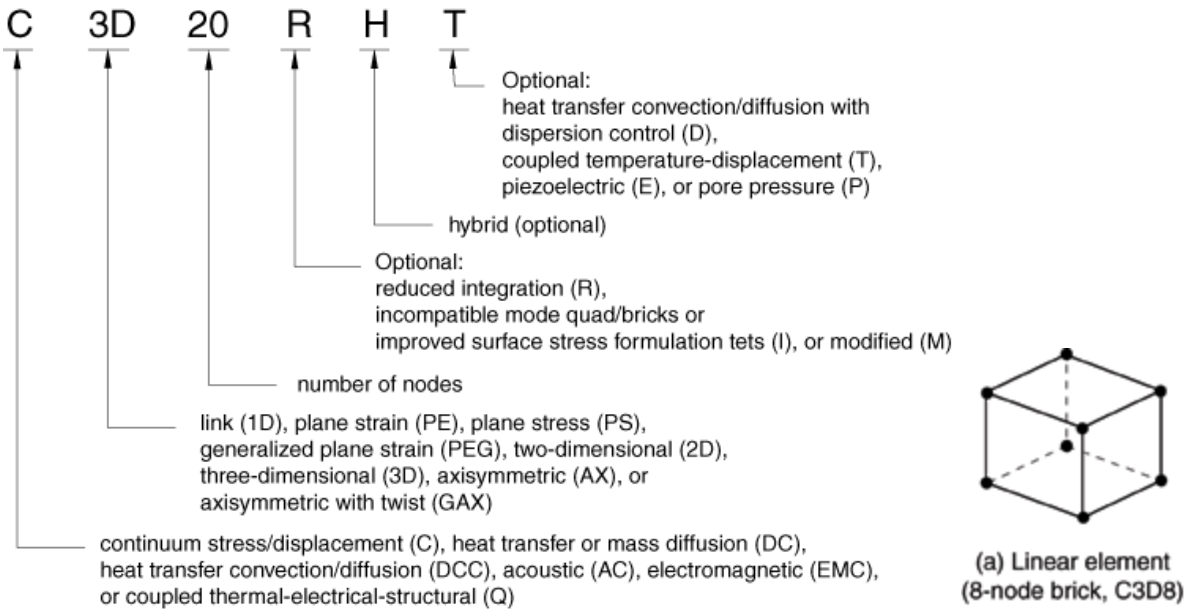

Figure 4.23: Different characteristics and properties of solid elements in Abaqus.

The applied surface element is SFM3D4R, which is a membrane-like, three-dimensional surface element with four nodes and one integration point (reduced integration), see Figure 4.24.

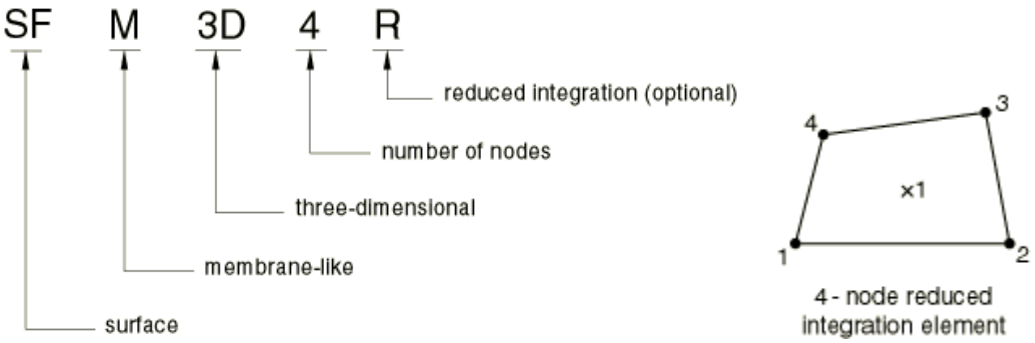

Figure 4.24: Different characteristics and properties of surface elements in Abaqus.

Once the mesh of the model is defined, a first test can be performed in order to check the data of the model. In this so-called 'data check' all input parameters are reviewed by the Abaqus solver as well as the stable times of the elements are calculated. The results of the data check show whether changes or improvements of the model are required or beneficial for the accuracy, stability and duration of the analysis.

4.7. Summary chapter 4

In this chapter the steps of the modelling process and the applied modelling techniques were discussed. Several modelling techniques were elaborated and some of the input parameters were verified and validated through tests. These tests showed that the applied material model for concrete (concrete damaged plasticity) works as defined and expected. Furthermore, a description of the possible types of analysis was presented, which showed that the explicit method is preferred for an analysis in which plasticity is expected. Also the interactions between the parts were discussed; since the building mainly consists of cast in place concrete, most of the interactions were defined as ties. This type of interaction 'couples' all the degrees of freedom of the interface surfaces of the parts. Last but not least, the definition of the boundary conditions was considered, together with the method of application of the different loads in the analyses. The earthquake load was applied as accelerations in several directions at the boundary conditions of the piles.

In the following chapter, the results of the NLTH analyses are presented and discussed.

5. NLTH Analyses

After the 3D model is developed in Abaqus, as described in chapter 4, the next step is to determine the sensitivities of the model. Sensitivities are parameters within the model which are 'sensitive' to changes, which means that these parameters influence the results to a large extend if subjected to relative small changes. In order to develop a reliable calculation model, these parameters are of importance.
The sensitivities are determined through a process of analyses; this modelling process consists of multiple analyses of the model with varying input and parameters. The starting point of this process, besides two elastic analyses, is a most basic model with the smallest analysis time. During the process, several parameters are adjusted or enabled, which influences the duration of the analysis; because next to the reliability, also the efficiency plays a role in developing this calculation model.

In the table below, an overview of the performed analyses is given. In the column 'property' the main property for the analysis is described. Basically each following analysis is an improvement or rectification of the previous analysis. Analyses which are further discussed and elaborated below, are marked with a green filling in the last column. The elastic analysis of the model are used for verification of the 3D model with the 1D model and are marked with the yellow mark in the last column.

Table 5-1: Overview of the performed analyses in the modelling process.

Analysis	**Property**	**Remarks**	
E_0	Initial stiffness	Analysis with elastic material properties	
E_{red}	Reduced stiffness	Analysis with elastic material properties	
1	High fracture energy.	No tensile cracks, concrete behaves tough/viscous.	
2	'normal' fracture energy ($\sim 90\ [\mathrm{J/m^2}]$).	Analysis becomes unstable within 0.1 seconds; tension damage occurs in whole model.	
3	'higher' fracture energy ($\sim 500\ [\mathrm{j/m^2}]$) and second order accuracy.	Analysis finishes, but the concrete behaves too tough.	
4	'normal' fracture energy ($\sim 90\ [\mathrm{J/m^2}]$) and second order accuracy.	Analysis becomes unstable after 1.5 seconds. Second order accuracy improves analysis, compared to analysis number 2	
5	Stiffness recovery set to zero for both tension and compression.	Analysis runs without instability but the concrete has no stiffness anymore as soon as damage occurs due to tension or compression.	
6	Analysis with nonzero beta-factor for damping (Rayleigh).	Analysis runs without instability; the beta-factor solves instability problem of previous runs; however, it has a significant influence on the analysis time.	

6a-d	Non-zero beta-factor with fixed stable time or mass scaling.	With fixed stable time, results are not accurate since explicit solver ‘jumps’ over peak strains/accelerations. With mass scaling, the results are incorrect; amount of mass scaling too high.	
7	Analysis with element deletion on tensile plastic strains in order to prevent increasing mass scaling.	Threshold for element deletion is not reached and so mass scaling is still too high.	
8-10,12	Improved mesh with significant finer mesh size and more cubic element shape	Analysis runs with small amount of mass scaling. In these three analyses, mesh is further improved and some small (prefab) parts are removed.	
11	Changed material properties and earthquake loading (magnitude of signal) according to NPR 9998:2015 annex F	Analysis runs but due to different material properties, mass scaling becomes rather high.	
13	Material properties corrected, with different Young’s moduli.	Analysis finishes; no mass scaling, no elements deleted.	
14	‘combined’ hourglassing control instead of ‘enhanced’	Analysis finishes; no mass scaling, no elements deleted.	

5.1. Verification 3D NLTH Analysis

The 3D model in Abaqus is verified by means of a comparison of the results of the elastic analyses of the 1D and 3D model. As described in chapter 3, the 1D model consists of three elements and the nodes of these elements correspond to the foundation and the 4^{th}, 12^{th} and 22^{nd} floor of the building.

In chapter 3 the factors of the Rayleigh damping of the 1D model are described and determined; these damping factors correspond to a ratio of 2.5% damping. However, in the 3D Abaqus model, a ratio of 0.33% is applied for the higher frequency (corresponding to a small β-factor), in order to achieve a reasonable analysis time. Therefore, the same ratio is applied in the Matlab model, which corresponds with the following damping factors:

$$\alpha = 0.324; \beta = 0.000034$$

For the analysis of the 1D model in Matlab, these damping factors are applied to the system.

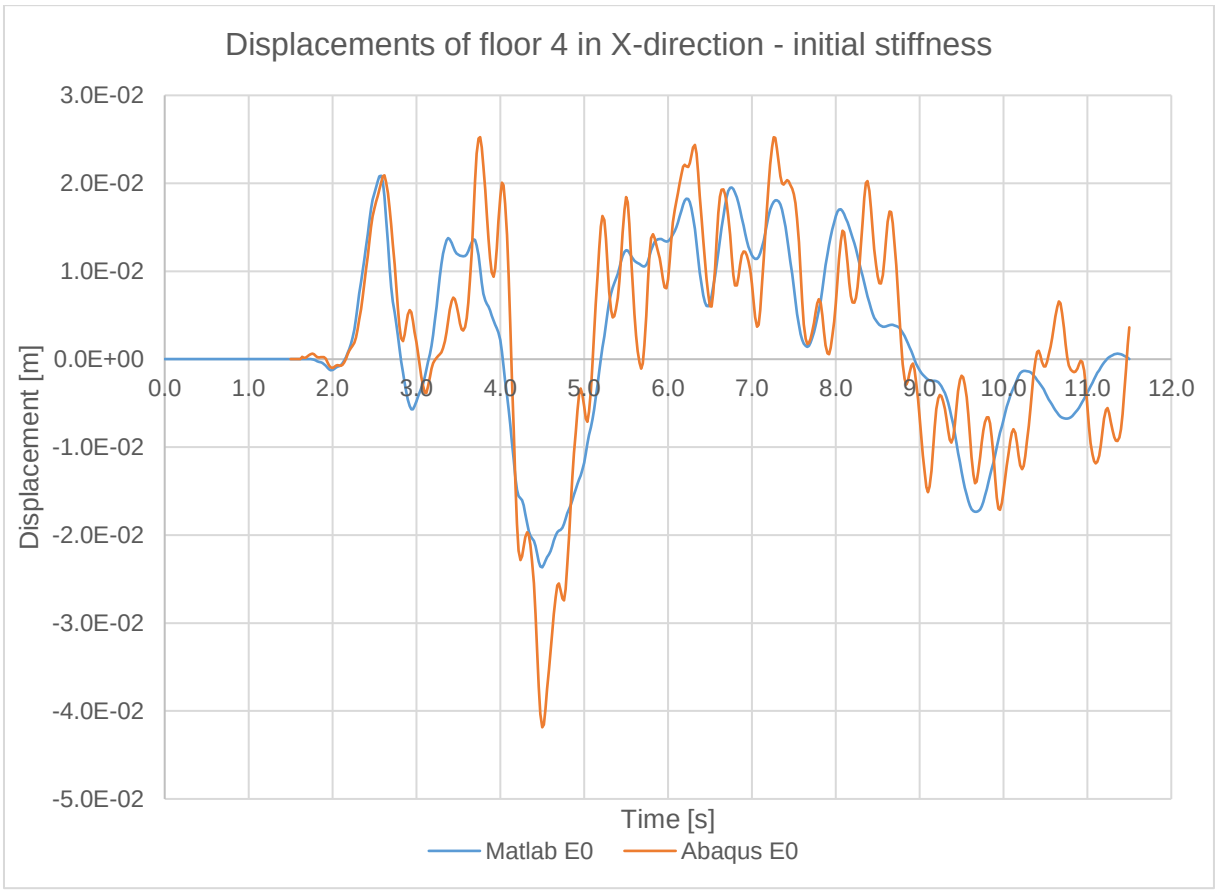

Figure 5.1: Displacements of the 4th floor in X-direction of 1D model (blue) and 3D model (orange) with initial stiffness.

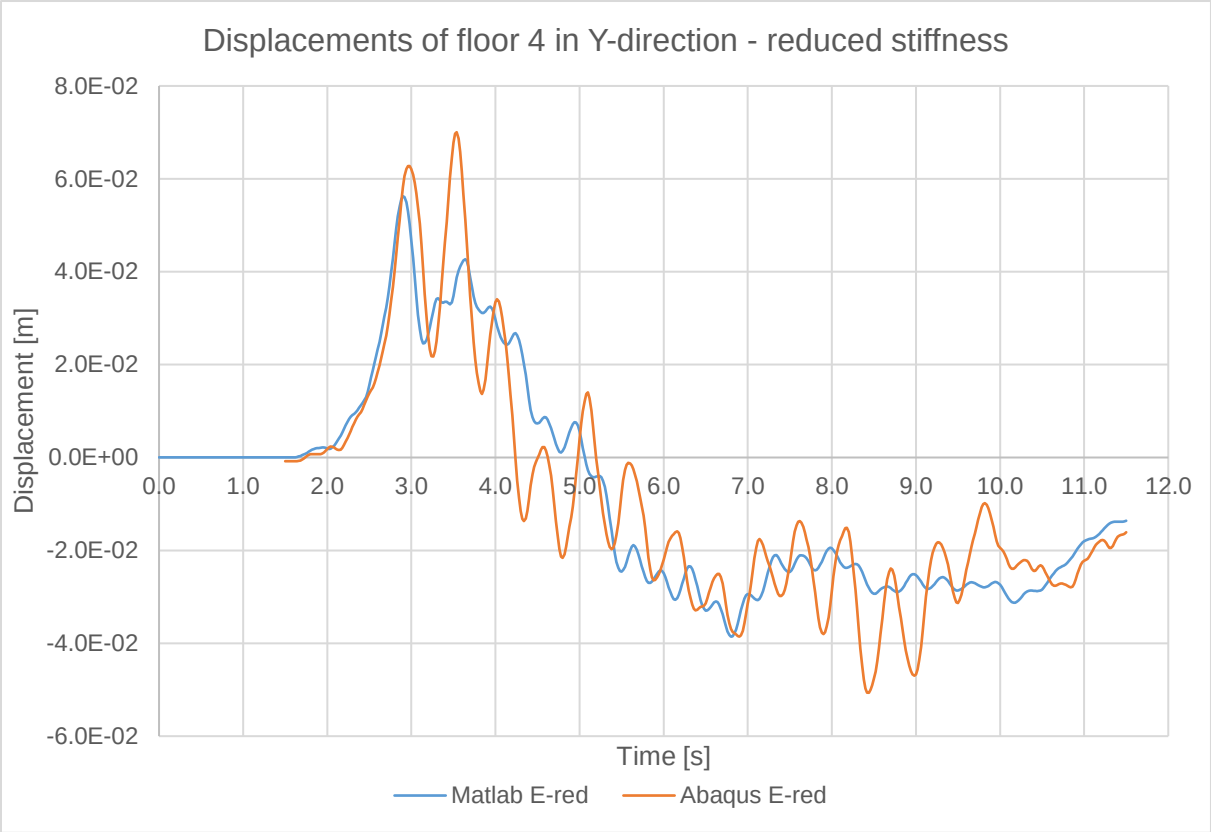

Figure 5.2: Displacements of 4th floor in Y-direction of 1D model (blue) and 3D model (orange) with reduced stiffness.

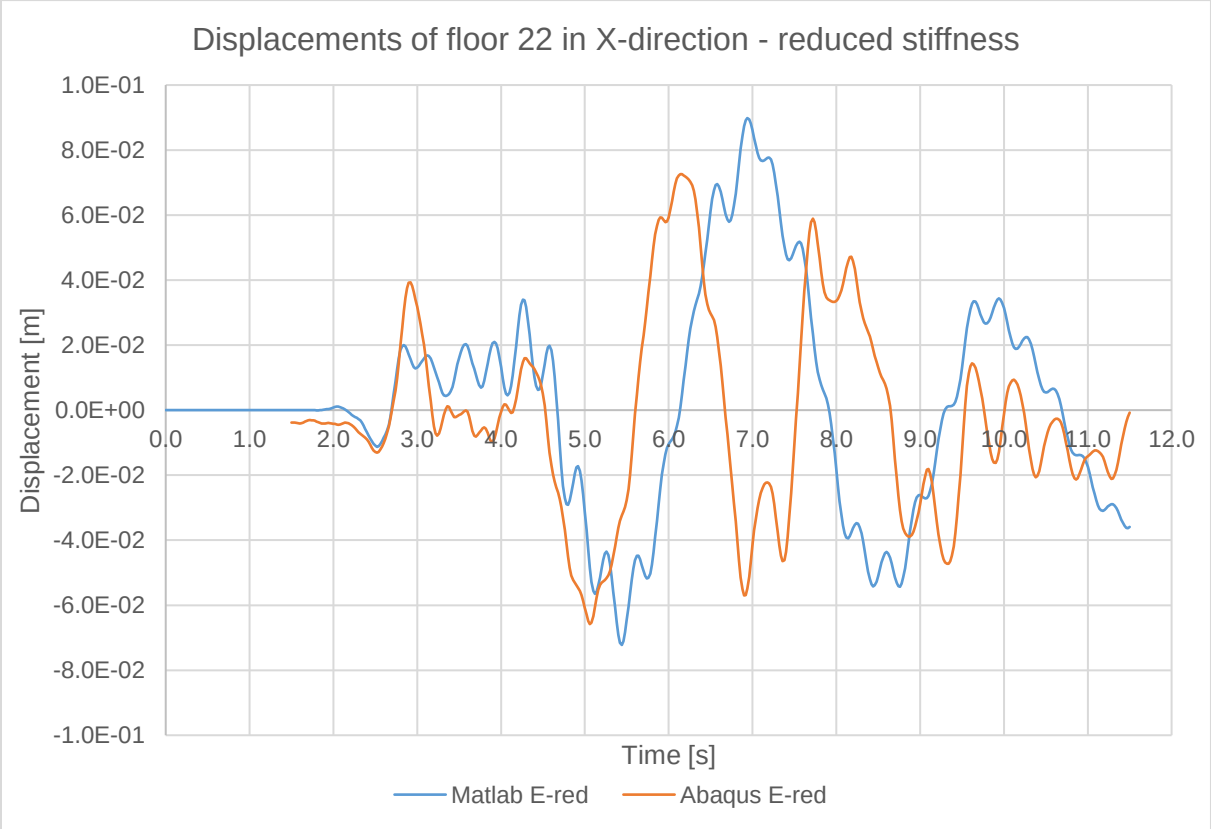

Figure 5.3: Displacements of 22nd floor in X-direction of 1D model (blue) and 3D model (orange) with reduced stiffness.

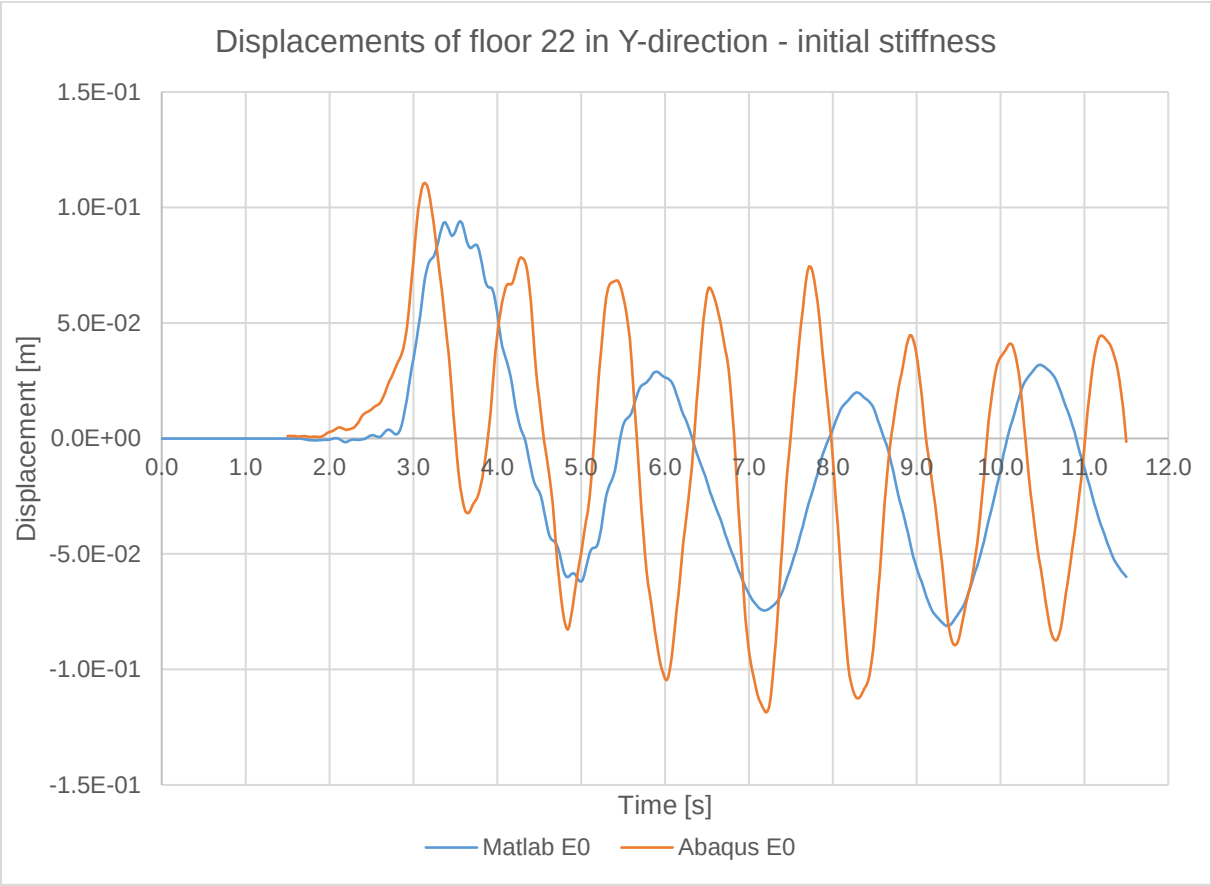

Figure 5.4: Displacements of 22nd floor in Y-direction of 1D model (blue) and 3D model (orange) with initial stiffness.

Even though the graphs show displacements in the same order of magnitude, the 3D model has a larger amount of peaks than the 1D model.

Despite the deviations between the 3D and 1D model, the similarities are sufficient for verification of the 3D model. Especially the trend of both displacements shows significant similarities.

5.2. Results of analyses

The results of the green marked analysis in Table 5-1 are further discussed and elaborated in this paragraph.

5.2.1. Analysis 2 – Excessive damage

In the second analysis, instability occurs due to excessive damage in the building. The analysis stops after 0.073 seconds due to excessive distortion error, since this analysis is performed without element deletion and critical elements are not deleted.

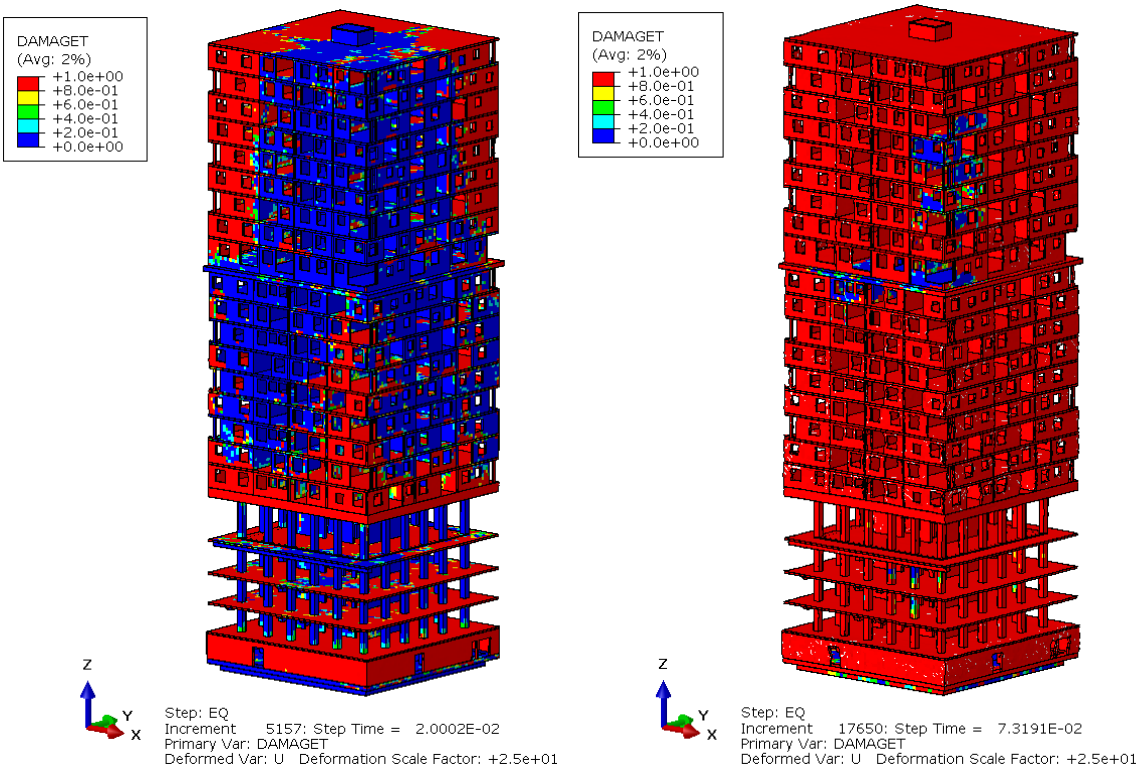

Figure 5.5: Tension damage (red) occurs over whole building within 0.02 seconds (left) and analysis stops after 0.073 seconds (right).

5.2.2. Analysis 4 – Second order accuracy

According to the manual of Abaqus, it is recommended to enable second order accuracy for analyses with a large number of revolutions (> 5). This second order accuracy is an element control option, which enables a second order accurate element formulation. This parameter improves the result of the analysis significantly. The analysis with second order accuracy still becomes unstable, but only after 1.5 seconds.

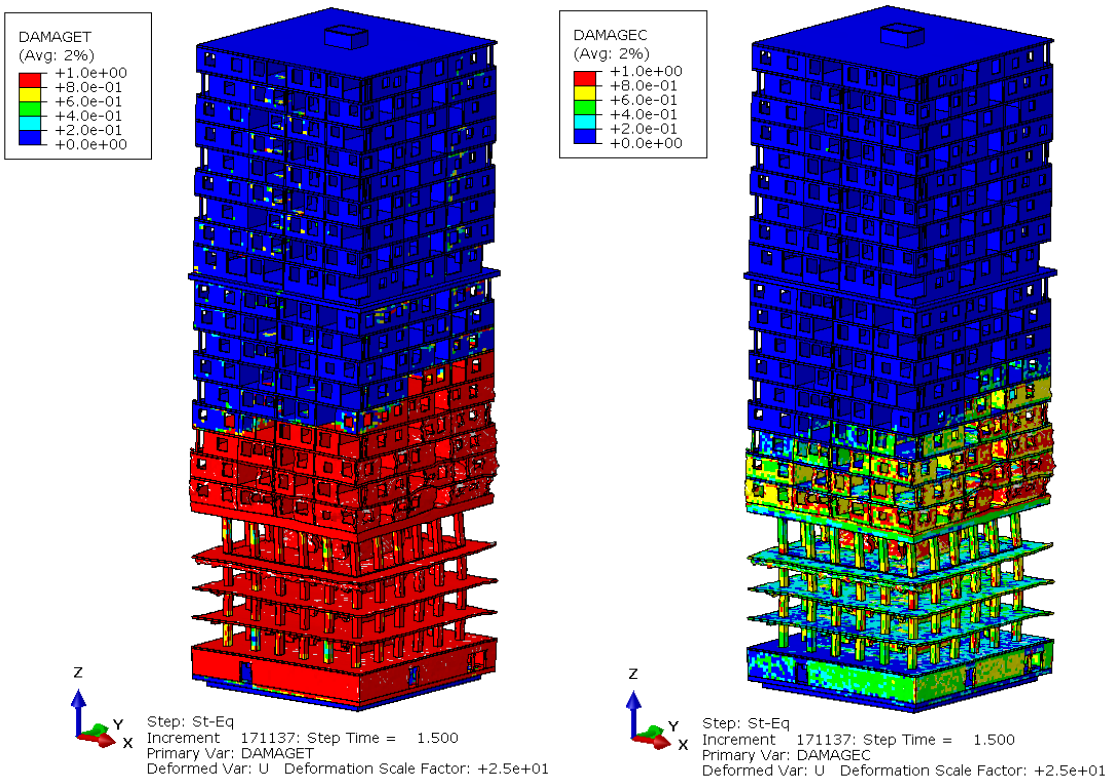

Figure 5.6: Tension (left) and compression (right) damage occurs at an extensive part of the building before the analysis stops after 1.5 seconds.

The results in Figure 5.6 show that the second order accuracy formulation improves the analysis. Still, a large amount of damage occurs.

5.2.3. Analysis 6 – Beta damping

A striking detail of the previous analyses is that the damage due to compression occurred at the same location as the damage due to tension, Figure 5.6. This indicates that the stiffness recovery of the material model does not perform correctly. Figure 5.7 shows the tensile stress-strain diagram with and without compression stiffness recovery ($w_c = 1$ and $w_c = 0$).

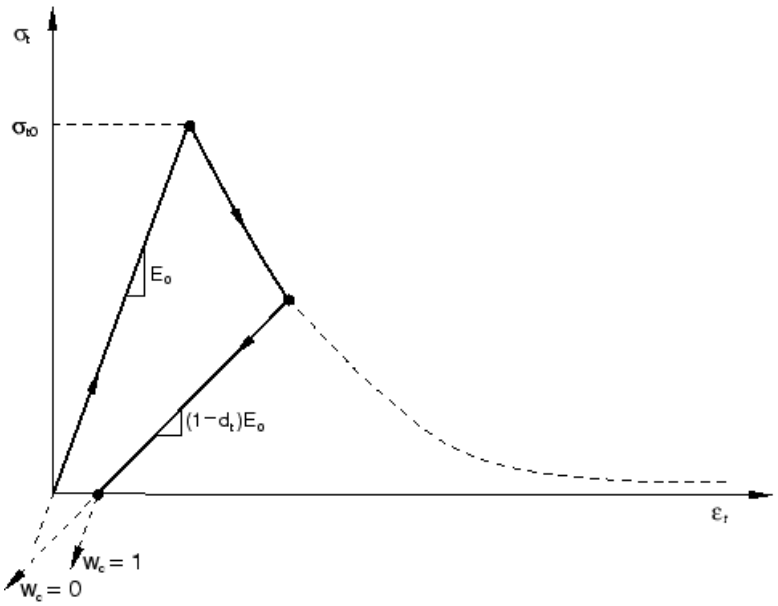

Figure 5.7: Tensile stress-strain diagram and stiffness recovery of CDP material model.

Since damage due to tension and compression occurred at the same locations in the previous analyses, the following analysis (analysis 5) is performed with the stiffness recovery set to 0 for both w_t and w_c. Although the stiffness degradation is too high with these settings, instability does not occur as in the previous analyses. Which is remarkable and implies that the instability of the previous analyses is related to the settings of the stiffness recovery. The switch from tension to compression, in combination with the stiffness recovery seems to cause instability and thus the excessive damage, as shown in Figure 5.5 and Figure 5.6.

The following analysis (analysis 6) is performed with a nonzero β-factor of the Rayleigh damping and the default settings for the stiffness recovery ($w_c = 1;\ w_t = 0$). However, the β-factor has a significant negative impact on the stable time of the explicit solver in Abaqus and therefore on the total analysis time. In order to decrease the analysis time, a fixed stable time or mass scaling can be used. With mass scaling, the mass of the critical element is increased in order to keep the stable time at a certain level. As long as the applied mass scaling is smaller than $5\% - 10\%$ of the total mass, the influence on the results of the analysis is minimal.

5.2.3.1. Analysis 6a: fixed stable time

The stable time in this analysis is fixed and can therefore not change due to damage. However, due to the fixed stable time peak accelerations or material nonlinearity could be missed by 'overstepping'. In order to check whether the results are physically correct a comparison between the kinetic and total energies is made. The total energy should be approximately constant, in relation to the kinetic energy, during the analysis; since the law of conservation of energy should be fulfilled. In Figure 5.8, it can be seen that the total energy (orange line) is not constant, and therefore, the results are not reliable.

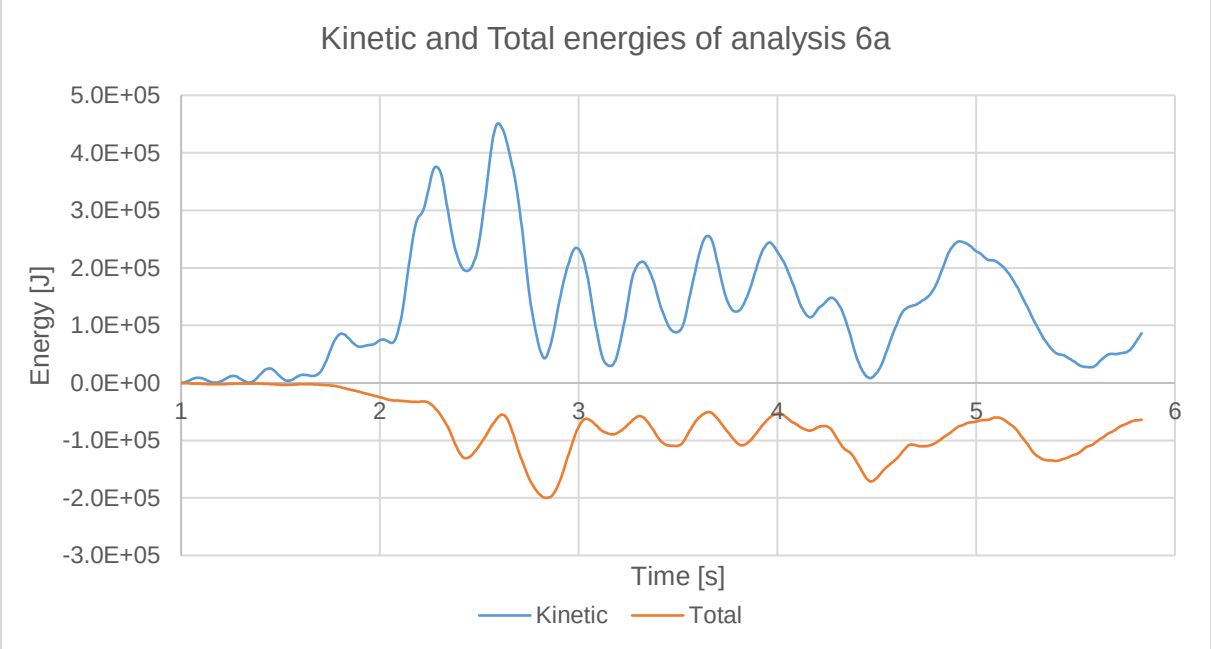

Figure 5.8: Comparison between total and kinetic energies of analysis 6a with a fixed stable time.

5.2.3.2. Analysis 6b: Mass scaling

In this analysis, the option “mass scaling” is applied which basically means that the mass of the critical element is increased, in order to keep the stable time at a certain level, because the stable time of the critical element determines the stable time of the whole analysis.
In the graph below, the energies of this analysis are shown and the graph shows that the mass scaling increases the kinetic energy substantially.

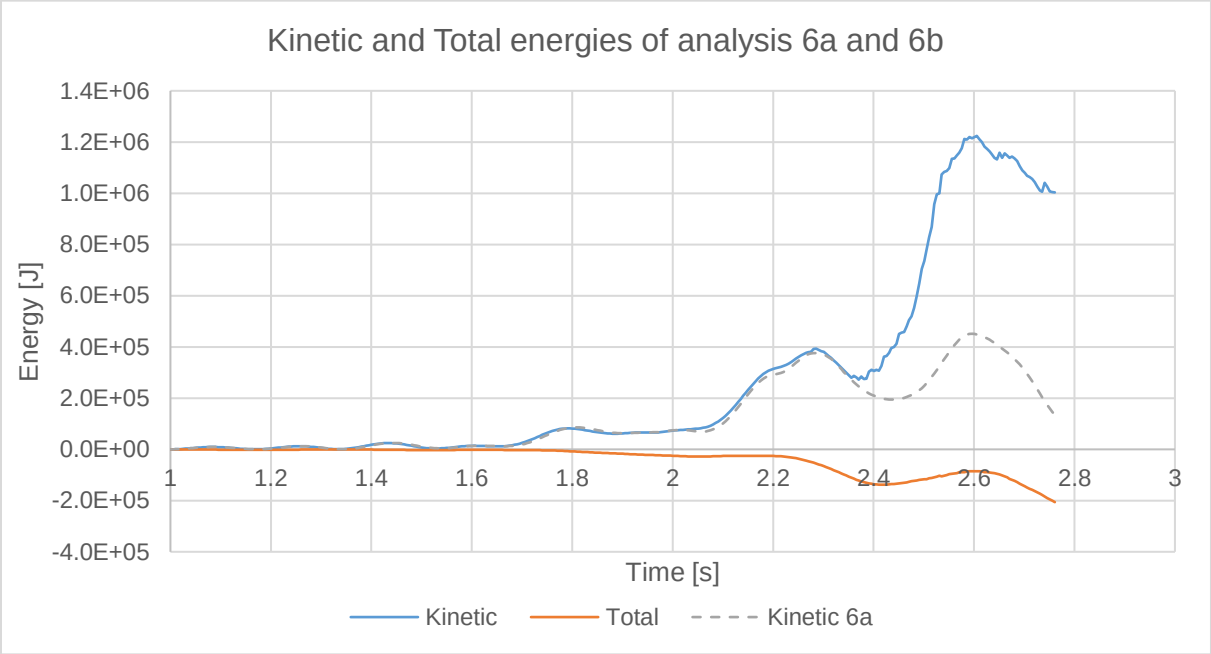

Figure 5.9: Comparison between the total and kinetic energies of analysis 6a and 6b with mass scaling.

Also the amount of mass scaling is too high, approximately $250\,\%$ of the total mass of the model. In Figure 5.10, the mass scaling factor per element is shown. The mass of the purple elements is increased with more than $10\,\%$.

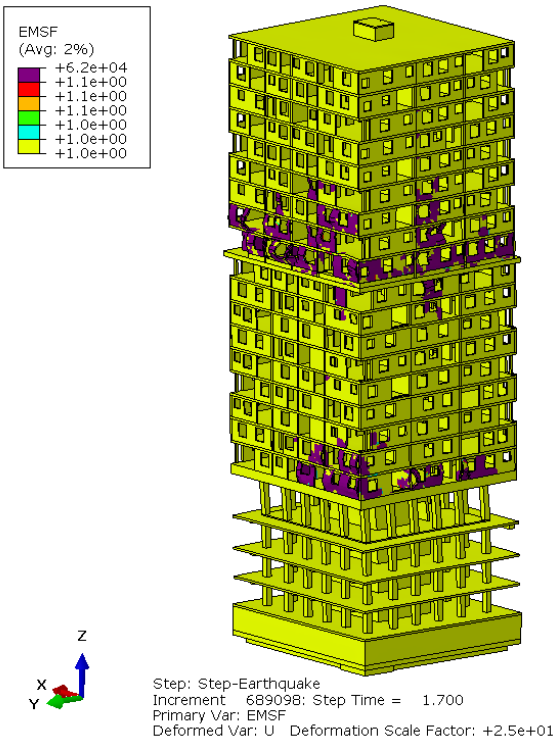

Figure 5.10: Mass scaling factor for the elements of analysis 6b.

Although the results of the sixth analysis are physically incorrect, they clearly show that a non-zero β factor of the Rayleigh damping results in a more stable analysis. According to the theory of Rayleigh damping, the β factor mainly corresponds to the damping of the higher modes/frequencies of the system. In other words, if the β factor is zero, the higher modes will be assigned a small amount of damping.

In conclusion, the beta factor of the Rayleigh damping is a crucial parameter for dynamic explicit analyses in combination with the concrete damaged plasticity material model. However, the beta factor increases the total analysis time significantly. A solution for this problem is to use mass scaling. Yet, for this model, the amount of mass scaling is too high and in case of a fixed stable time, the peak accelerations can be 'missed' by overstepping, which makes the results in both cases unreliable and physically incorrect.

5.2.4. Analysis 8-10 and 12 – Refined mesh

In order to reduce the amount of mass scaling and improve the stable time, some small parts of the model are removed and the mesh of the model is improved. These small parts appeared to have a large negative influence on the stable time. This is because the stable time also depends on the dimension of the elements. However, with the solid elements (reduced integration) in this model, at least two elements should be used over the thickness of a part. Hence, thin parts, as walls with a small thickness, significantly decrease the stable time.
The mesh is improved by reducing the mesh size which results in more cube-like elements; the length to width ratio of the elements is improved to a maximum of 1 to 3.

The analysis with the refined mesh shows a significant improvement of the stable time compared to the previous analyses; the applied mass scaling is less than 1 %. This seems

contradictory, since the size of the elements decreases and so the stable time decreases as well. However, the cube-like elements result in more stability during the analysis, which prevents a large reduction of the stable time due to damage occurring during the analysis. So, with a finer mesh, the initial stable time is smaller but less sensitive for damage. Therefore, the ratio of the dimensions of the elements is an important factor for explicit dynamic analyses with a large amount of elements.

5.2.5. Analysis 14 – Hourglassing control

The applied elements in the model are first order 'reduced integration' elements, which means that each element has only one integration point. The advantage of these elements is that they are cheap and effective and they minimize the computational costs of element calculations.
However, the reduced integration scheme has a disadvantage: it can result in mesh instability, commonly referred to as 'hourglassing'. According to the Abaqus lecture about elements, "the hourglass mode does not cause any strain and does not contribute to the energy integral. Its behaviour is similar to that of a rigid body mode" (Simulia Abaqus, 2005).
One of the main causes of hourglassing is bending of a part with a small amount of elements in the bending direction; for example in case of bending of a beam with only two elements over the height of the beam.
This problem can be solved by applying more elements, at least four, over the height of the beam. However, this will reduce the mesh size and thus the stable time of the critical element.
Another solution is applying hourglassing control, what basically consists of adding (artificial) stiffness or (artificial) viscosity to the elements.
Multiple methods are available for applying hourglassing control in Abaqus. The Abaqus manual states that enhanced hourglassing control gives sufficient accurate results for a relative course mesh. However, the enhanced hourglassing control might give too stiff results if plasticity occurs. The enhanced hourglassing control is based on the pure stiffness method, in which the stiffness coefficients are based on the enhanced assumed strain method. These coefficients are based on the initial stiffness of the material and remain therefore the same during the analysis, even if the stiffness is degraded due to damage in the material model.
A different method of hourglassing control in Abaqus, is the combined hourglassing control which is a linear combination of stiffness and viscous hourglassing control.

The previous analyses in the process are performed with the enhanced hourglassing control. However, since this hourglassing control might give too stiff results, the combined control is applied in the model for comparison.
First, a comparison between the enhanced and combined hourglassing control is made with a small model of a beam on two supports. Next, the 3D model of the building is analysed with the combined hourglassing control.

5.2.5.1. Small scale test

With a small model of a beam on two supports, a comparison between the enhanced hourglassing control and the combined hourglassing control is made. A point load is applied in the middle of the beam. The beam is modelled as a simply supported beam.

Table 5-2 shows the parameters which are applied as input for the test.

Table 5-2: Overview of input for small model test of simply supported beams.

Parameter	**Value**
Length	5 m[1]
Width x height	0.6x0.6 m[1]
Volume	$5 * 0.6 * 0.6 = 1.8$ m^3
Section modulus	$\frac{1}{6} * 0.6 * 0.6^2 = 0.036$ m^3
Moment of Inertia	$5 * 0.6 * 0.6 = 1.8$ m^3
Concrete class	$C20/25$
E-modulus	2996195.05 kN/m^2
Self-weight	$\frac{1.8}{5} * 2400 * \frac{9.81}{1000} = 8.4758$ kN/m
Point load (F)	24.525 kN
Moment	$\frac{1}{8} * 8.4758 * 5^2 + \frac{1}{4} * 24.525 * 5 = 57.146325$ kNm
Stress	$\frac{57.14325}{0.036} = \frac{1587.3}{1000} = 1.587$ N/mm^2
Deflection	$\frac{5}{384} * \frac{q*l^4}{EI} + \frac{1}{48} * \frac{F*l^3}{EI} = 0.4105$ mm

The hand calculations of the stress and deflection, shown in Table 5-2, are elastic calculations and do not account for plasticity.
In the figure below, the model of the beam on two supports is shown. The point load is applied through a non-structural mass (green squares) in the middle of the beam in order to prevent local distortion of elements.

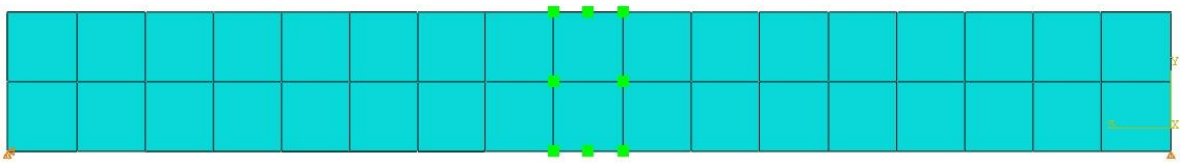

Figure 5.11: Model of beam on two supports

As shown in Table 4-3, the maximum tensile strength of C20/25 is approximately 0.85 N/mm^2. According to the hand calculation, the resulting stress is equal to 1.587 N/mm^2, which is larger than the tensile strength of the concrete. Therefore, tension damage is expected once the gravity is applied.
In the figures below, the results of the test with the combined and the enhanced hourglassing control are shown.

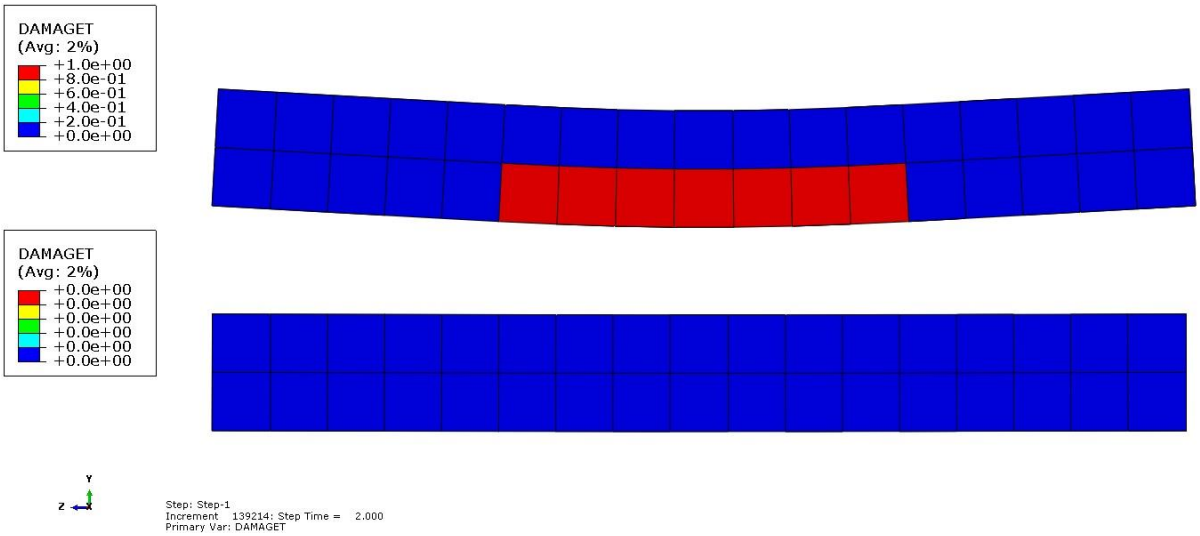

Figure 5.12: Tension damage with combined (top) and enhanced (bottom) hourglassing control.

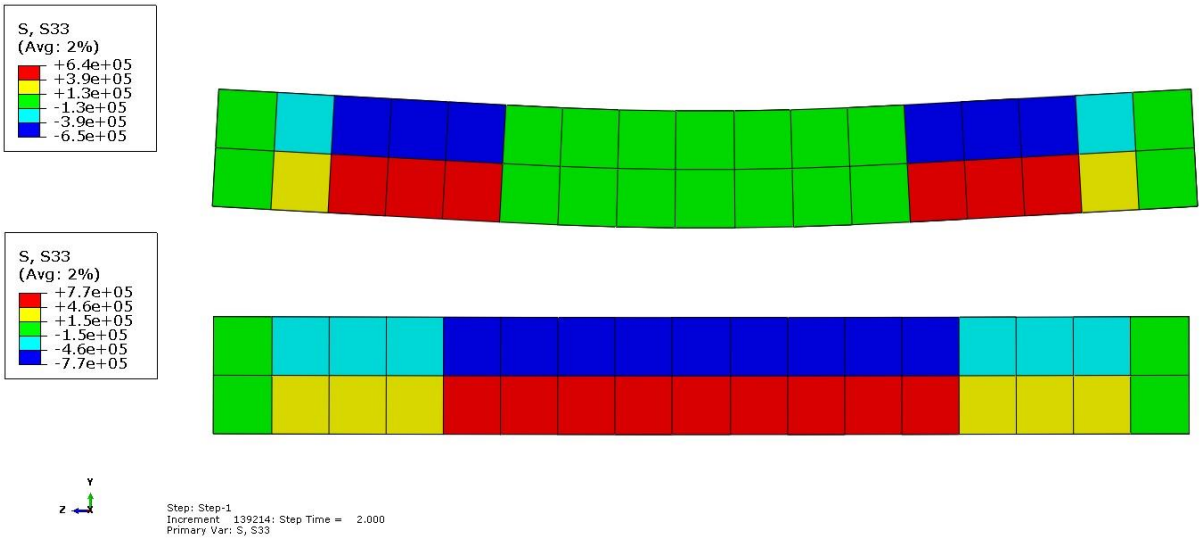

Figure 5.13: Stresses in Z-direction (longitudinal) with combined (top) and enhanced (bottom) hourglassing control.

The figures clearly show a significant difference between the two hourglassing control mechanisms. Damage, due to tension, occurs in the beam with the combined hourglassing control, but not in the beam with the enhanced hourglassing control. Figure 5.13 shows a decrease of stress in the damaged elements of the beam with combined hourglassing, while the stress is higher in the beam with enhanced hourglassing control. This is also shown in the graph below, which shows the stress-strain diagrams of the bottom elements in the middle of the beam.

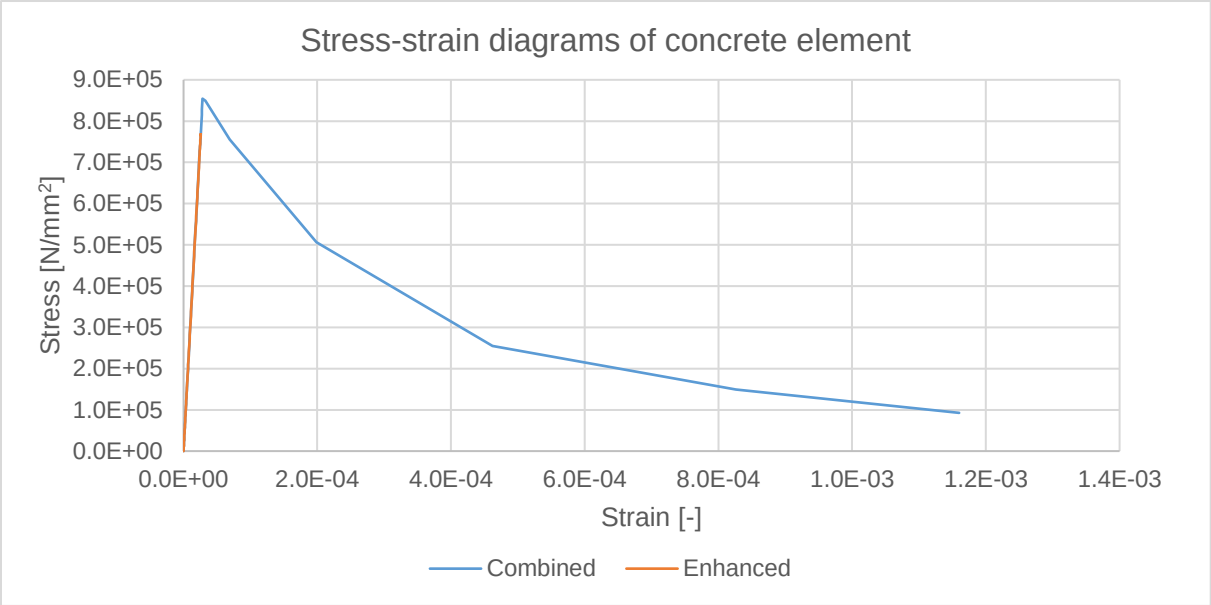

Figure 5.14: Stress-strain diagram of bottom elements of the beams

5.2.5.2. Model La Liberté

The test with the small model showed that the enhanced hourglassing control gives too stiff results for bending if plasticity occurs. The following analysis of the model of La Liberté is performed with the combined hourglassing control. The following graphs show a comparison between the two hourglassing mechanisms for the model of the building.

The graphs below show the displacement of the ground floor and the 22nd floor; the displacements of the ground floor of the enhanced and combined analysis are approximately equal.

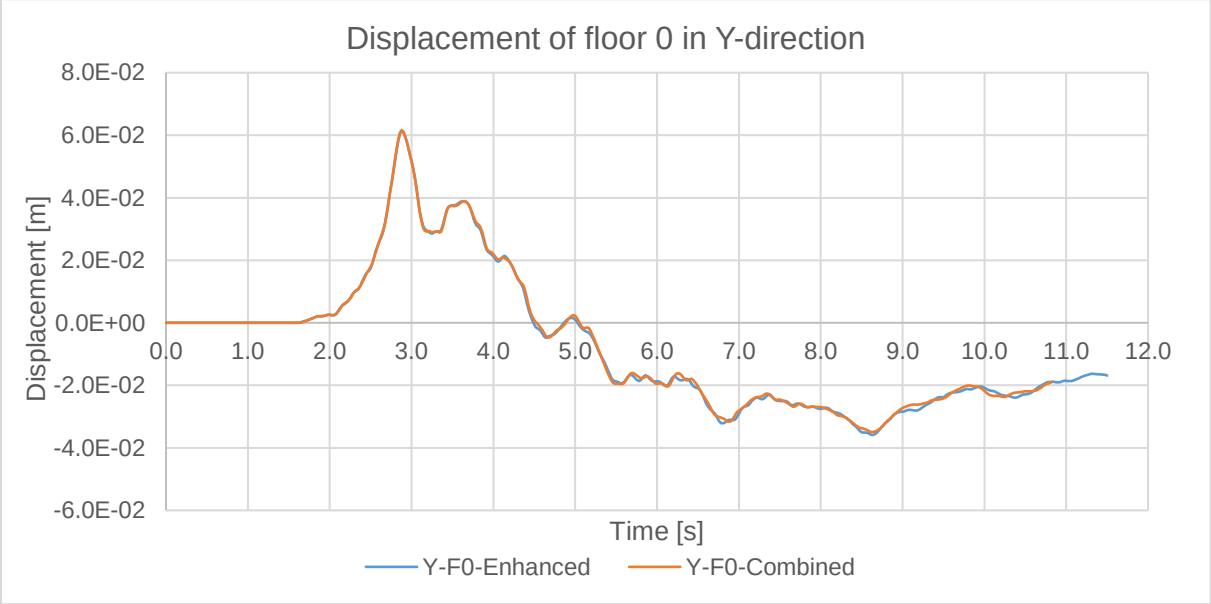

Figure 5.15: Displacement of the ground floor in Y-direction with enhanced (blue) and combined (orange) hourglassing control.

The following graph shows more deviation between the displacements of the enhanced and combined analyses. In the first 1.5 seconds, the gravity loading is applied and after that, the earthquake signal is applied. In the first 3 seconds of the total analysis, till the top of the peak, the displacements are approximately equal. Due to the peak acceleration in the earthquake signal, plasticity occurs. From the moment that plasticity occurs, the displacements of both hourglassing mechanisms differ.

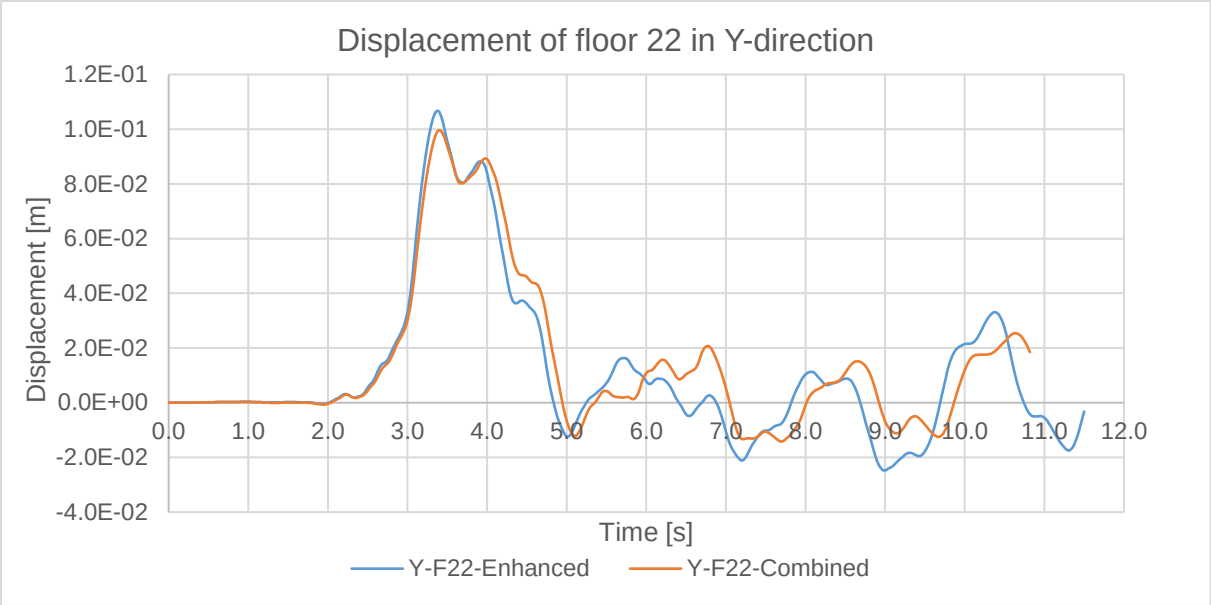

Figure 5.16: Displacement of the 22nd floor in Y-direction with enhanced (blue) and combined (orange) hourglassing control.

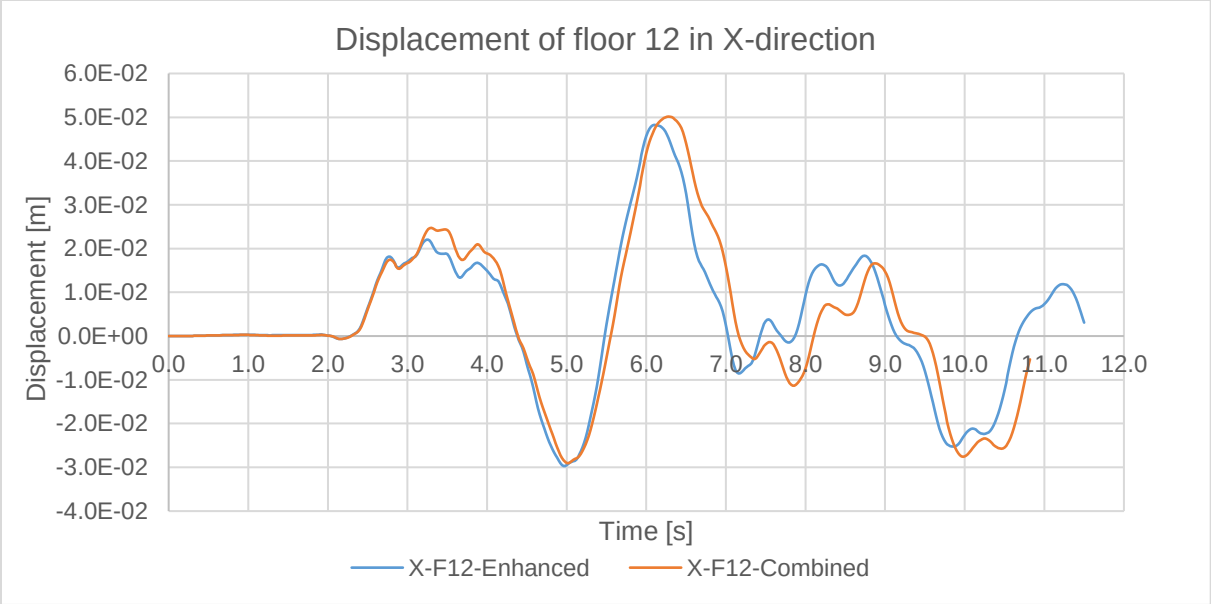

Figure 5.17: Displacement of the 12th floor in X-direction with enhanced (blue) and combined (orange) hourglassing control.

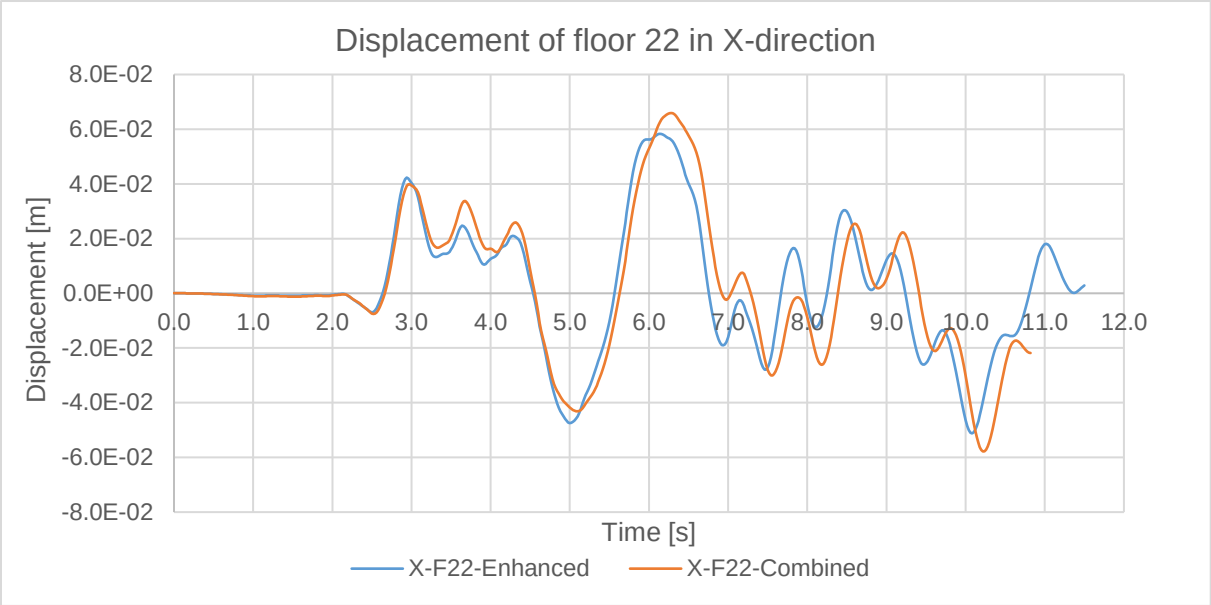

Figure 5.18: Displacement of the 22nd floor in X-direction with enhanced (blue) and combined (orange) hourglassing control.

The graphs in Figure 5.16 till Figure 5.18 indicate that the model with the combined hourglassing control responds a bit later or slower on the accelerations of the earthquake than the enhanced model.

The following graphs show a comparison of the shear forces of the analyses with the two different hourglassing mechanisms. The first two graphs show the base shear, the shear forces at the top of the piles, in X and Y direction. The next graphs show the maximum shear forces occurring at the first four floors in X and Y direction. These maxima occur at different times during the analysis.

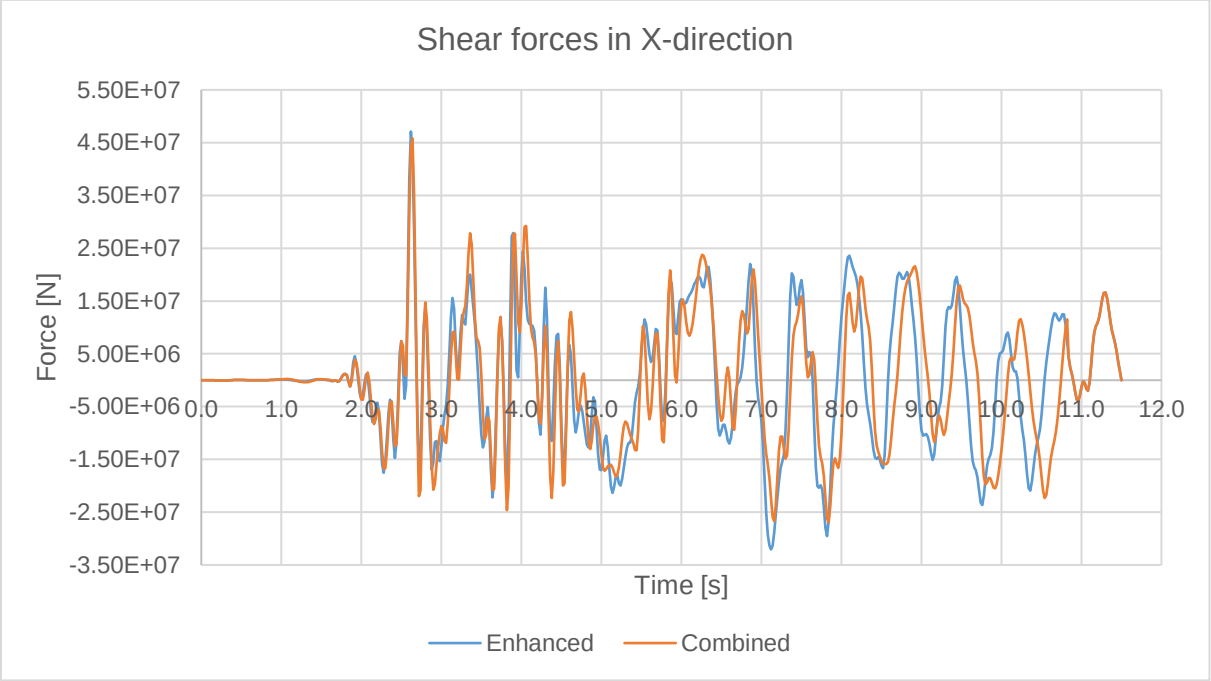

Figure 5.19: Plot of the shear forces in the piles in X-direction with enhanced (blue) and combined (orange) hourglassing control.

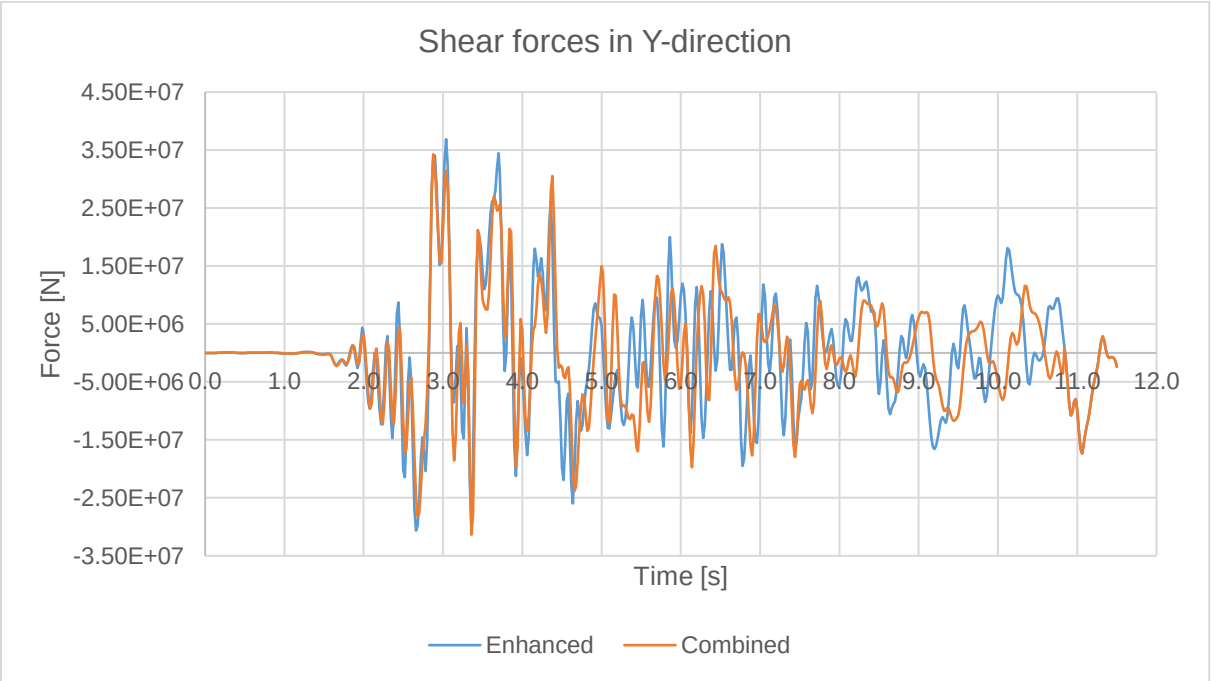

Figure 5.20: Plot of the shear forces in the piles in Y-direction with enhanced (blue) and combined (orange) hourglassing control.

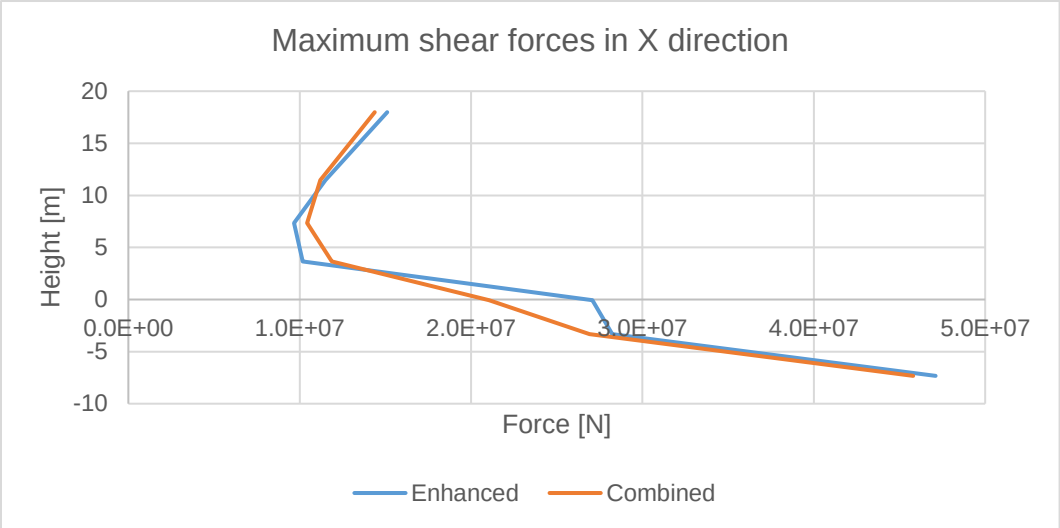

Figure 5.21: Maximum shear forces over the height of the first four floors of the building in X-direction with enhanced (blue) and combined (orange) hourglassing control.

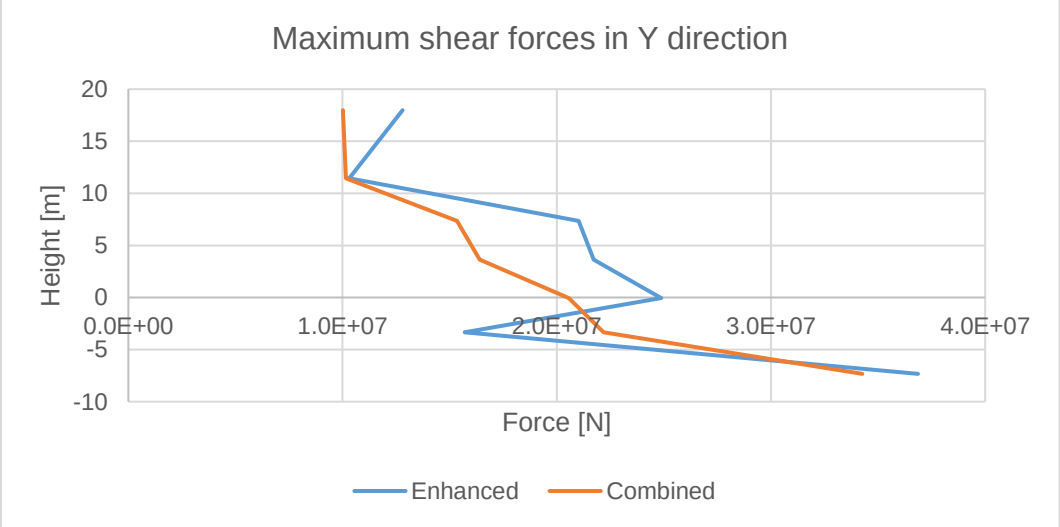

Figure 5.22: Maximum shear forces over the height of the first four floors of the building in Y-direction with enhanced (blue) and combined (orange) hourglassing control.

The graphs in Figure 5.19 and Figure 5.20 show that the shear forces of the combined hourglassing analysis are not significant different compared to the enhanced hourglassing control. The shear forces of the combined analysis are a bit smaller, especially the forces in Y-direction and the graph of the combined analysis (Figure 5.20) has less peaks and has a different frequency than the enhanced analysis.

Table 5-3: Comparison of base shear forces of enhanced and combined analysis.

Direction	Maximum base shear force [kN]	
	Enhanced	Combined
X	47105.8	45797.7
Y	36864.8	34264.1

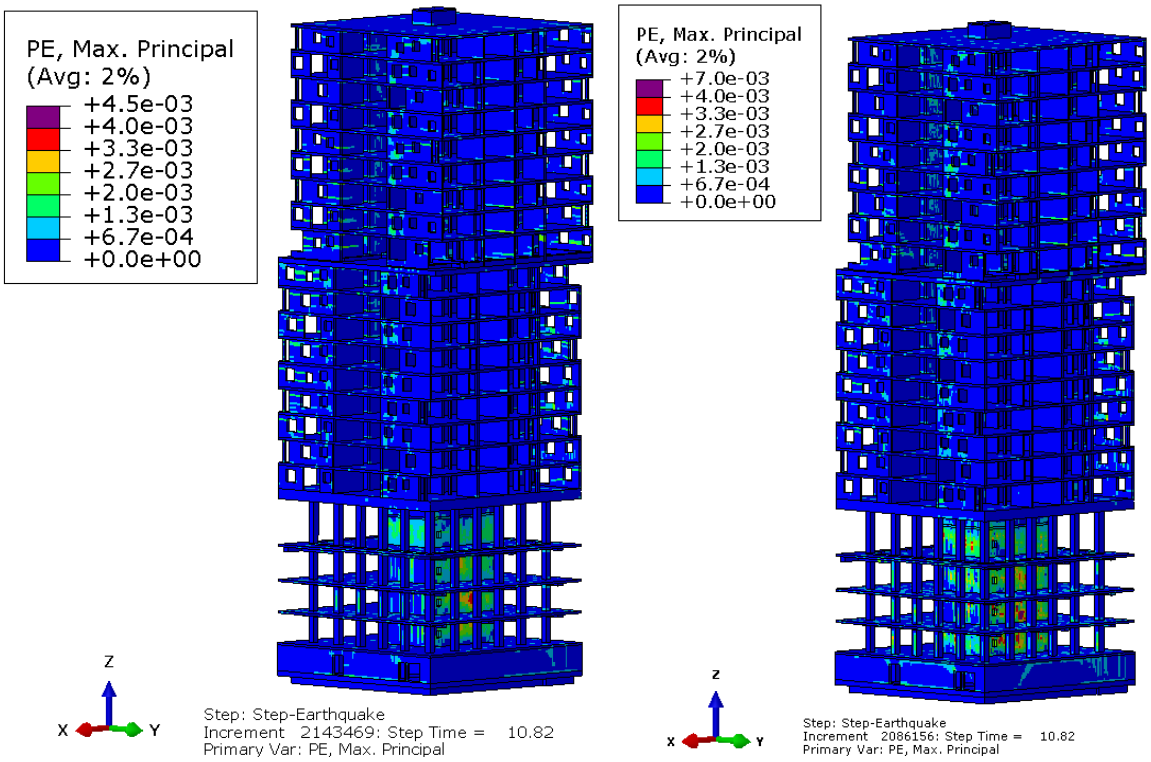

Figure 5.23: Maximal plastic strain with enhanced (left) and combined (right) hourglassing control.

Figure 5.23 shows the plastic strain almost at the end of both analyses ($t = 9.32$ s). The maximum plastic strain in the combined analysis is significant larger than the maximum plastic strain in the enhanced analysis. Especially in the core at the first three floors, a large amount of plasticity occurs.

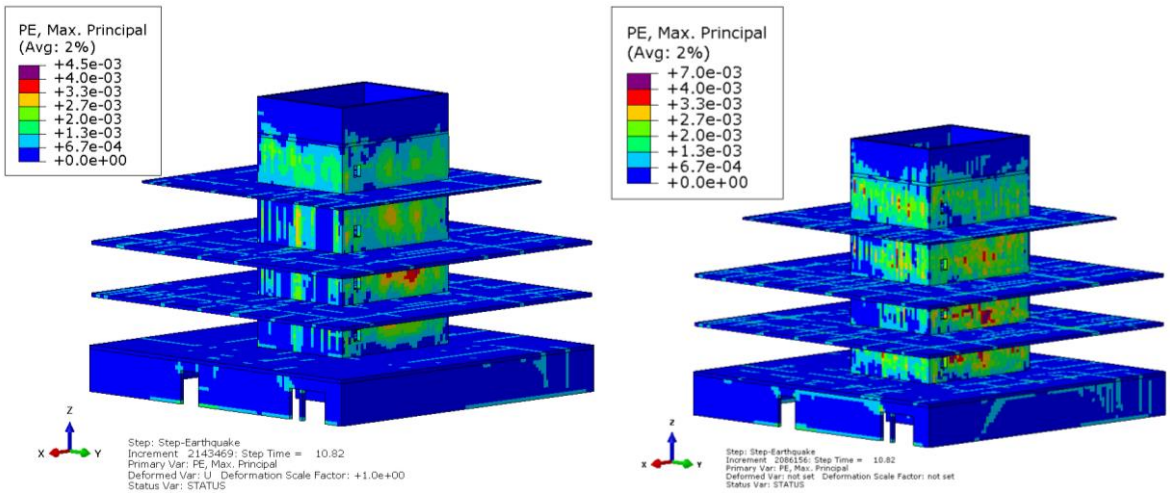

Figure 5.24: Maximal plastic strain in the core of floor 0 till 3 with enhanced (left) and combined (right) hourglassing control.

The following figures show the plasticity in the reinforcement steel of the core walls. They show that the amount of plasticity is relative small, compared to the plasticity in the concrete. Although, the combined analysis shows a larger maximum plasticity than the enhanced analysis.

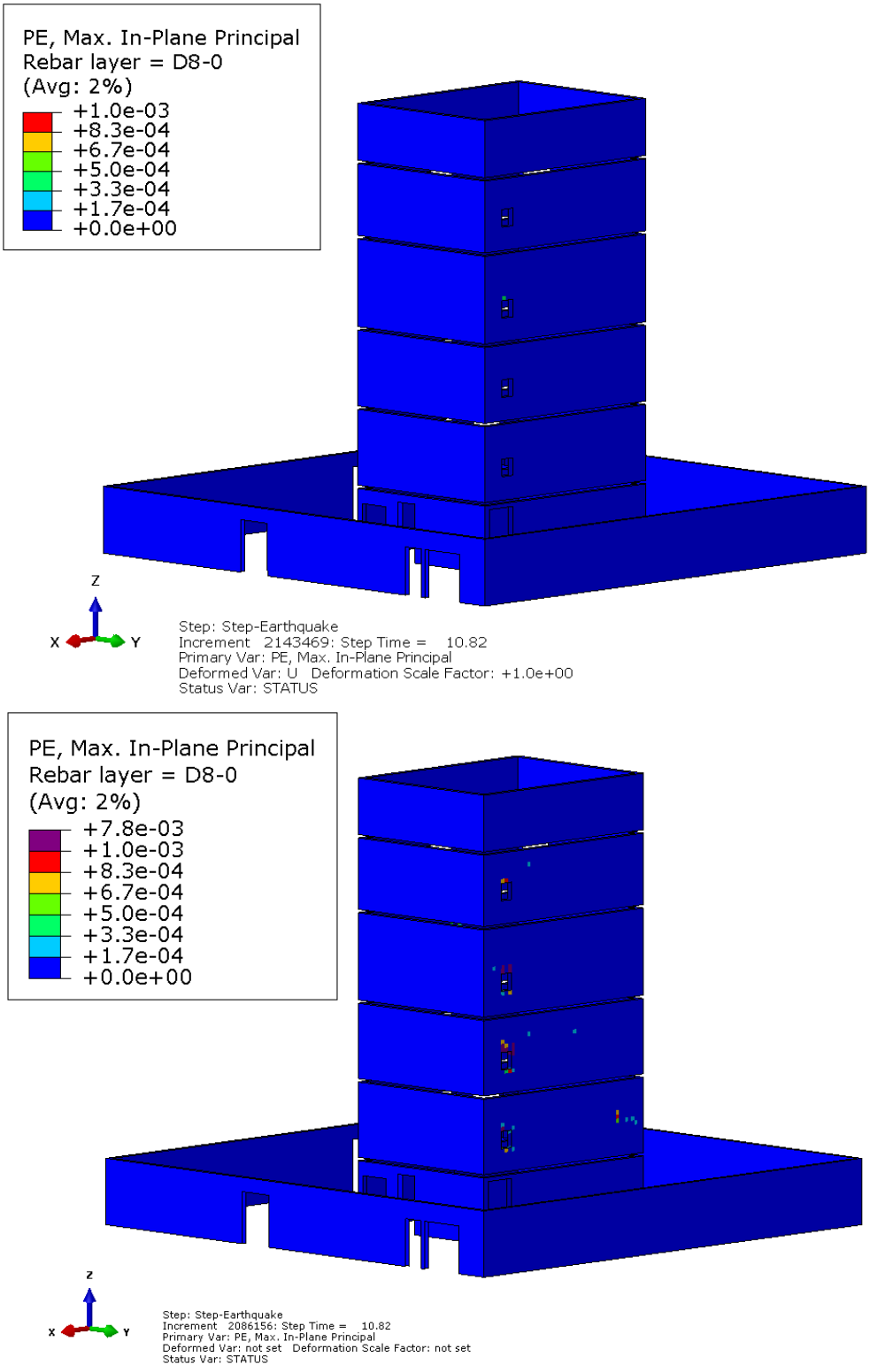

Figure 5.25: Maximum plastic strain in the reinforcement of the core with enhanced (top) and combined (bottom) hourglassing control.

5.2.5.3. Conclusion hourglassing control

The results of the small test with the simply supported beam and the analysis of the model of La Liberté, show that the enhanced hourglassing control results in a more stiff response than the combined hourglassing control, especially when plasticity occurs.
Based on the fact that the displacements and forces are in the same order of magnitude, the combined hourglassing control is recommended for analyses for which plasticity is expected.

5.3. Summary chapter 5

This chapter discussed the verification and sensitivities of the 3D model, as developed in Abaqus; the sensitivities were determined through multiple analyses with varying parameters. First, the analyses with elastic material properties were performed for the verification of the 3D model with the results of the 1D model analyses of Matlab. This verification showed that the Abaqus model has more peaks of displacements, yet it showed that the displacements are in the same order of magnitude and follow the same trend.
Next, several analyses of the process were discussed; these analyses showed the influence and impact of several parameters of Abaqus, so-called sensitivities. Through this process, a reliable and efficient calculation model was developed together with a thorough understanding of the dynamic behaviour of the building.
The sensitivities determined through the process of analyses are briefly addressed below.

First of all, the second order accuracy parameter, which is a mesh control option, enables a more accurate element formulation and results in more stability during the analysis.

A parameter with significant impact on the analysis is the β factor of the Rayleigh damping. In Abaqus, damping is implemented by material damping according to the theory of Rayleigh. The drawback of this type of damping in combination with the applied analysis type (explicit) is that the β factor increases the analysis time significantly. However, the results showed that a non-zero β factor is required for a dynamic analysis in combination with the concrete damaged plasticity material model.

Also, the ratio of the dimensions of the elements is an important factor for the stability of the analysis. Through a mesh refinement, smaller and more cube-like elements are applied. Although the initial stable time decreased due to smaller elements, more cube-like elements improved the stability of the stable time during the analysis, since they were less sensitive for plasticity and damage and so excessive decrease of the stable time did not occur.

The applied elements contain only one integration point which makes them sensitive for mesh instability or hourglassing. In order to prevent hourglassing modes, several control mechanisms are available in Abaqus. However, the choice of the mechanism has a significant influence on the stiffness and behaviour of the model. As initial mechanism, the enhanced control was applied; this mechanism adds artificial stiffness to the elements in order to prevent or resist hourglassing modes which do not contribute to the energy balance. However, since the enhanced mechanism is based only on the initial stiffness, the amount of artificial stiffness added remains the same throughout the analysis; even if plasticity occurs. And so, this mechanism results in overly stiff results in plastic analyses, especially in case of bending. Another mechanism of hourglassing control in Abaqus, is the combined hourglassing control which is a linear combination of stiffness and viscous hourglassing control. This method is less dependent on the (initial) stiffness of the element and gives less stiff results in case of plasticity. Therefore, the combined mechanism is recommended for (highly) plastic analyses.

The following chapter discusses the analysis of the seismic behaviour of the building. Since the 3D model is improved and optimised during the process of multiple analyses, the model of analysis 14 is used for the analysis of the seismic behaviour of the building in the following chapter; see also Table 5-1.

6. Analysis of seismic behaviour

In the previous chapters the Abaqus model and the process of analyses are discussed and elaborated. In this chapter, the analysis of the seismic behaviour of the structure is presented. First a comparison with a 'modal response spectrum analysis' calculation of the base shear force is presented. Next, the results of the analyses of the 3D model are shown as the displacements, drifts, plasticity and damage occurring during the earthquake.

6.1. Modal response spectrum analysis

The base shear force, which is the shear force at the foundation of the building, can be determined by a method called the 'modal response spectrum analysis' (MRS analysis); in this analysis the force corresponding to each mode separately is calculated and then, the total force can be calculated with the *'Complete Quadratic Combination'* (CQC) method or the *'Square Root of the Sum of the Squares'* (SRSS) method. For these calculations the results of the frequency analysis of the model are used for determining the frequencies of the building and the activated mass in each frequency. The response of each mode shape which contributes significantly to the global response of the building should be taken into account. This condition is met if the sum of the activated mass of the considered modes is at least 90% of the total mass; or if all modes with an effective activated mass more than 5% of the total mass are considered (Nederlands Normalisatie-Instituut, 2015).

The response per mode (F_i) is calculated by multiplying the activated mass, in that specific mode, with the value of the response spectrum, corresponding to the frequency of that specific mode:

$F_i = m_i * Se(T_i)$

The calculation of the CQC method is performed with the following formula (Wilson, 1981):

$$F_b = \sqrt{\sum_{i=1}^{n}\sum_{j=1}^{n} F_i \alpha_{ij} F_j}\,; \quad \alpha_{ij} = \frac{8\xi^2(1+\beta)\beta^{\frac{3}{2}}}{(1-\beta^2)^2 + 4\xi^2\beta(1+\beta)^2}$$

In which:

- F_b is the maximum response from all modes;
- F_i is the maximum response in the i^{th} mode;
- F_j is the maximum response in the j^{th} mode;
- α_{ij} is the correlation coefficient;
- ξ is the damping ratio in the modes
- β is the ratio between the frequencies i and j (≥ 1)

The calculation of the SRSS method is performed with the following formula:

$$F_b = \sqrt{\sum_{i=1}^{n} F_i^2}$$

The first 13 mode shapes of the model are used for the MRS analysis and displayed in the table below.

Table 6-1: Overview of the results of the frequency analysis of the 3D model.

MODE NO	EIGENVALUE	FREQUENCY		Total activated mass [%]	
		(RAD/TIME)	(CYCLES/TIME)	X-COMPONENT	Y-COMPONENT
1	23.986	4.8976	0.77947	10.5%	58.4%
2	25.022	5.0022	0.79613	67.8%	68.5%
3	39.327	6.2712	0.99809	68.9%	68.7%
4	271.53	16.478	2.6226	73.3%	69.2%
5	362.95	19.051	3.0321	73.5%	85.9%
6	418.84	20.466	3.2572	85.6%	85.9%
7	974.02	31.209	4.9671	85.8%	86.0%
8	1244.6	35.28	5.6149	85.8%	86.0%
9	1847.1	42.978	6.8401	87.4%	86.0%
10	1927	43.898	6.9865	87.4%	87.5%
11	3074.9	55.451	8.8254	87.4%	87.5%
12	4384.2	66.213	10.538	87.8%	87.5%
13	4648.4	68.179	10.851	87.9%	87.9%

Up to the thirteenth mode shape 87.9% of the total mass is activated for both directions and all modes with an effective activated mass more than 5% are taken into account.

The results of the MRS analysis are shown in the table below.

Table 6-2: Base shear forces according to the CQC and SRSS-method.

Direction	CQC [kN]	SRSS [kN]
X	21799.8	20524.8
Y	23922.7	22997.4

6.2. NLTH Analysis shear forces

The base shear forces are also calculated by the analysis of the 3D model in Abaqus; these forces are shown in the graph below.

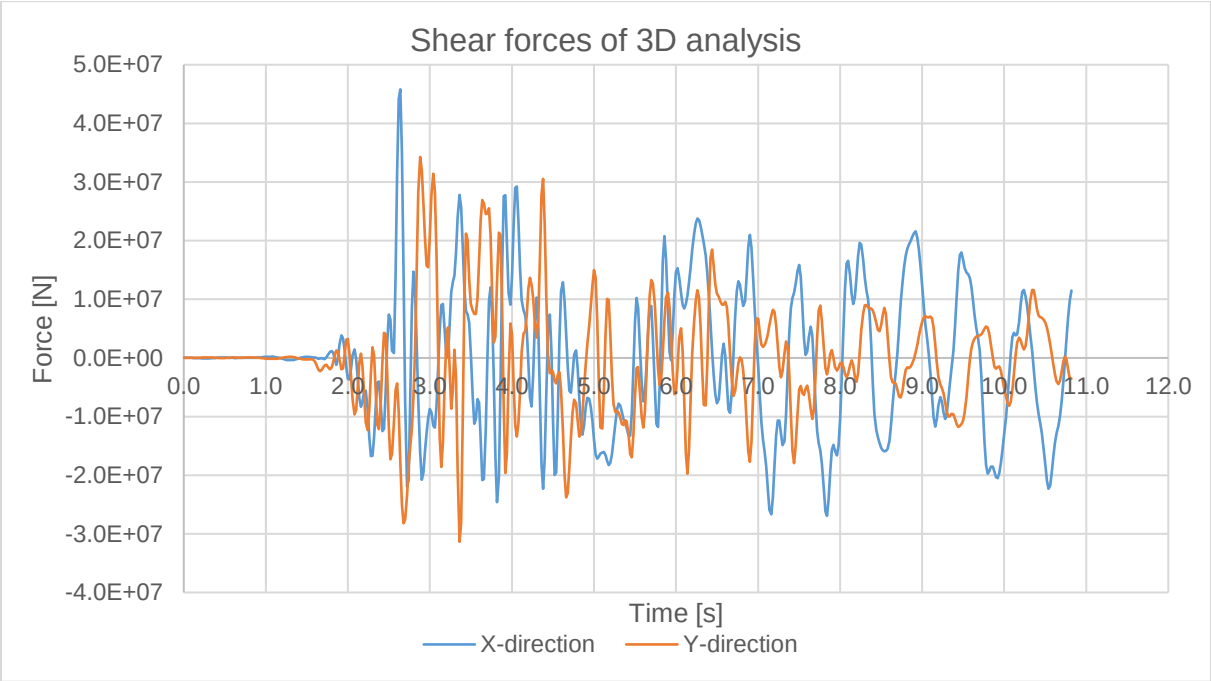

Figure 6.1: Base shear forces of 3D analysis in X (blue) and Y (orange) direction.

The base shear forces of the 3D analysis deviate significantly from the values of the MRS analysis, especially in the X-direction; see also Table 5-3. The base shear forces of the 3D analysis as shown in Figure 6.1 are determined in a section of the piles and so, all mass above this section contributes to these shear forces. The MRS analysis does not take into account the mass of the foundation and the walls and columns in the basement, since these masses are hardly activated in the frequency analysis, see also chapter 4. A better comparison with the MRS analysis would be to consider the forces right above the basement, at floor 0. The locations of the sections are shown in Figure 6.2.

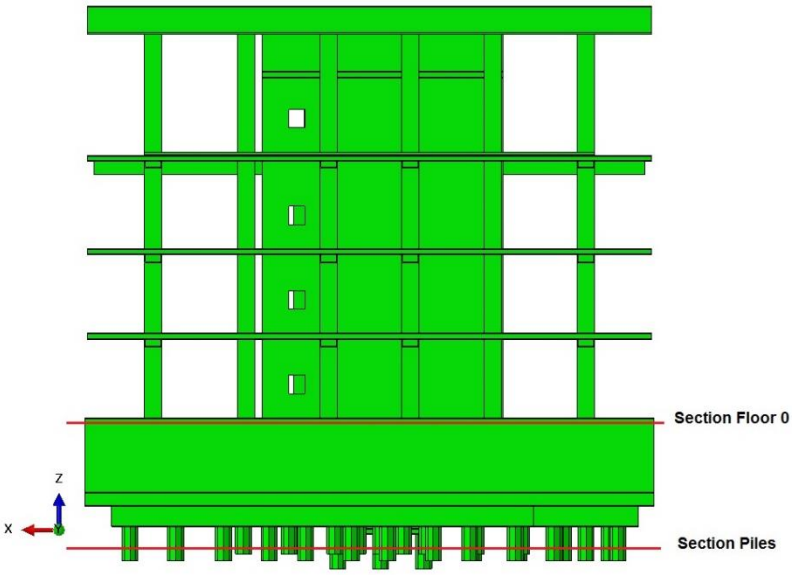

Figure 6.2: Locations of the sections for determining the base shear forces of the 3D model in Abaqus.

The shear forces of the MRS analysis and the two sections in the 3D model are shown in the table below.

Direction	CQC [kN]	SRSS [kN]	Section piles [kN]	Section Floor 0 [kN]
X	21799.8	20524.8	45797.7	21048.7
Y	23922.7	22997.4	34264.1	20556.3

Table 6-3: Overview of the base shear forces of the MRS analysis and the 3D analysis of Abaqus.

The shear forces of the section at floor 0 are significant smaller than the forces of the section in the piles.

The following graph shows the maximum shear forces for each floor over the height of the building. Each maximum value occurs at a different moment/time in the analysis.

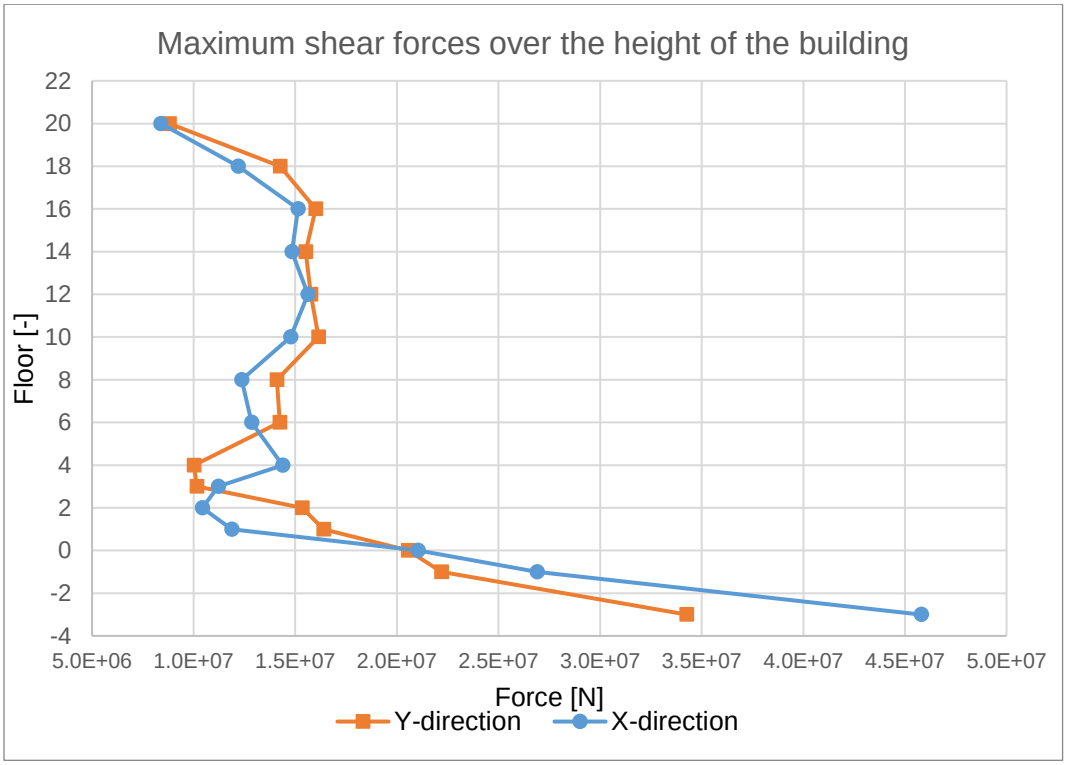

Figure 6.3: Maximum absolute shear forces for each floor over the height of the building.

At the first four floors, the stability in horizontal direction is mainly ensured by the walls of the stiff core. The occurring shear forces at these floors are therefore mainly transferred through these walls which results in rather high shear forces and stresses. In chapter 6.4 the plasticity and damage as a result of these large shear forces are displayed and discussed.

6.3. Displacements

In this paragraph the displacements and interstorey drifts are displayed and discussed. The first two graphs show the displacement of the building plotted over the height of the building at the moment of the peak accelerations in X- and Y-direction ($t = 2.64$ and $t = 2.88$ seconds; see Figure 4.22).

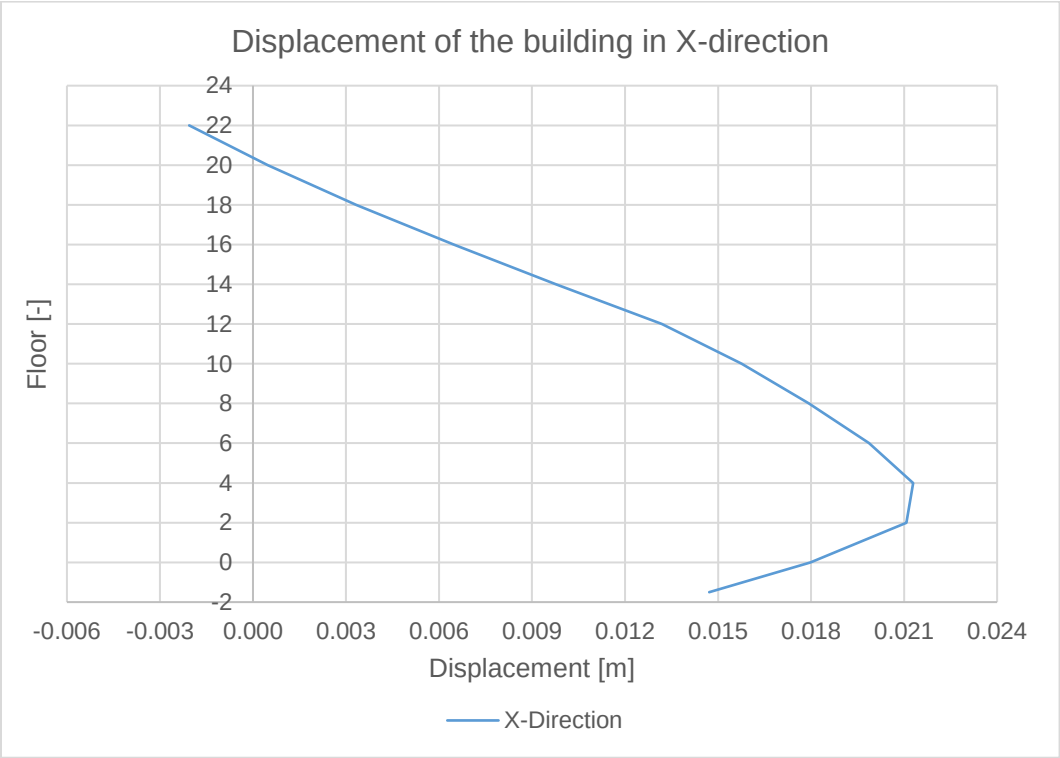

Figure 6.4: Displacement of each floor in X-direction at t=2.64 seconds, plotted over the height of the building.

Figure 6.5: Displacement of each floor in Y-direction at t=2.88 seconds, plotted over the height of the building.

The following graph shows the maximum displacements of each floor of the building. Each maximum displacement occurs at a different time in the analysis; the graph shows that the maximum displacement increases over the height of the building.

Figure 6.6: Absolute maximum displacement in X-direction (blue) and Y-direction (orange) of each floor over the height of the building.

The displacement graph in Figure 6.6 shows a significant increase of the maximum displacement between the second and fourth floor. This makes sense, since the bearing structure of the first four floors consists of a core with columns, while the bearing structure of the remaining part of the building consists of shear walls. This bearing structure of the core with the columns results in a sort of soft storey in the building; this soft storey is also visible in the plot of the maximum drifts.
The drifts are calculated by the following formula:

$$D_{int} = \frac{D_j - D_i}{\delta_h}$$

In which:

- D_i is the displacement of floor i;
- D_j is the displacement of floor j ($j > i$);
- δ_h is the height of the floor.

The interstorey drift is displayed in Figure 6.7, plotted over the height of the building.

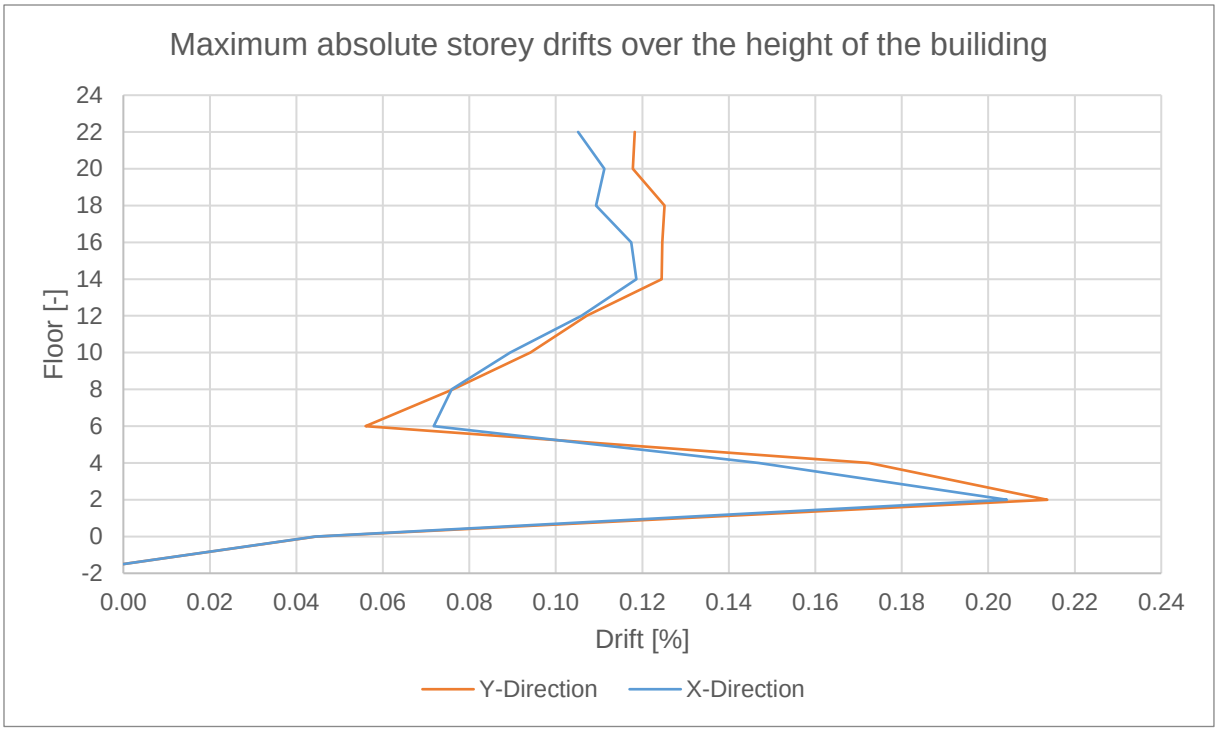

Figure 6.7: Absolute maximum storey drift of each floor over the height of the building in X (blue) and Y-direction (orange).

According to the Eurocode, the maximum allowed interstorey drift is 0.53%. This limit is not exceeded, as shown in the graph above; since the maximum occurring drift is about 0.21%.

6.4. Plasticity and damage

The (base) shear forces indicate that the impact of the earthquake is significant and causes plasticity and damage in the building. The figures in this paragraph show the amount of plasticity occurring during the earthquake.

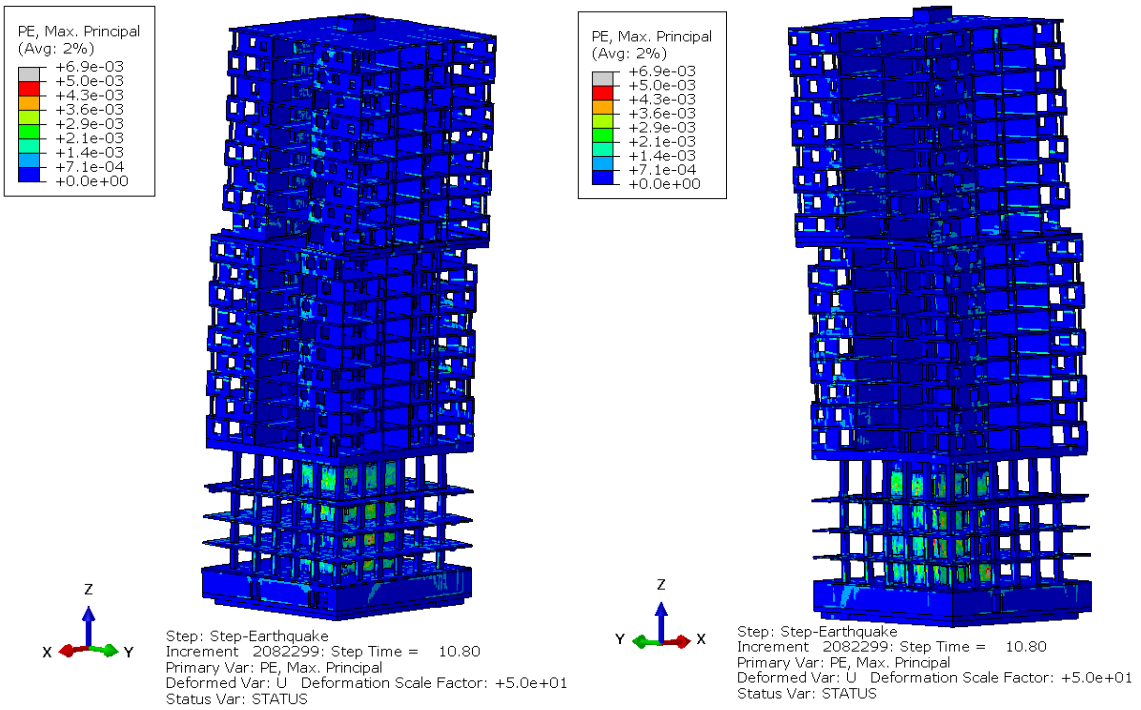

Figure 6.8: Plastic strains in the concrete of the building at the end of the earthquake analysis (t=10.8 seconds; viewpoint from two different directions).

As discussed in the previous paragraph, the soft storey shows a significant larger drift than the other storeys and as expected, this causes more plasticity and damage in the walls of these floors, compared to the rest of the building. This is shown in the following figures; the first two figures show the plastic strain in the whole building right after the peak in X-direction; the major amount of plasticity is developed in the walls of the first four floors.

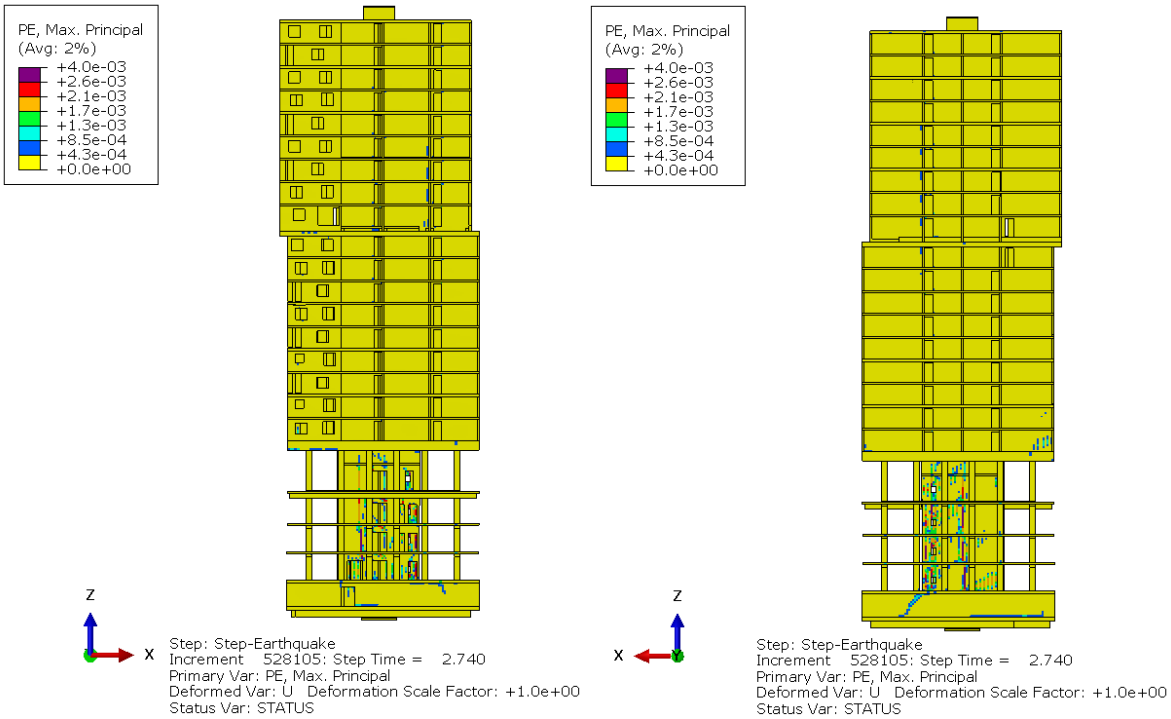

Figure 6.9: Plastic strain of concrete right after the peak acceleration in X-direction; t=2.74 seconds.

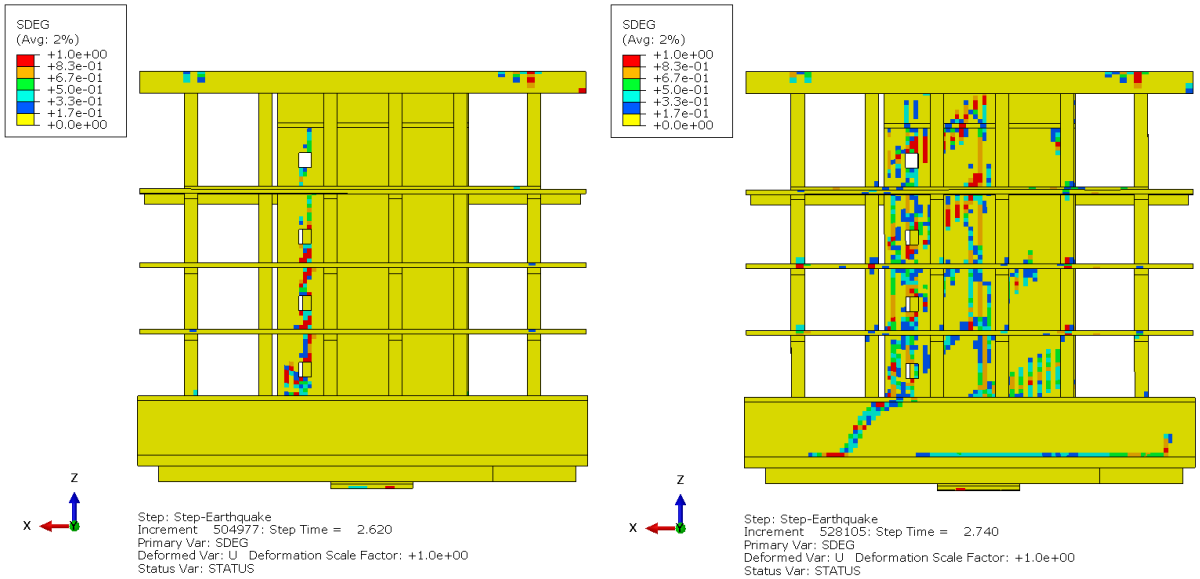

Figure 6.10: Stiffness degradation due to damage of concrete before (t=2.62 s) and after (t=2.74 s.) the peak acceleration in X-direction.

The following figures show the same principle for the Y-direction.

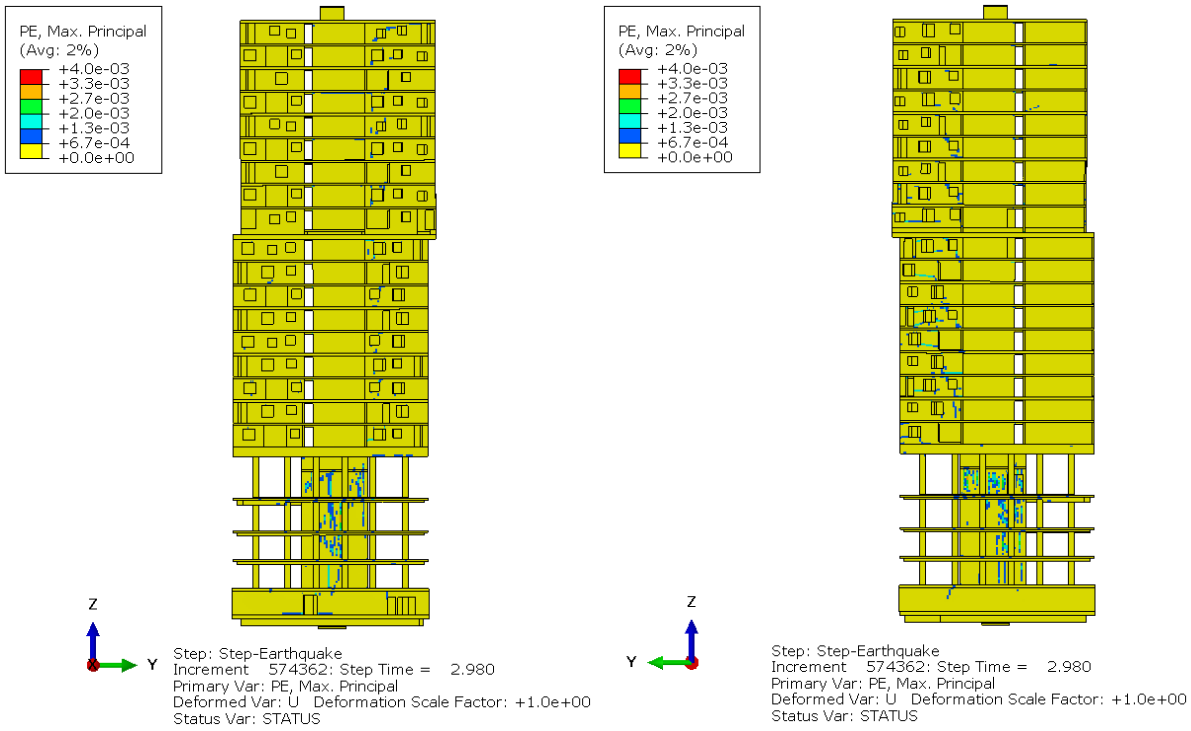

Figure 6.11: Plastic strain of concrete right after the peak acceleration in Y-direction; t=2.98 seconds.

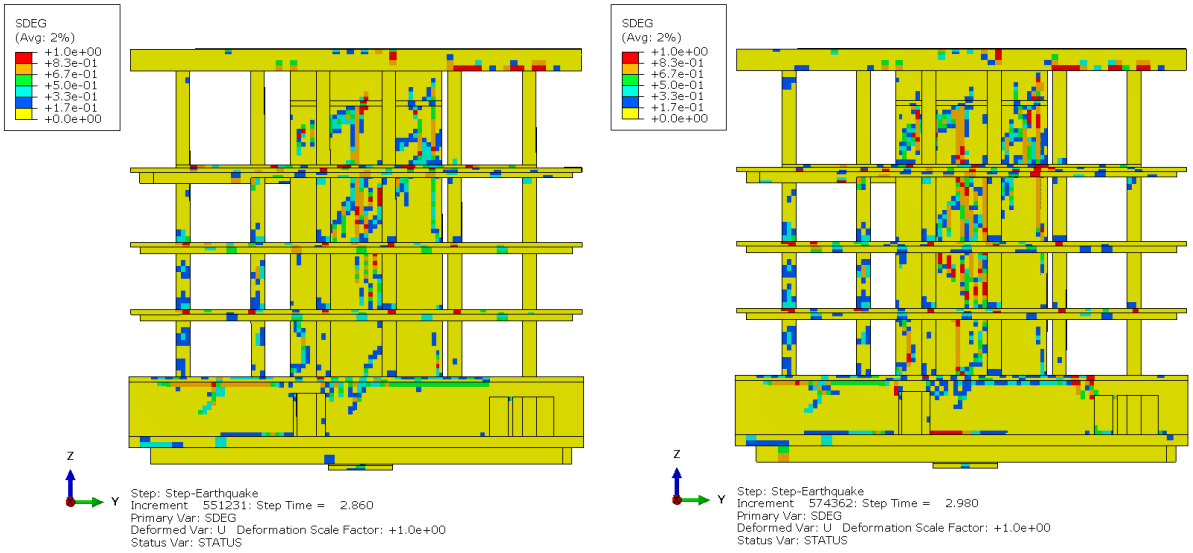

Figure 6.12: Stiffness degradation due to damage of concrete before (t=2.86 s) and after (t=2.98 s.) the peak acceleration in Y-direction.

The figures show that the impact of the peak in Y-direction is smaller than the impact of the peak in x-direction. The reason for this could be that the peak acceleration in X-direction already causes plasticity and therefore the stiffness reduces which results in smaller forces. Also, the stiffness of the top part of the building in Y-direction is smaller than the stiffness in X-direction (Table 3-1), which results in a smaller impact in Y-direction on the lower part of the building.

Figure 6.13 shows the stiffness degradation of the concrete at the end of the analysis at $t = 10.8$ seconds. The damage, due to tension and compression mainly develops in the core walls of the first four floors.

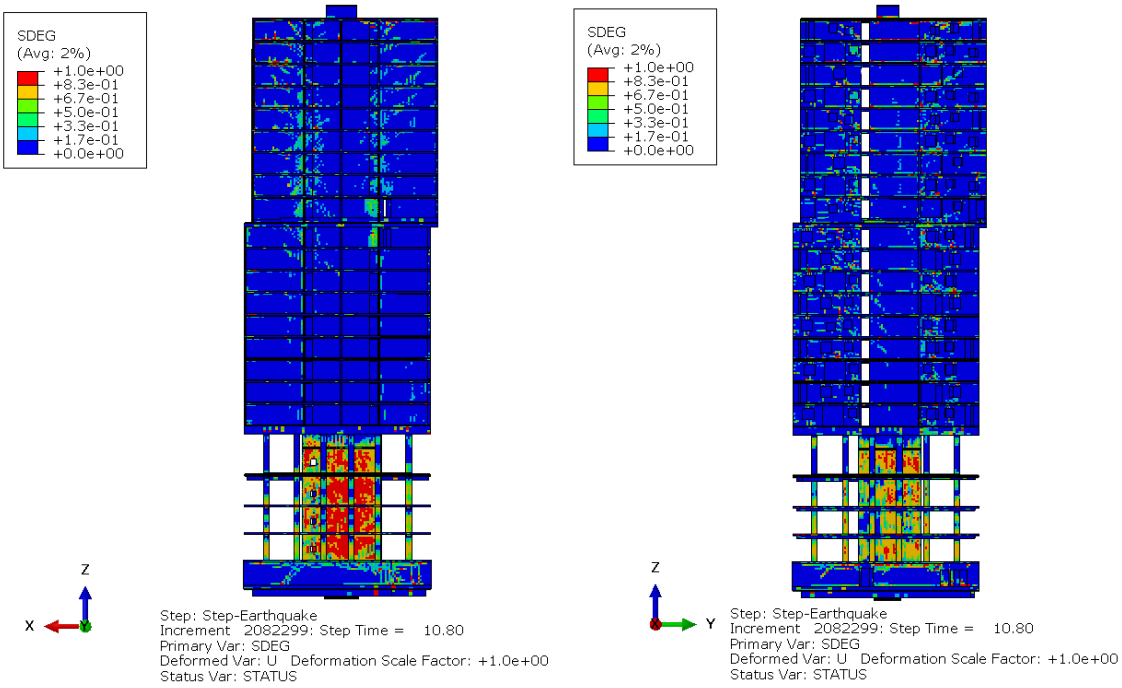

Figure 6.13: Stiffness degradation of the concrete at the end of the analysis, t=10.8 seconds; X- and Y-direction.

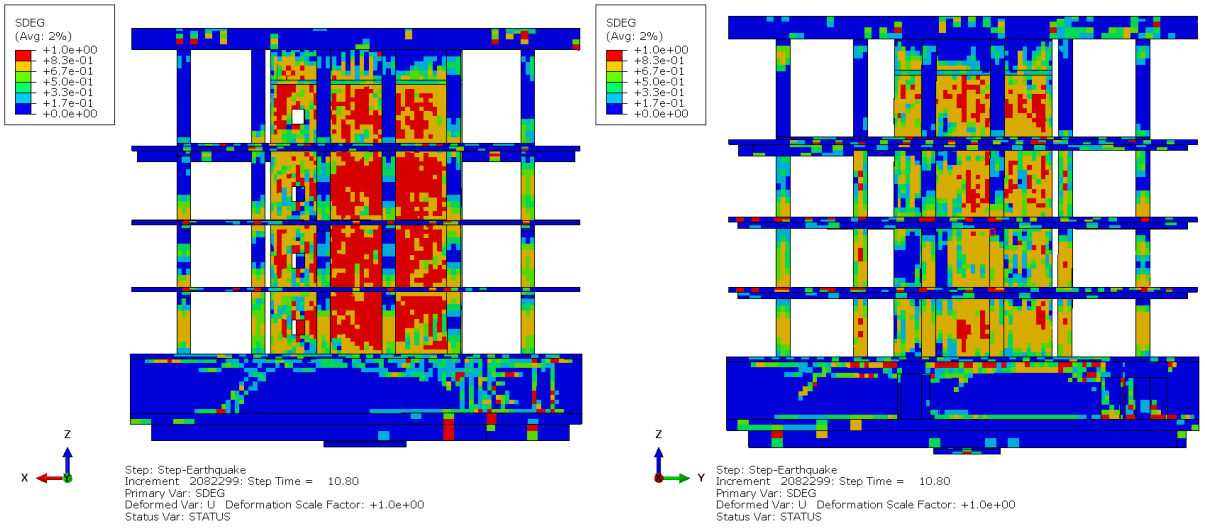

Figure 6.14: Stiffnes degradation of the concrete of the first four floors at the end of the analysis, t=10.8 seconds; X- and Y-direction.

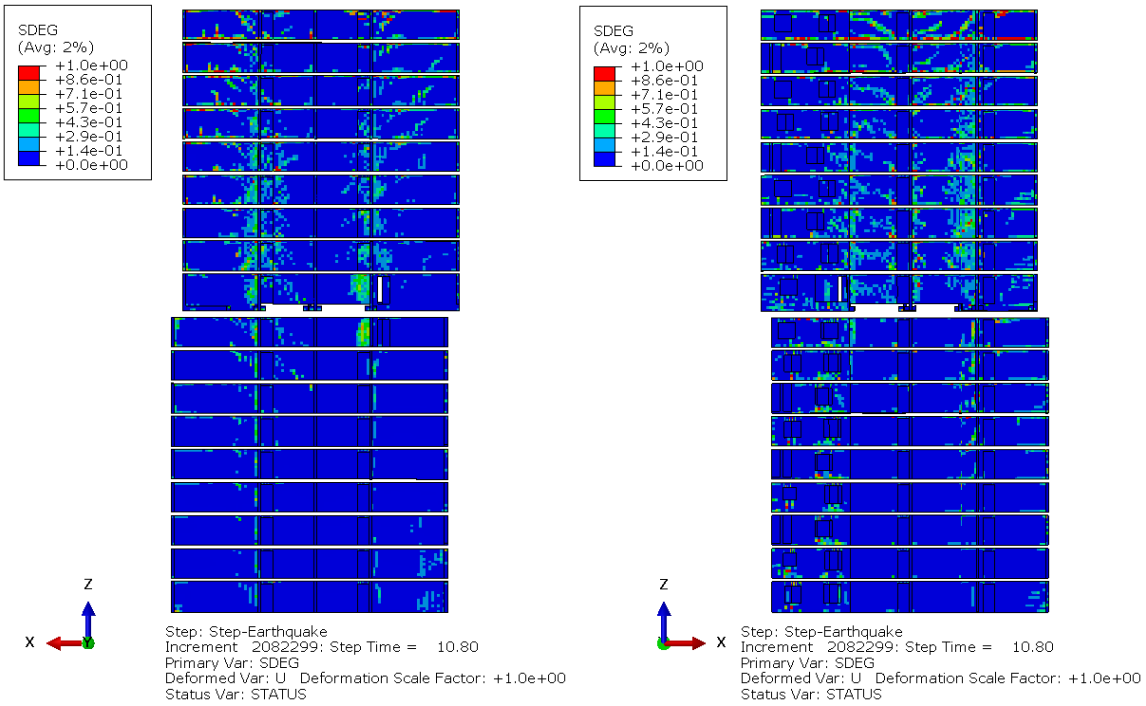

Figure 6.15: Stiffness degradation of the walls of the top part of the building at the end of the analysis in X-direction.

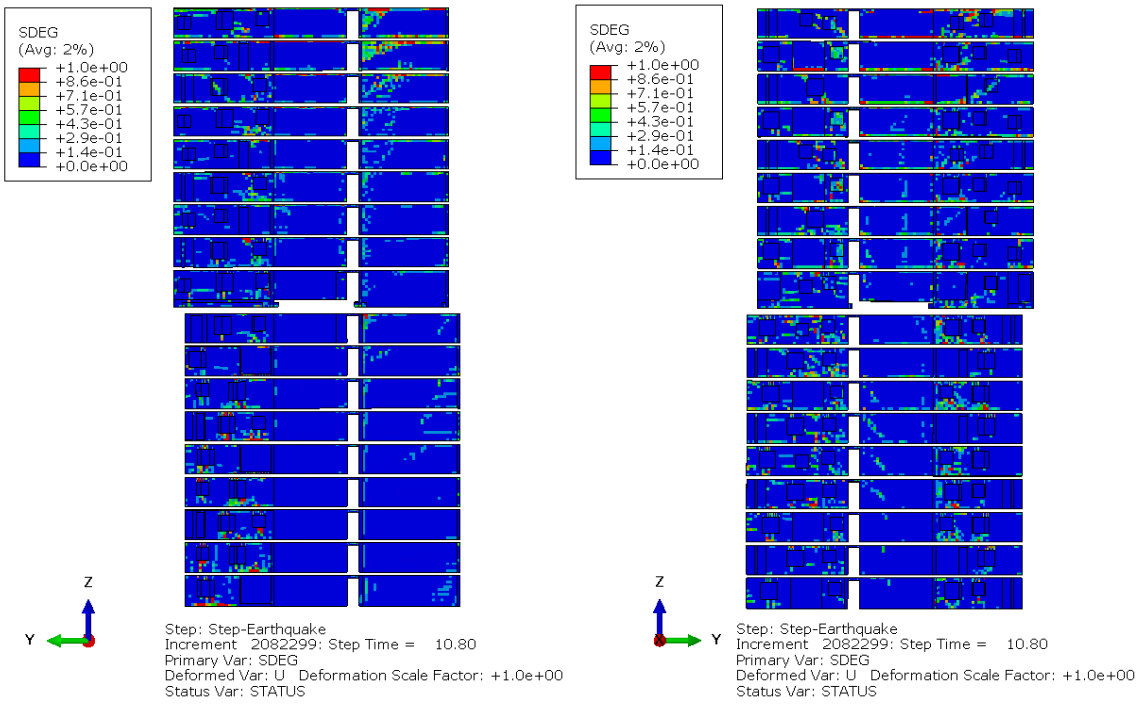

Figure 6.16: Stiffness degradation of the walls of top part of the building at the end of the analysis in Y-direction.

The results of the analysis show that the plasticity and damage occur at logical moments in time, corresponding to the time of the (peak) accelerations and displacements of the earthquake.

6.5. Reinforcement steel

The reinforcement steel is 'activated' once a crack occurs in the concrete. At the location of the crack the concrete is no longer able to take up any tensile force and the force is transferred to and through the reinforcement. This principle is clearly shown in the figures below; the first figure shows the stiffness degradation in the concrete, just after the peak acceleration ($t = 2.74$ s) and the second figure shows the stresses in the reinforcement steel at the same time.

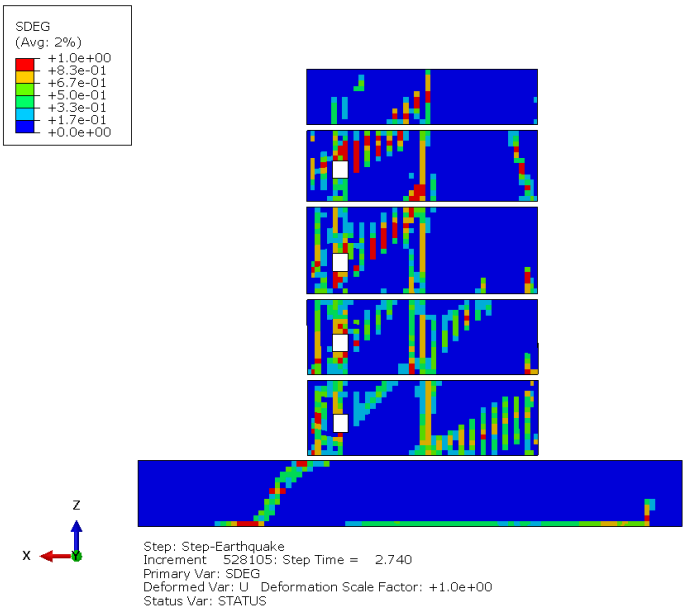

Figure 6.17: Stiffness degradation of concrete walls, floor 0 till floor 4, just after the peak acceleration in X-direction (t=2.74 seconds).

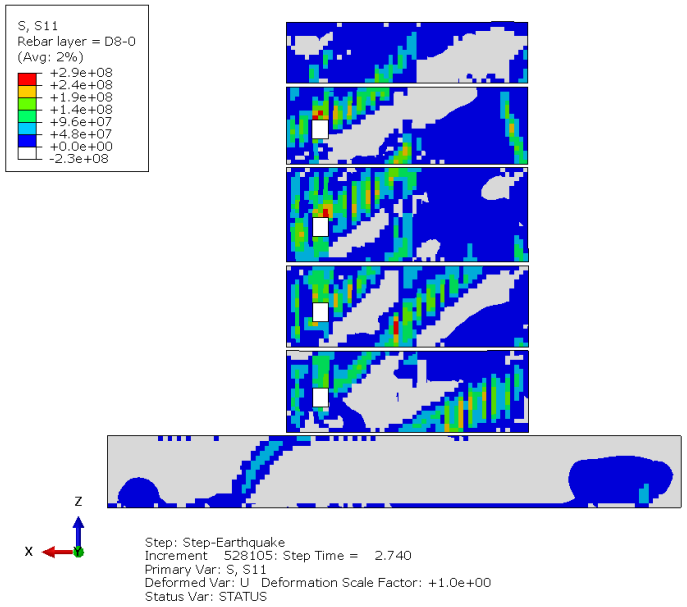

Figure 6.18: Stresses in the horizontal rebars of the walls of floor 0 till floor 4 just after the peak acceleration in X-direction (t=2.74 seconds); grey colour represents the compression stresses.

The following figures show the same principle in Y-direction, right after the peak at acceleration ($t = 2.98$ s).

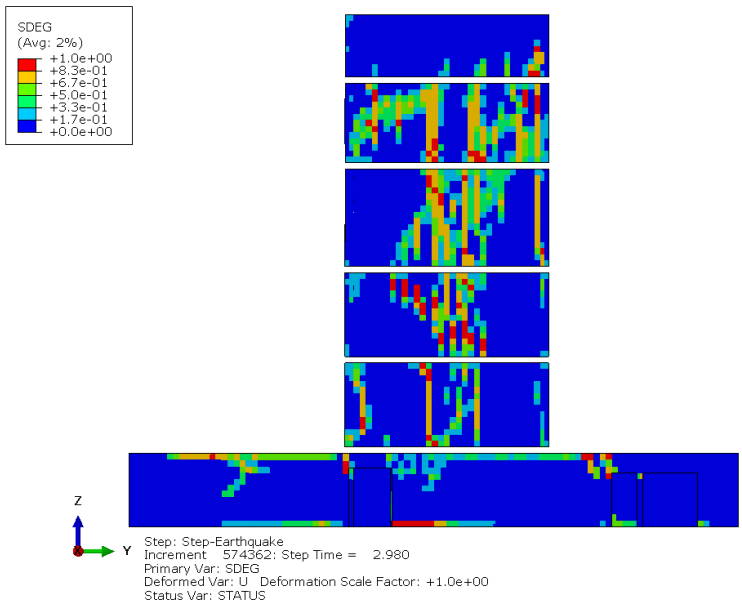

Figure 6.19: Stiffness degradation of concrete walls, floor 0 till floor 4, just after the peak acceleration in Y-direction (t=2.98 seconds).

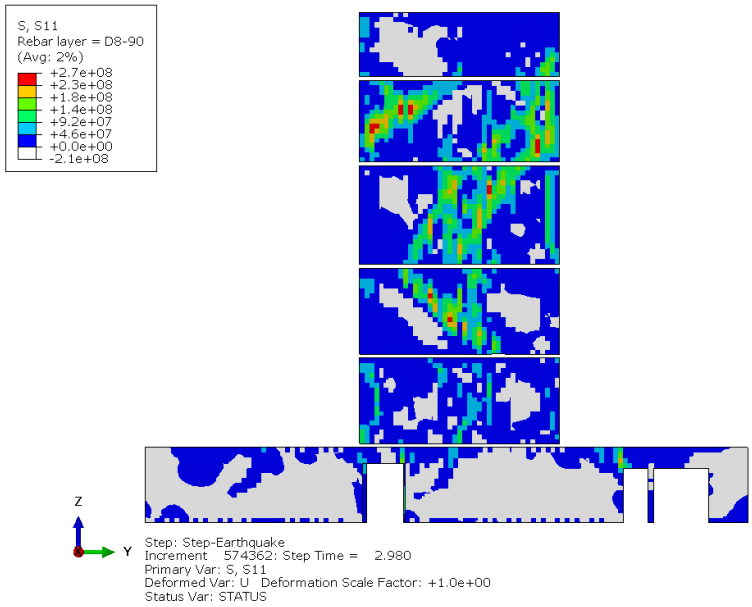

Figure 6.20: Stresses in the horizontal rebars of the walls of floor 0 till floor 4 just after the peak acceleration in Y-direction (t=2.98 seconds); grey colour represents the compression stresses.

Figure 6.17 till Figure 6.20 show that the stresses in the reinforcement increase substantial at the locations where the stiffness of the concrete is degraded.

As shown in the figures above, the core walls are quite damaged and a significant amount of stiffness degradation occurs. Despite the damage of the core walls, the reinforcement does not show a large amount of plastic strains. Only in some reinforcement parts of the first four floors plastic strains are developed.

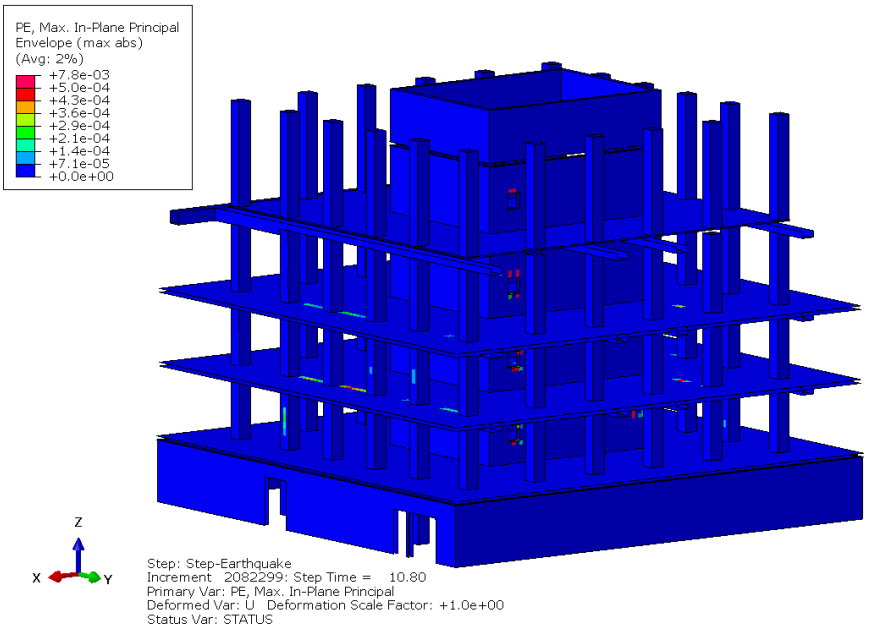

Figure 6.21: Envelope of absolute maximum plastic strain at the end of the analysis (t=10.8 seconds).

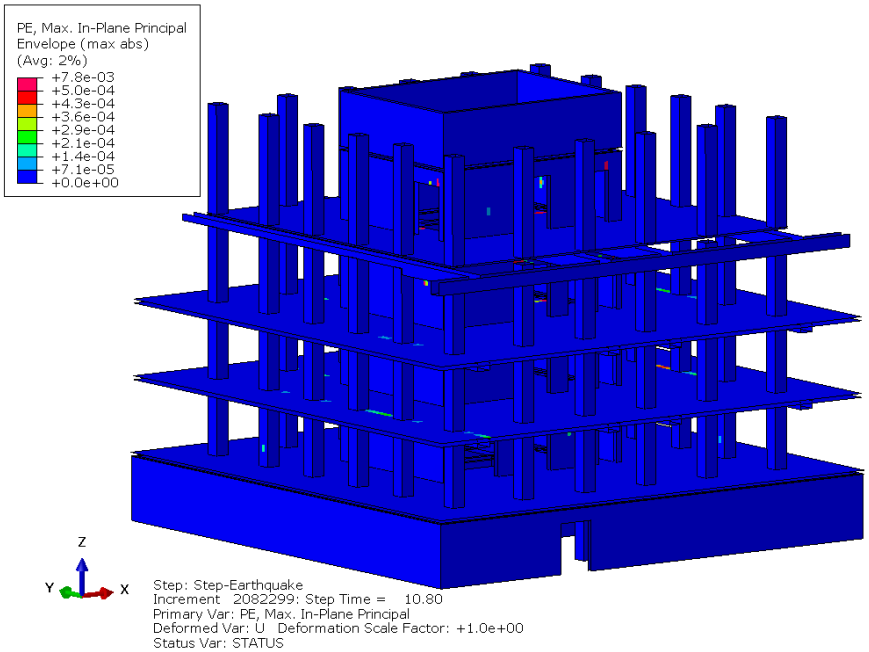

Figure 6.22: Envelope of absolute maximum plastic strains at the end of the analysis (t=10.8 seconds).

6.6. Summary chapter 6

In this chapter the analysis of the seismic behaviour of the building is presented through the consideration of the shear forces, displacements, plasticity and damage of the concrete and the strains and stresses in the reinforcement steel. The results showed that the displacements, the cracks and the damage of the structure correspond to the applied acceleration of the earthquake, since they occur at, or right after, peak accelerations and in the directions of the accelerations.
As discussed in chapter 2, the analysis was performed according to the 'Near Collapse' limit state as defined in the NPR; this limit state is defined by the following definition:

"The structure is heavily damaged and the remaining strength and stiffness in horizontal direction is relatively small; the structural members are still able to sustain the vertical loads. Most of the non-structural elements have collapsed and large permanent drifts are present. Progressive collapse does not occur; however, the structure is not able to withstand another earthquake or other load, regardless the intensity.

As presented in this chapter, severe damage was developed during the earthquake, especially in the core walls of the first four floors. However, progressive collapse of the building did not occur, even though this is possible with the enabled element deletion option. Also, the drift limits were not exceeded during the earthquake. On the other hand, the NPR also states that at least 7 accelerograms should be applied in order to determine the seismic capacity of a building through the analysis of a 3D model.

In conclusion, based on the results of the analysis - with only one accelerogram - the building meets the criterion for the Near Collapse limit state of the NPR. The building did not collapse and excessive permanent drifts were not developed.

However, the building might not meet the criterion of the NC limit state, based on a complete analysis with seven various accelerograms. In order to perform further analysis of the seismic behaviour and to increase the seismic capacity of the building, three strengthening measures are developed and initially analysed with the 1D model in Matlab. Next to this, also from a structural point of view, it is interesting to develop and analyse these strengthening measures for this specific building.

The developed strengthening measures and the initial analysis, performed with the 1D model in Matlab, are elaborated and discussed in the following chapter.

7. Strengthening proposals

As discussed and elaborated in the previous chapter, severe damage and plasticity occurs due to the earthquake, especially in the core walls of the first four floors. In this chapter some basic strengthening measures are proposed and discussed; these measures mainly focus on the first four floors in order to reduce the forces in the core walls. Also the impact of these strengthening measures on the dynamic behaviour is tested initially by means of the 1D model in Matlab.

7.1. Steel plating

A relative simple method of strengthening is applying a layer of steel on the concrete walls of the core at the first four floors of the building. This method is effective, since a steel plate is able to withstand high shear forces; this will reduce the high shear forces, and so the plasticity and damage in the core walls.

The shear force at the fourth floor is approximately 14500 kN in X-direction and 10500 kN in Y-direction, see Figure 6.3. These forces need to be transferred to the foundation of the building. Since the columns at the first four floors hardly contribute to the shear resistance, it is assumed that the shear forces are transferred through the core walls. In the calculation of the required thickness of the steel plate, the maximum shear capacity of the concrete is considered to be 1.0 N/mm^2. For the calculation of the shear stresses, a thickness of 45 millimeters per steel plate at each side of the concrete wall is assumed.

The dimensions of the core walls and applied steel plate are shown in the table below.

Table 7-1: Dimensions of core walls and steel plates for reinforcement.

	Concrete walls	Steel plates
Effective length X [m]	7.06	7.06
Effective length Y [m]	6.74	6.74
Thickness (b_i) [m]	$2 * 0.35 = 0.7$	$2 * 0.09 = 0.18$
Area x direction [m^2]	$7.06 * 0.7 = 4.942$	$7.06 * 0.18 = 1.27$
Area y direction [m^2]	$6.74 * 0.7 = 4.718$	$6.74 * 0.18 = 1.21$
I_{xx} [m^4]	106.51	27.38
I_{yy} [m^4]	152.11	39.10
$E_{modulus}$ [N/m^2]	$3.4 * 10^{10}$	$2.1 * 10^{11}$
n_i [-]	1	$\frac{2.1 * 10^{11}}{3.4 * 10^{10}} = 6.18$

The core walls (red and green) and the applied steel plates (blue) are shown below.

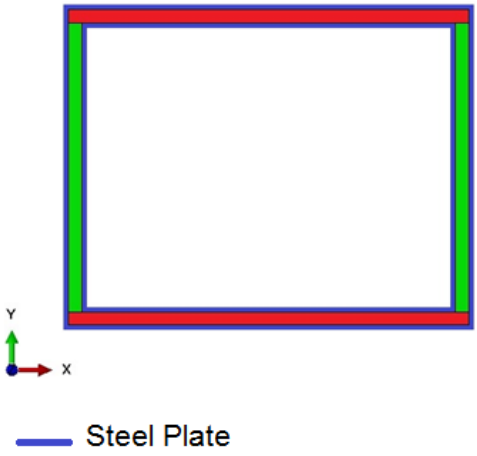

Figure 7.1: Top view of core walls with applied steel plates.

The shear force per material is determined by the following formula:

$$V_i = \frac{n_i * b_i}{n_c * b_c + n_s * b_s} * V$$

In which

- V_i is the shear force in material i;
- n_i is the ratio of the elasticity moduli; for concrete (n_c) equal to 1 and for steel (n_s) equal to 6.18;
- b_i is the width of the shear plane of material i, for concrete (b_c) equal to 0.7 and for steel (b_s) equal to $2 * 0.09 = 0.18$;
- V is the total shear force in X or Y-direction.

The shear force in the concrete cross section in X- and Y-direction is equal to:

$$V_{x,y;\,concrete} = \frac{1 * 0.7}{1 * 0.7 + 6.18 * 0.18} = 0.39 V_{x,y}$$

$$V_{x,y;\,steel} = \frac{6.18 * 0.18}{1 * 0.7 + 6.18 * 0.18} = 0.61 V_{x,y}$$

The shear stress in each material is calculated with the following formula:

$$\tau_{i,max} = \frac{V_i * S_i}{b_i * I_i}$$

In which

- τ_i is the shear stress in material i;
- V_i is the occurring shear force in material i;
- S_i is the statical moment of area, which is equal to $A_{shear\ plane} * z$;
- I_i is the moment of inertia of the cross-section of the material i.

For the calculation of $\tau_{i,max}$ it is assumed that the maximum shear stress occurs at the center of the cross section. Therefore, the area of the shear plane is equal to half of the total area and z is determined by the ratio of the area and the distance to the center of gravity (c.o.g.).

$$A_{shear\ plane} = \frac{A_x + A_y}{2}$$

$$z_x = \frac{\left(\frac{A_y * X_{c.o.g}}{2} + \frac{A_x * X_{c.o.g}}{4}\right)}{\frac{A_x}{2} + \frac{A_y}{2}} = 3.93\ [\text{m}]\ ;\ \ z_y = \frac{\left(\frac{A_y * Y_{c.o.g}}{4} + \frac{A_x * Y_{c.o.g}}{2}\right)}{\frac{A_x}{2} + \frac{A_y}{2}} = 3.15\ [\text{m}]$$

The calculation of the static moment of area (S_i) is displayed in the figure below. The black area corresponds to $A_{shear\ plane}$. The measures $X_{c.o.g.}$ and $Y_{c.o.g.}$ correspond to the distance of the center of gravity of the cross section in X and Y direction.

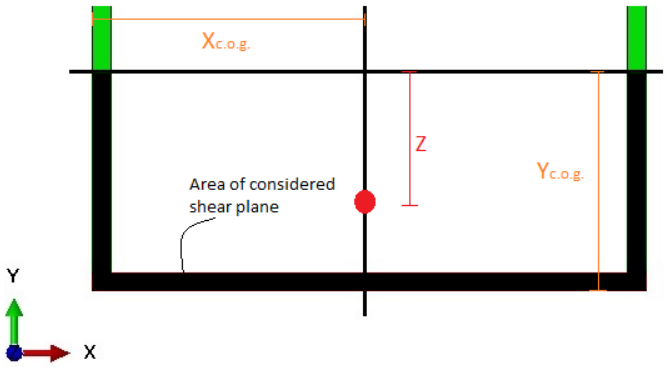

Figure 7.2: Calculation of static moment of inertia of core walls.

The calculations of the shear stress in the concrete and steel cross section are shown below:

$$\tau_{x,concrete} = \frac{0.39V_x * 18.98}{0.7 * 152.11} = 0.0689V_x$$

$$\tau_{y,concrete} = \frac{0.39V_y * 15.22}{0.7 * 106.51} = 0.0789V_y$$

$$\tau_{x,steel} = \frac{0.61V_x * 4.88}{0.18 * 39.10} = 0.425V_x$$

$$\tau_{y,steel} = \frac{0.61V_y * 3.91}{0.18 * 27.38} = 0.487V_y$$

The total shear forces at the fourth floor are equal to:

$V_x = 14500$ kN
$V_y = 10500$ kN

Which results in the following shear forces and stresses in the concrete core and the steel plate:

$V_{c,x} = 0.39 * 14500 = 5602.3$ kN; $\tau_{c,x} = \frac{0.0689*14500}{10^3} = 1.0$ N/mm^2;
$V_{c,y} = 0.39 * 10500 = 4056.8$ kN; $\tau_{c,y} = \frac{0.0789*10500}{10^3} = 0.83$ N/mm^2.

$V_{steel,x} = 0.61 * 14500 = 8897.7$ kN; $\tau_{steel,x} = \frac{0.425*14500}{10^3} = 6.17$ N/mm^2;
$V_{steel,y} = 0.61 * 10500 = 6443.2$ kN; $\tau_{steel,y} = \frac{0.487*10500}{10^3} = 5.12$ N/mm^2.

The calculation shows that the steel plate effectively reduces the shear force and stress in the concrete cross section. However, the thickness, and so the total amount of steel, is rather large which increases the total mass of the building.
With a thickness of the steel plate of 45 mm at each side of the core walls, the total mass of the steel is equal to:

$Mass_{steel} = (0.045 * 2) * \big((7.06 * 2) + (6.74 * 2)\big) * 3.3 * 7.85 * 4 = 257$ [tonnes]

This mass is rather high which has a negative effect on the shear forces at the first 2 floors of the building.

7.1.1. Initial analysis strengthening measure 1

The strengthening measure is analysed with the 1D model in Matlab. This analysis gives an initial insight in the effect and impact of the strengthening on the behaviour of the structure during an earthquake. The results of this analysis are compared with the analysis results of the existing structure, as shown in chapter 3.
The measure is modelled in Matlab as an ‘extra’ element in the model, with the bending and area related properties (moment of inertia) of the cross section of the steel plating, Table 7-1. The extra element is combined with the existing element for the first four floors by adding up the element mass and stiffness matrices.
Some of the comparisons between the displacements of the floors are shown in the following graphs.

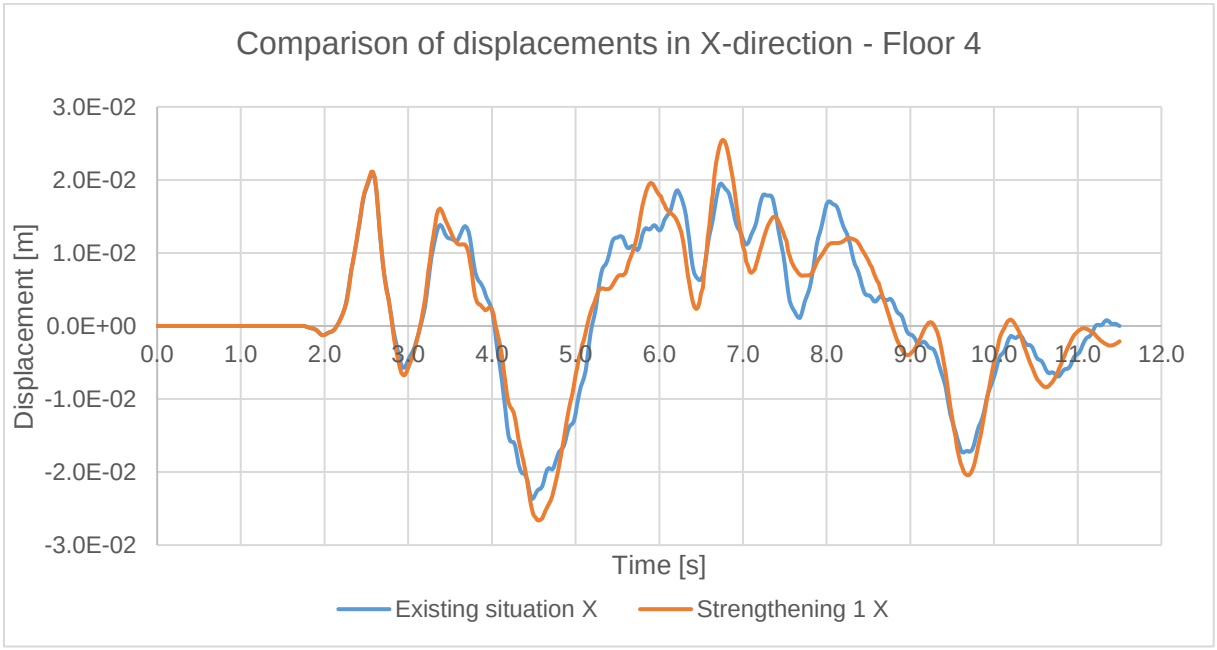

Figure 7.3: Comparison of the displacements of the existing building and the building with strengthening measure 1 – floor 4 in X-direction.

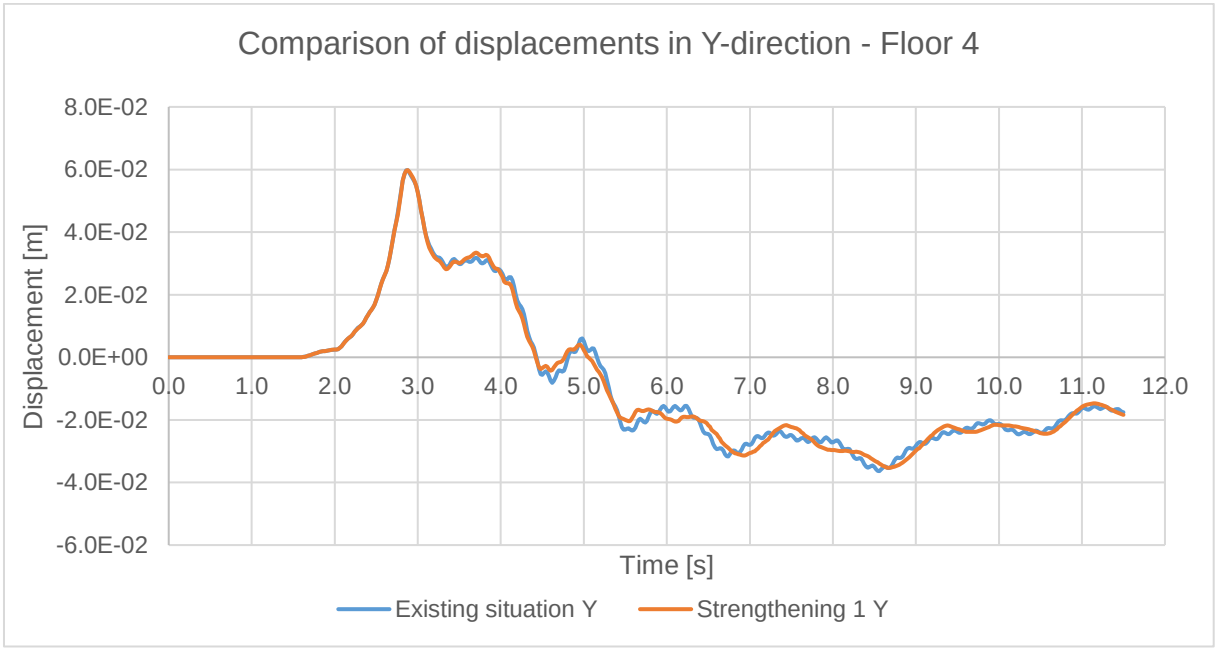

Figure 7.4: Comparison of the displacements of the existing building and the building with strengthening measure 1 – floor 4 in Y-direction.

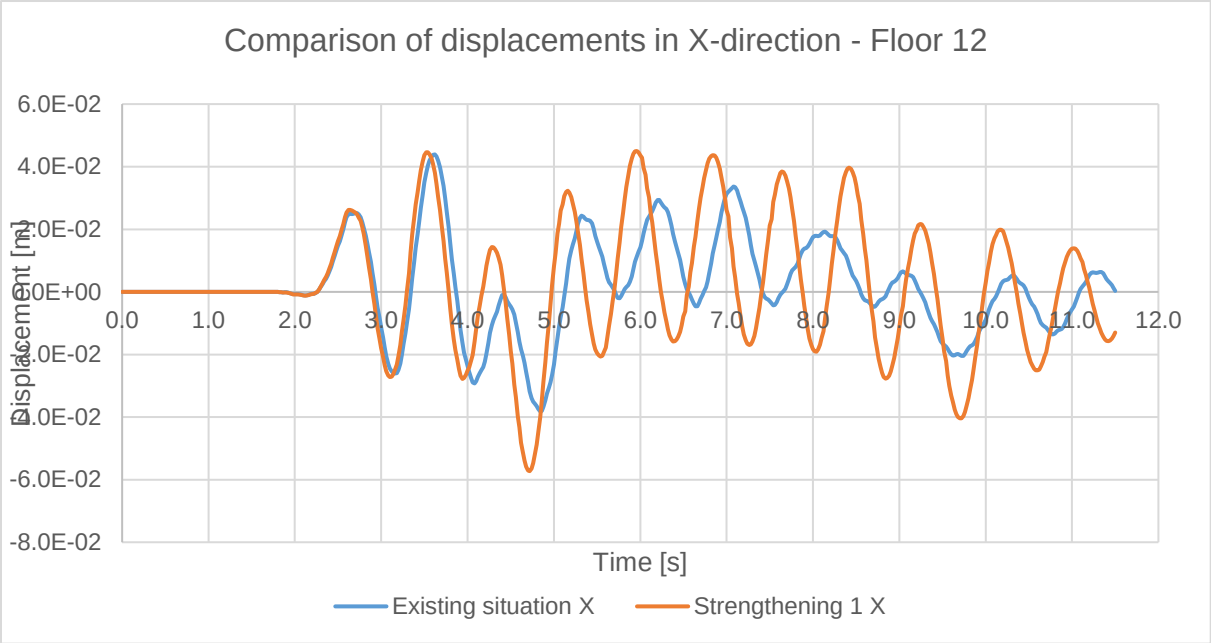

Figure 7.5: Comparison of the displacements of the existing building and the building with strengthening measure 1 – floor 12 in X-direction.

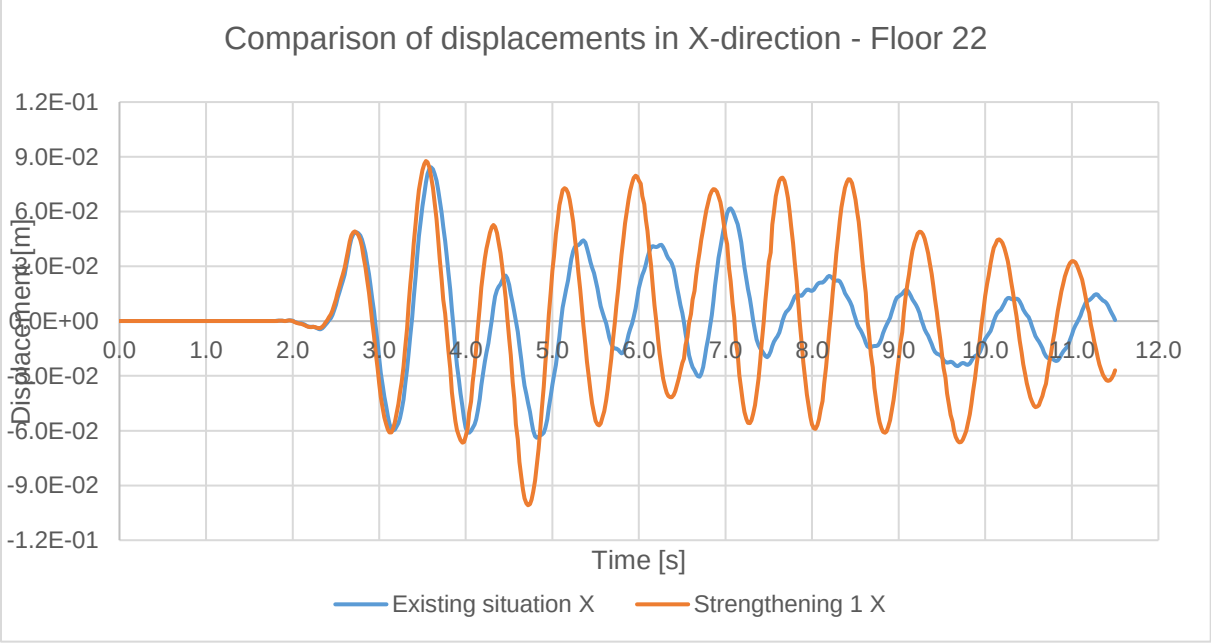

Figure 7.6: Comparison of the displacements of the existing building and the building with strengthening measure 1 - floor 22 in X-direction.

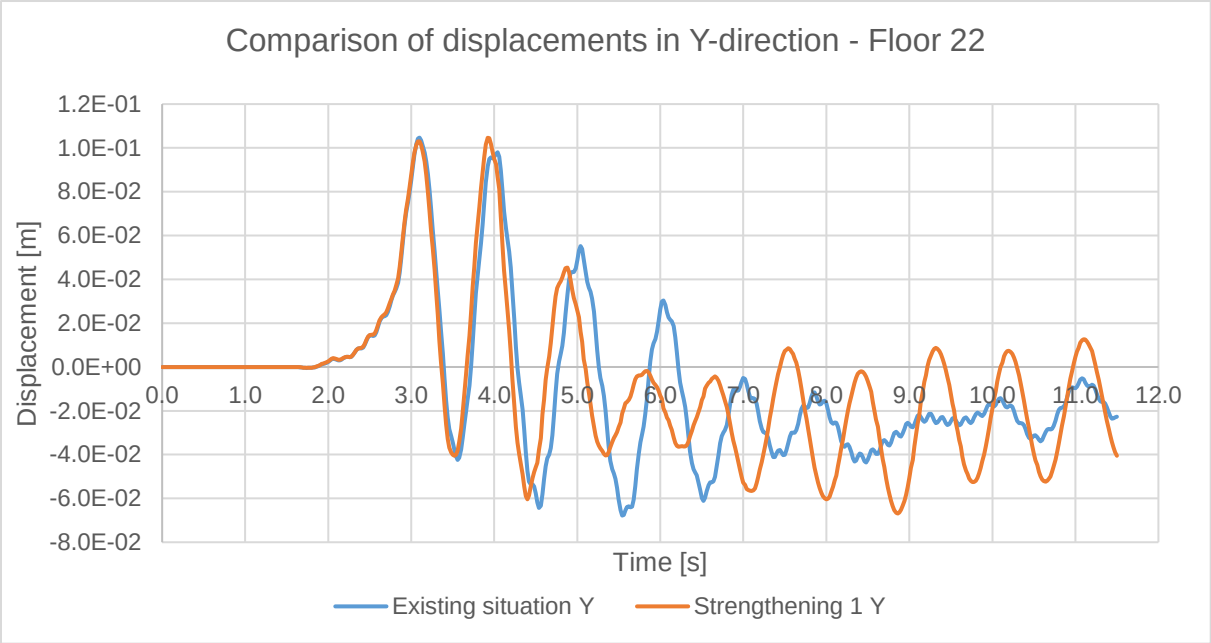

Figure 7.7: Comparison of the displacements of the existing building and the building with strengthening measure 1 – floor 22 in Y-direction.

The increase of stiffness results in a higher frequency of the displacements, especially of the 12th and 22nd floor. An overview of the displacements is given in the table below.

Table 7-2: Overview of displacements and drifts of existing building and strengthened building.

Direction	Maximum displacement [m]		
	Floor 4	Floor 12	Floor 22
X (initial)	0.0238	0.0435	0.0834
X (strengthened)	0.0266	0.0573	0.1009
Drift X (initial)	0.111%	0.108%	0.137%
Drift X (strength.)	0.125%	0.116%	0.148%
Y (initial)	0.0578	0.0680	0.101
Y (strengthened)	0.0598	0.0687	0.105
Drift Y (initial)	0.280%	0.110%	0.146%
Drift Y (strength.)	0.280%	0.110%	0.152%

The table shows that the maximum displacements of the strengthened building are higher, especially in the X-direction. The extra stiffness, and mass, added at the first four floors of the building seems to cause a resonance effect on the top part of the building.
The larger displacements in combination with the higher frequency will result in larger forces in the top of the building. Therefore, this strengthening measure might reduce the amount of plasticity in the walls of the first four floors, but it will increase the forces in the top part of the building. So, this measure does not solve the problem, but only moves the problem to a different location in the building.

7.2. Steel bracing

Since the amount of steel of the previous solution is rather high, a more integrated solution might result in a better solution. In order to reduce mass and increase the stiffness of the building, certain concrete parts can be replaced by steel parts and so a stiff steel framework can be created. Also the impact on the aesthetics of the building is smaller if concrete parts are replaced for steel parts instead of adding additional structural elements.
The principle of the reinforcement is shown in the figure below.

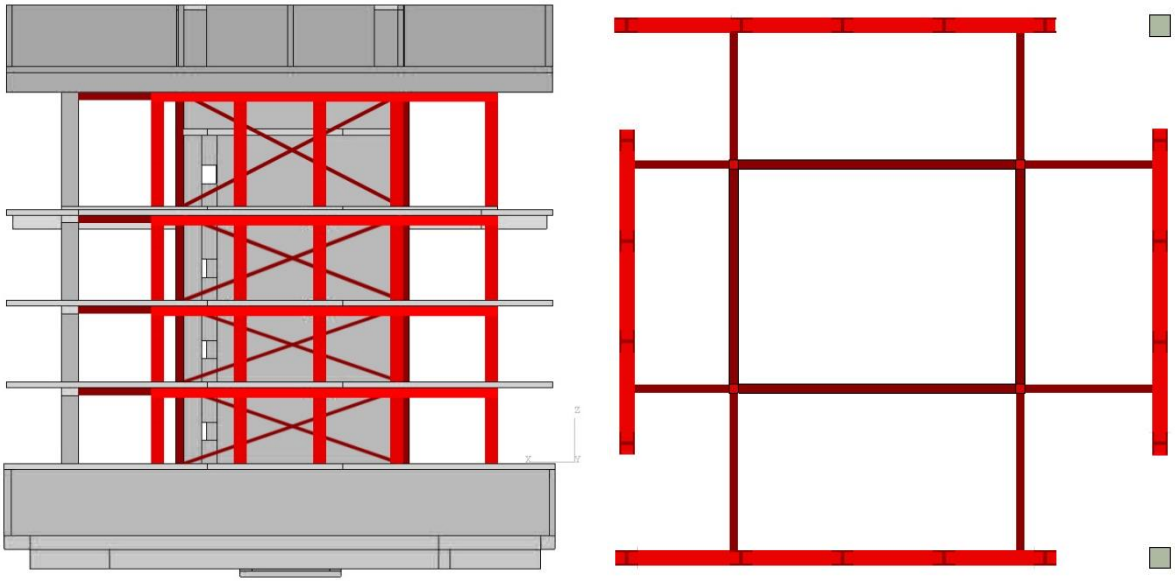

Figure 7.8: Side view (left) and top view (right) of the steel bracing (red) at the first four floors.

18 concrete columns will be replaced by steel columns with a steel plate at the bottom of the columns for the distribution of the vertical loading. The concrete at the corner of the core walls will be replaced by steel columns with an rectangular cross section. Steel beams are placed between the columns in order to create a stiff framework. At the outside of the concrete core walls, diagonal steel strips are applied between the top and bottom of the rectangular core columns. These strips will reduce the bending moment in the connection between the vertical column and horizontal beam. The frame needs to be applied at the first four floors of the building, which makes it a rather drastic method.

7.2.1. Initial analysis strengthening measure 2

With the 1D model in Matlab, an initial analysis of the strengthening measure is performed. The steel bracing is modelled as an 'extra' element, with the same principle as the first strengthening measure, 7.1.1.
For this extra element, the following parameters are applied:

Table 7-3: Overview of 1D Matlab parameters for implementation of strengthening measure 2.

Element	ρ [kg/m^3]	A [m^2]	E_0 [N/m^2]	I_{xx} [m^4]	I_{yy} [m^4]	l [m]
Concrete walls	19482.5	9.72	$3.41 * 10^{10}$	110	125	21.36
Steel bracing	19482.5	1.5	$21.0 * 10^{10}$	70.5	75.3	21.36

The parameters in Table 7-3 are based on the application HE-profiles for the steel columns with the same width as the concrete columns ($A_{s,col} = 0.0404\ [\mathrm{m}^2]$); therefore, the area is smaller while the mass is assumed to be the same. The following graphs show a comparison of displacements of the initial design and the building with the steel bracing.

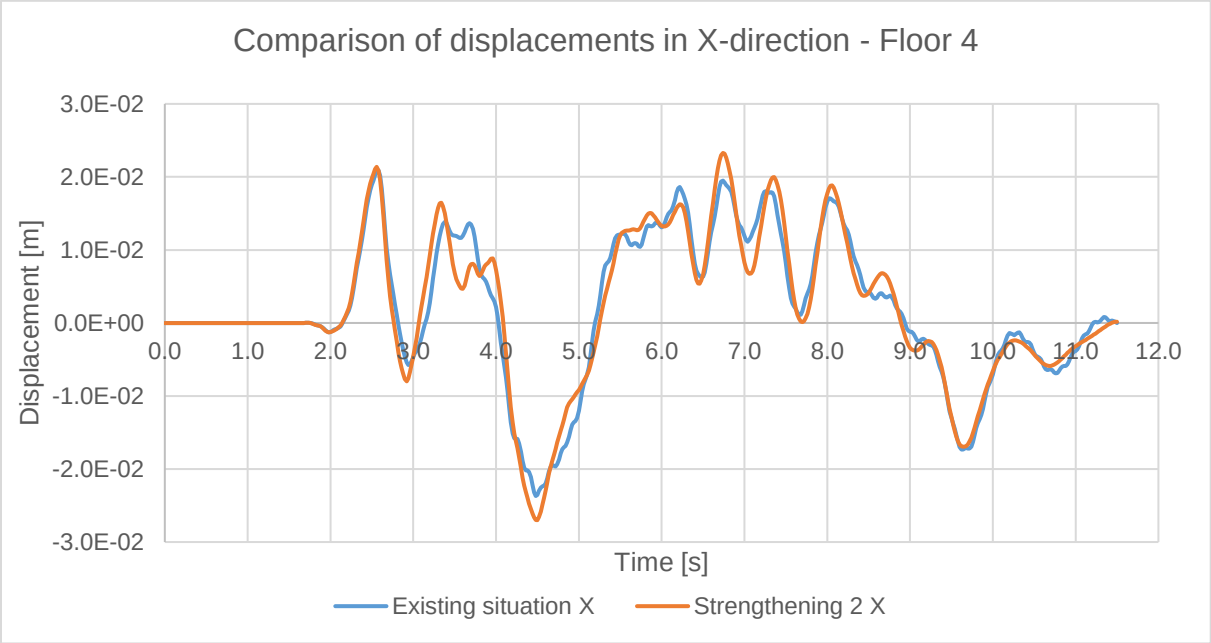

Figure 7.9: Comparison of the displacements of the existing building and the building with strengthening measure 2 – floor 4 in X-direction.

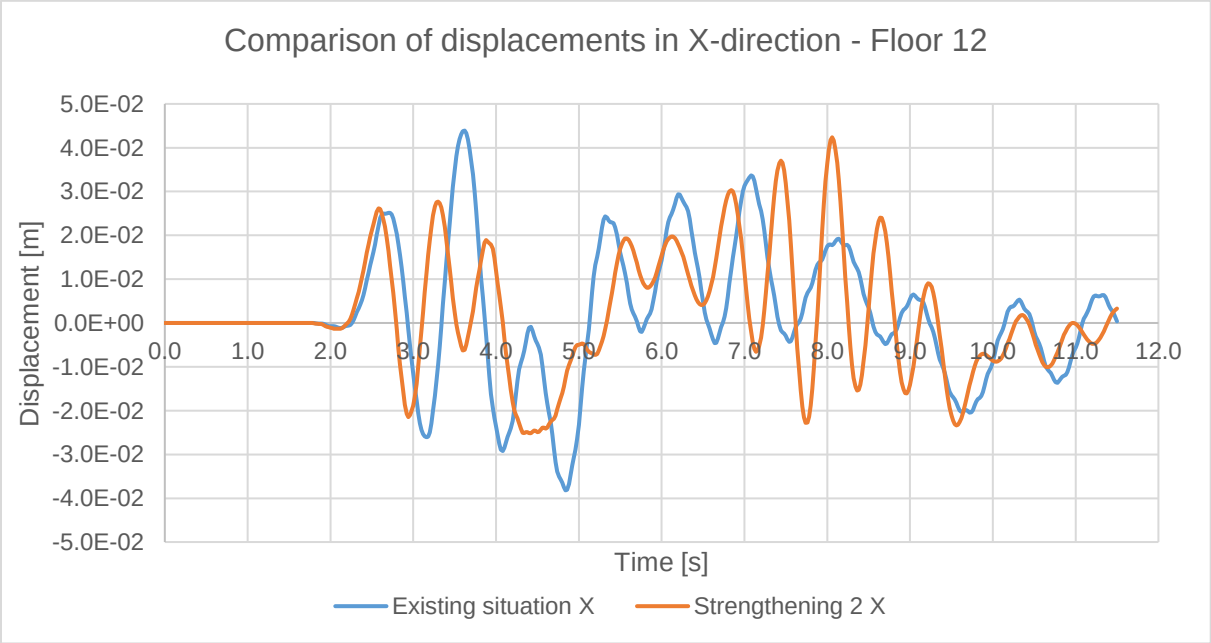

Figure 7.10: Comparison of the displacements of the existing building and the building with strengthening measure 2 – floor 12 in X-direction.

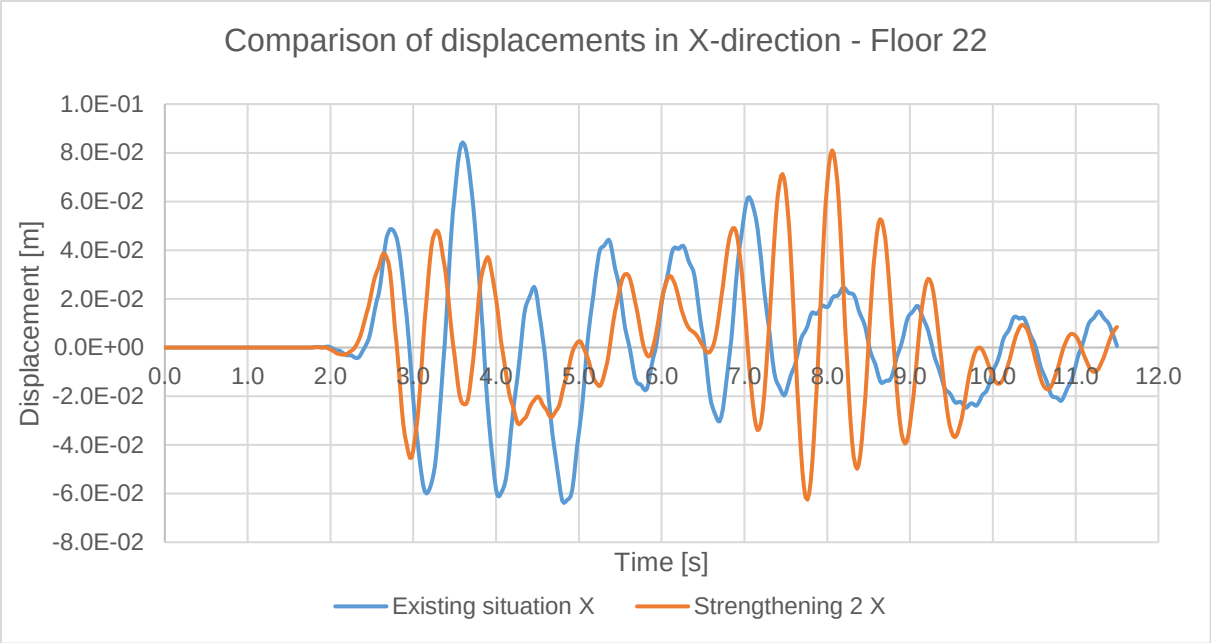

Figure 7.11: Comparison of the displacements of the existing building and the building with strengthening measure 2 - floor 22 in X-direction.

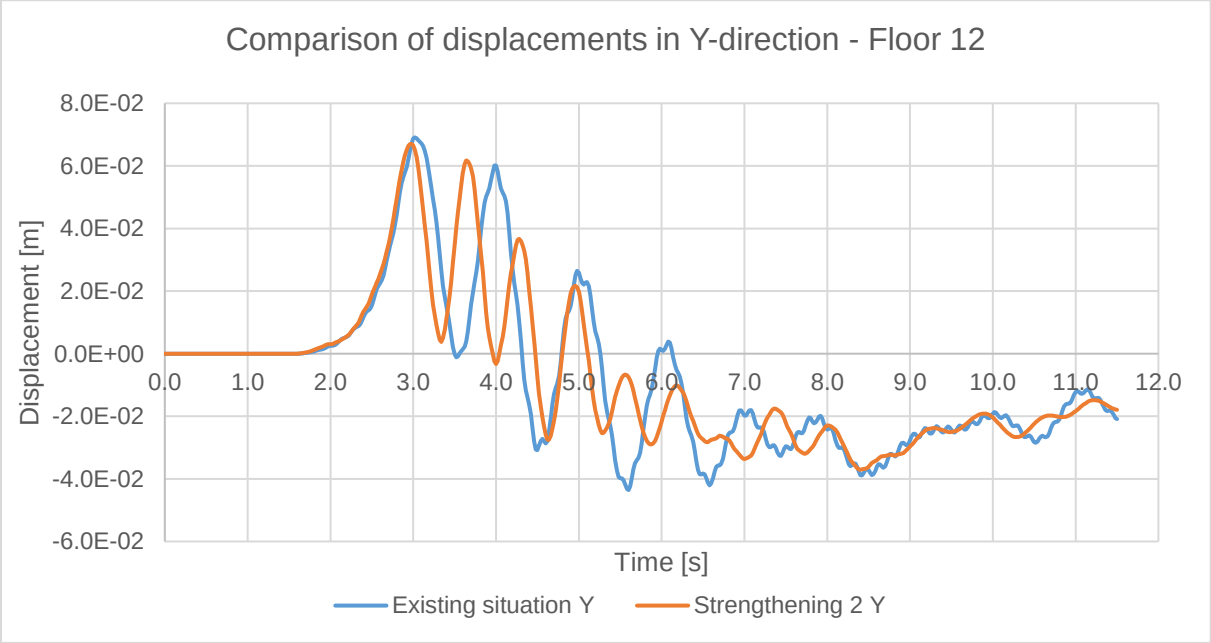

Figure 7.12: Comparison of the displacements of the existing building and the building with strengthening measure 2 - floor 12 in Y-direction.

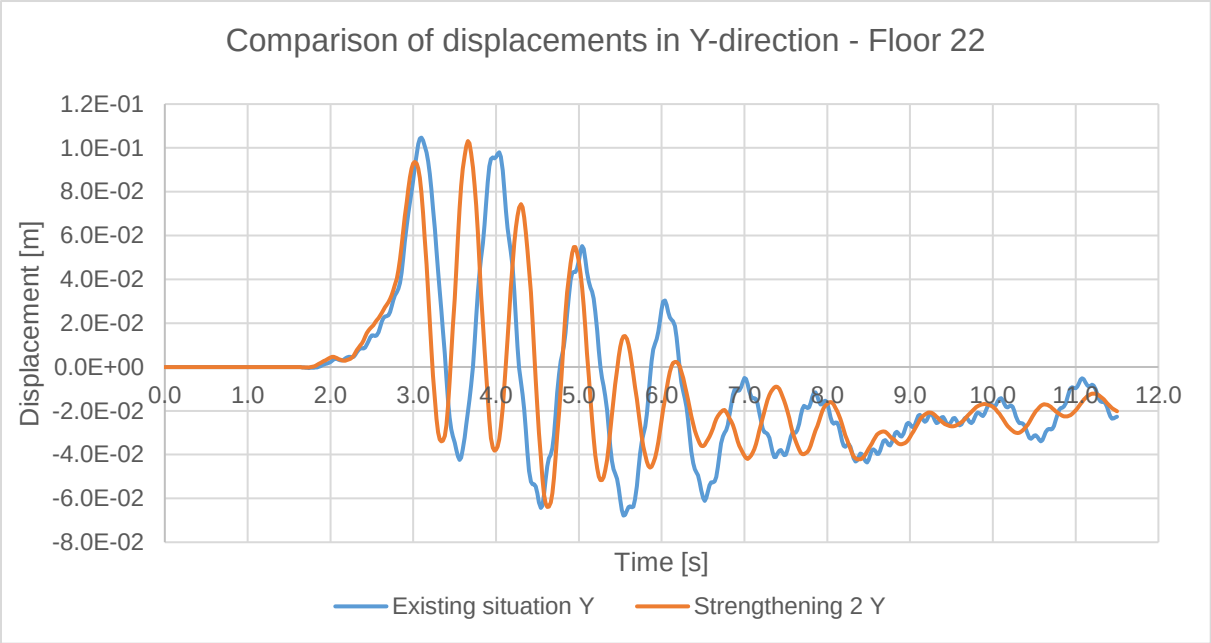

Figure 7.13: Comparison of the displacements of the existing building and the building with strengthening measure 2 - floor 22 in Y-direction.

The increase of stiffness results in a higher frequency of the displacements, especially of the 12th and 22nd floor. However, the impact of this measure on the dynamic behaviour is smaller than the impact of measure 1.
An overview of the displacements and drifts is given in the table below.

Table 7-4: Overview of the displacements of the existing building and the strengthened building.

Direction	Maximum displacement [m]		
	Floor 4	Floor 12	Floor 22
X (initial)	0.0238	0.0435	0.0834
X (strengthened)	0.027	0.0424	0.0810
Drift X (initial)	0.111%	0.108%	0.137%
Drift X (strength.)	0.126%	0.081%	0.135%
Y (initial)	0.0578	0.0680	0.101
Y (strengthened)	0.060	0.0670	0.103
Drift Y (initial)	0.280%	0.110%	0.146%
Drift Y (strength.)	0.282%	0.082%	0.141%

Despite the higher frequency of the displacements, the effect of this measure is rather minimal and the displacements are in the same order of magnitude; except for the displacements in X-direction around 8 seconds of the analysis. The applied signal of the NPR shows a peak of the acceleration at that specific time, see Figure 2.11; the strengthening measure increases the displacement of floor 12 and 22 at that specific time. Yet, the peak displacement is not higher than the displacements of the existing building.

Based on the results, it is expected that this strengthening measure reduces the amount of plasticity in the first four floors. The plasticity in the walls of the top part of the building will increase, due to the higher frequency which causes larger shear forces. However, it is expected that the increase of plasticity remains small.
This measure is therefore expected to be effective for the reduction of the plasticity in the core walls of the first four floors. However, as mentioned before, the method is quite drastic to implement in the existing design.

7.3. Base isolation

Since the behaviour of the soft storey at the first four floors is actually quite beneficial, the idea occurred to improve and optimise this behaviour in the building by means of base isolation.
Usually base isolation is applied at the base of the building, like the name already suggests. However, in an existing building it is quite difficult to apply this method at the base of that building. Besides, in this case it is not even necessary, since the building already has a soft storey till the fourth floor. Therefore, it is possible to implement the 'base' isolation at one of the first floors. Because of the beams at the top of the columns at the first three floors, the base isolation will be implemented at the third floor, below the thick fourth floor. The isolation is applied through sliders.

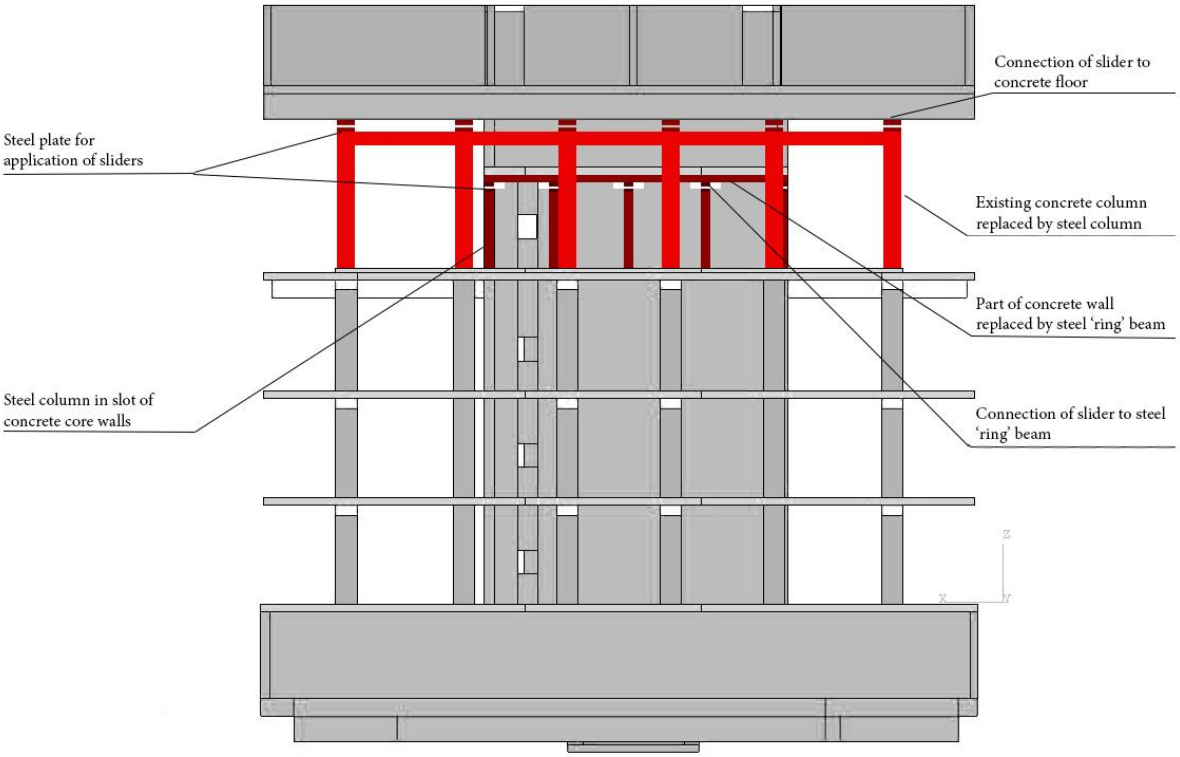

Figure 7.14: Side view of reinforcement applied through 'base' isolation with sliders.

All concrete columns at the third floor will be replaced by steel columns, with a steel plate at the top and bottom of the column. The sliders will be placed on top of the columns and connected with the concrete floor above.
Slots will be made in the concrete core walls, in which steel columns will be placed. On top of these columns and the core walls, a steel beam will be placed which will distribute the vertical forces from the floor above to the columns and prevents high peak stresses. The sliders are applied between the steel columns and the steel beam. This means that these columns will bear the vertical loading which are transferred through the walls in the original design. The remaining parts of the concrete wall will resist the remaining shear forces. An example of a slider is shown in Figure 7.15.

Figure 7.15: Example of a slider [fip industriale]

This method can be applied at one floor, as shown in Figure 7.14, which is an advantage compared to the other methods which need to be applied at four floors. Another advantage is that the shear forces in both the top and lower part of the building will decrease since the stiffness decreases as well, compared to the original design. This solution is a more durable solution, compared to the first two, since high forces are prevented instead of resisted and therefore a smaller amount of plasticity and damage is expected.

7.3.1. Initial analysis strengthening measure 3

With the 1D model in Matlab, the strengthening measure is analysed, in order to examine the impact of the measure on the dynamic behaviour of the building. In this case, the sliders are modelled as an extra, separate element with specific properties. Since the 1D model in Matlab performs elastic calculations, the plasticity of the sliders is defined artificially. The definition of the properties is based on the article of Junwon Seo and Jong Wan Hu (Seo & Wan Hu, 2016). Their example of hysteretic behaviour of a slider is shown in the figure below.

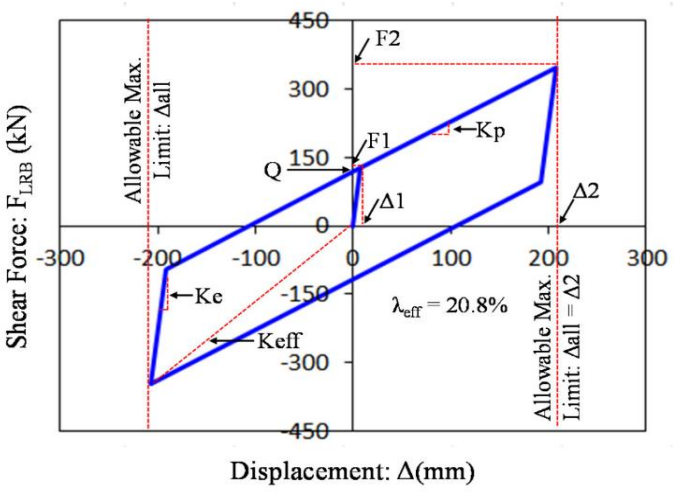

Figure 7.16: Example of hysteretic behaviour of a slider (Seo & Wan Hu, 2016).

This hysteretic behaviour as shown in Figure 7.16 cannot be modelled in the elastic 1D model; however, the behaviour can be approached through an elastic element, in combination with a certain amount of damping which corresponds to the energy loss due to the slider. For the calculation of the properties of the sliders, some applied parameters are based on assumptions.
The slider properties are shown in the table below.

Table 7-5: Overview of the slider properties, corresponding to Figure 7.16.

Property	Value	Description
μ	2 [%]	Friction coefficient of the sliders
Mass	$1.9895E7$ [kg]	Mass of top part of building above floor 4
Q	$3.903E6$ [N]	Friction force: $\mu * Mass$
Δ_1	0.0001 [m]	Assumption; represents the elastic stiffness of the slider
Δ_2	0.075 [m]	Assumption; based on displacement during earthquake
k_p	$7.807E7$ [N/m]	Assumption; equal to: $(Mass * 9.81)/2.5$
F_1	$3.911E6$ [N]	$Q + k_p * \Delta_1$
F_2	$9.76E6$ [N]	$Q + k_p * \Delta_2$
k_e	$3.91E10$ [N/m]	F_1/Δ_1
k_{eff}	$1.30E8$ [N/m]	Effective stiffness of the slider; equal to: F_2/Δ_2
Energy dissip.	$1.17E6$ [J]	Area of the hysteresis loop; equal to: $4 * Q * (\Delta_2 - \Delta_1)$
Potent. energy	$3.66E5$ [J]	$0.5 * k_{eff} * \Delta_2^2$
Effective damping (ξ)	0.25431	*Viscous damping coefficient* of the slider; equal to: $E_{diss.}/4 * \pi * E_{pot}$

The value of Q should be larger than the force due to wind load, in order to prevent the sliders being 'activated' due to the wind loading. The wind load on the building is approximately equal to: $F_{wind} * Width * Heigth = 2 * 25 * 71 = 3550$ kN, which is smaller than Q as in Table 7-5.
The effective damping is calculated by the ratio of the dissipated energy and the potential energy of the slider (Spijkers, Vrouwenvelder, & Klaver, 2005). In order to apply this effective damping of 25.4%, a large amount of Rayleigh damping is defined in the slider element; in the other elements of the 1D model, a normal amount of damping (2.5%) is applied. The parameters of the Rayleigh damping are determined through the same process as described in chapter 3.
The 'slider element' in the 1D model is defined as an Timoshenko beam element, since the shear deformation needs to be taken into account. The corresponding stiffness matrix is defined according to the theory of Felippa (Felippa, 1986). The shear stiffness (G) of the element is equal to:

$$G = \frac{k_{eff} * l}{A_s}$$

In which:

- l is the length of the slider element, set to 1 meter length;
- A_s is the area of the sliders, approximately equal to 12 m^2.

A comparison between the displacements of the original design and the building with the sliders is shown in the graphs below.

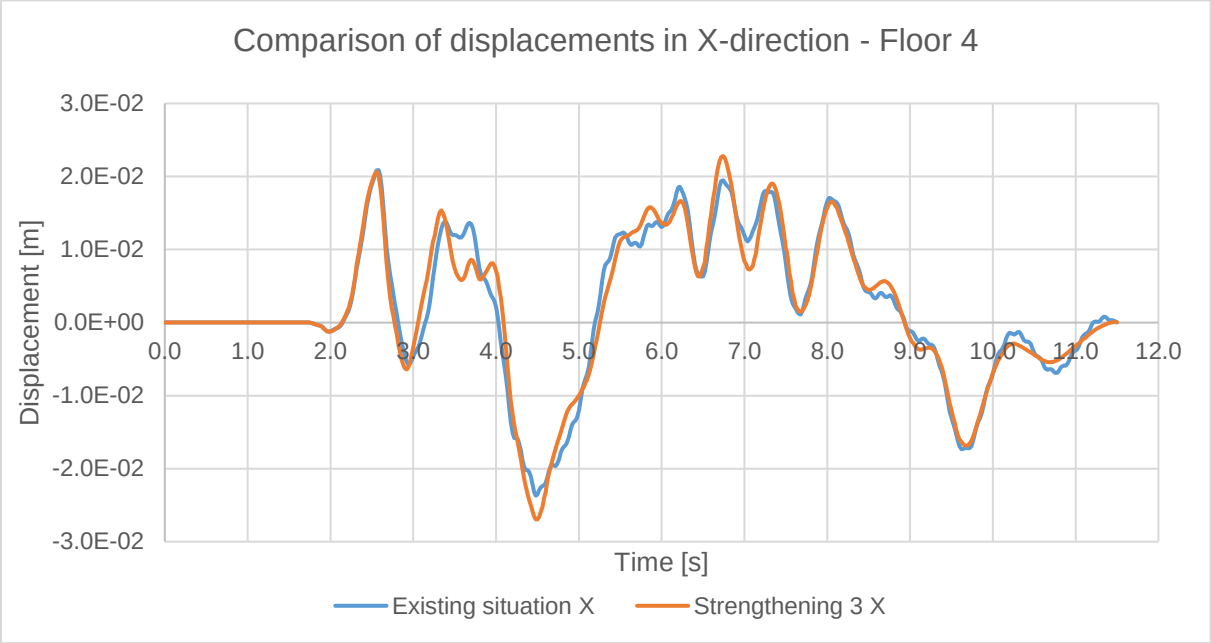

Figure 7.17: Comparison of the displacements of the existing building and the building with strengthening measure 3 - floor 4 in X-direction.

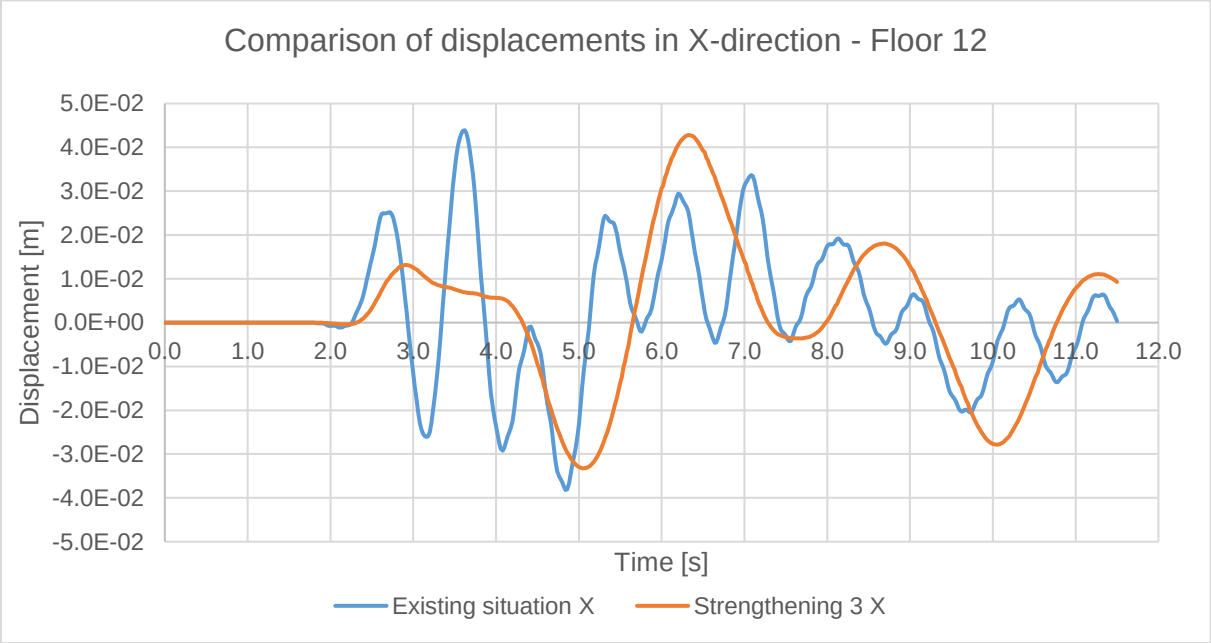

Figure 7.18: Comparison of the displacements of the existing building and the building with strengthening measure 3 - floor 12 in X-direction.

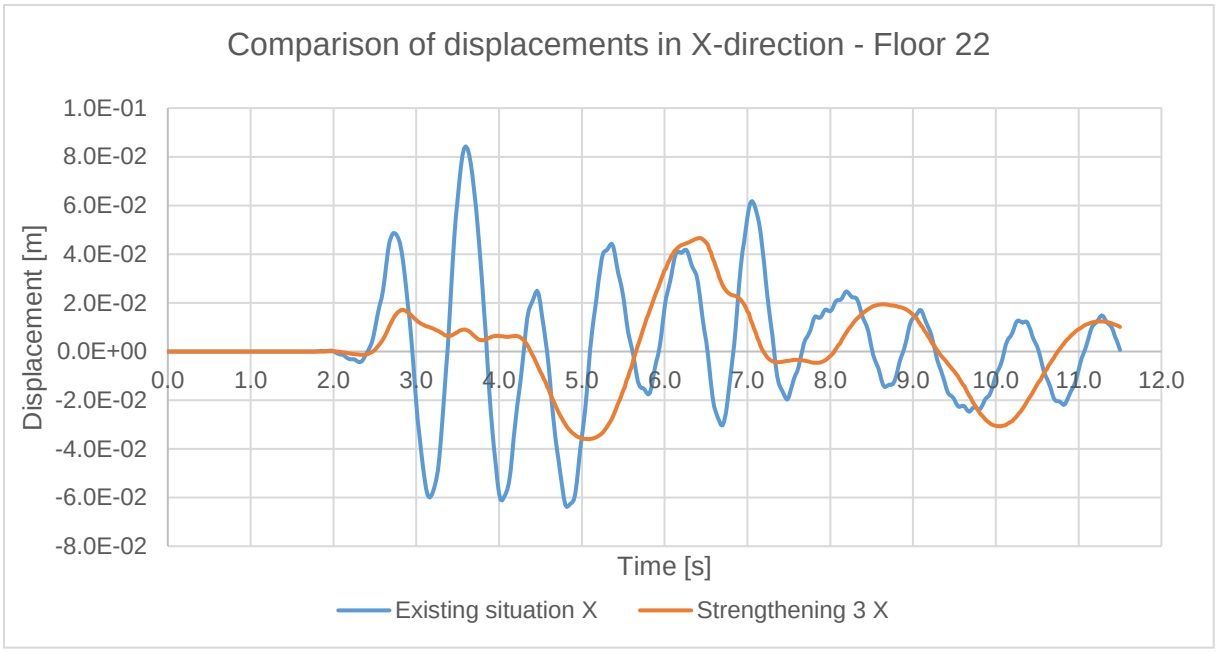

Figure 7.19: Comparison of the displacements of the existing building and the building with strengthening measure 3 - floor 22 in X-direction.

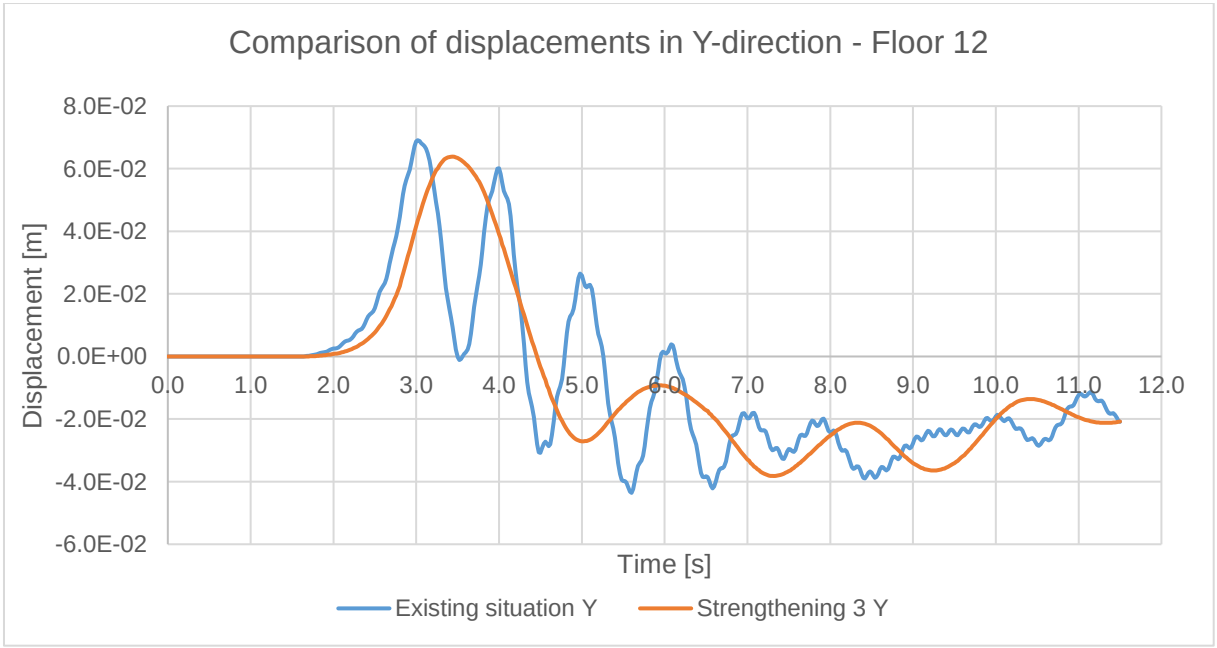

Figure 7.20: Comparison of the displacements of the existing building and the building with strengthening measure 3 - floor 12 in Y-direction.

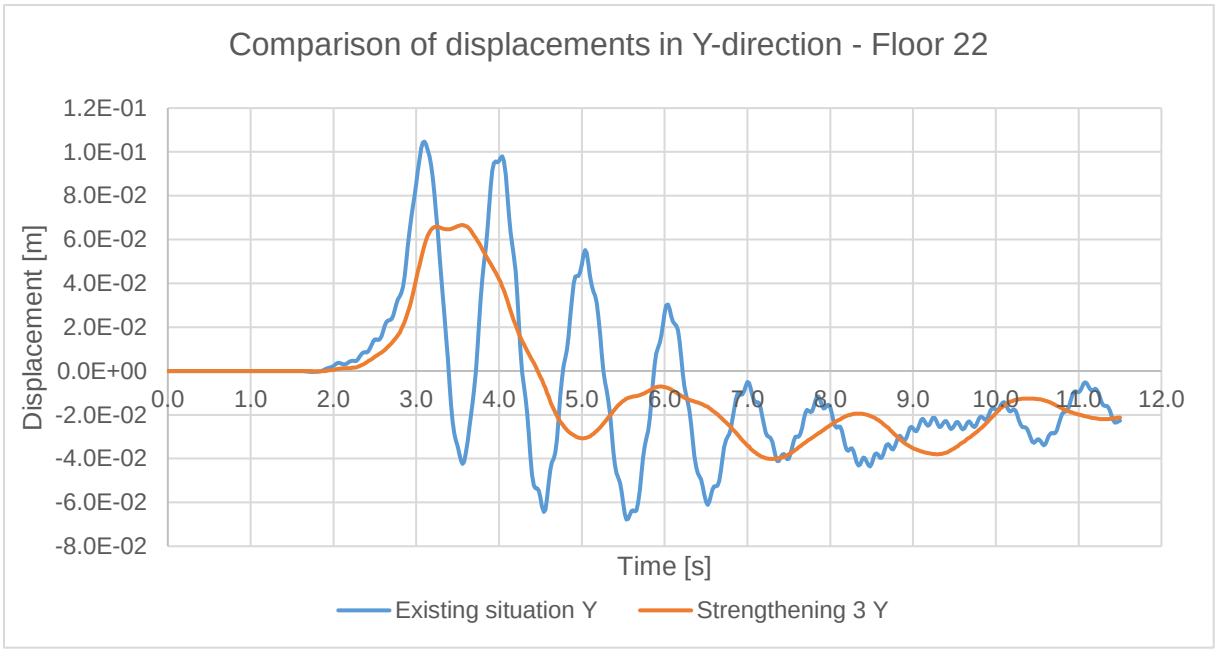

Figure 7.21: Comparison of the displacements of the existing building and the building with strengthening measure 3 - floor 22 in Y-direction.

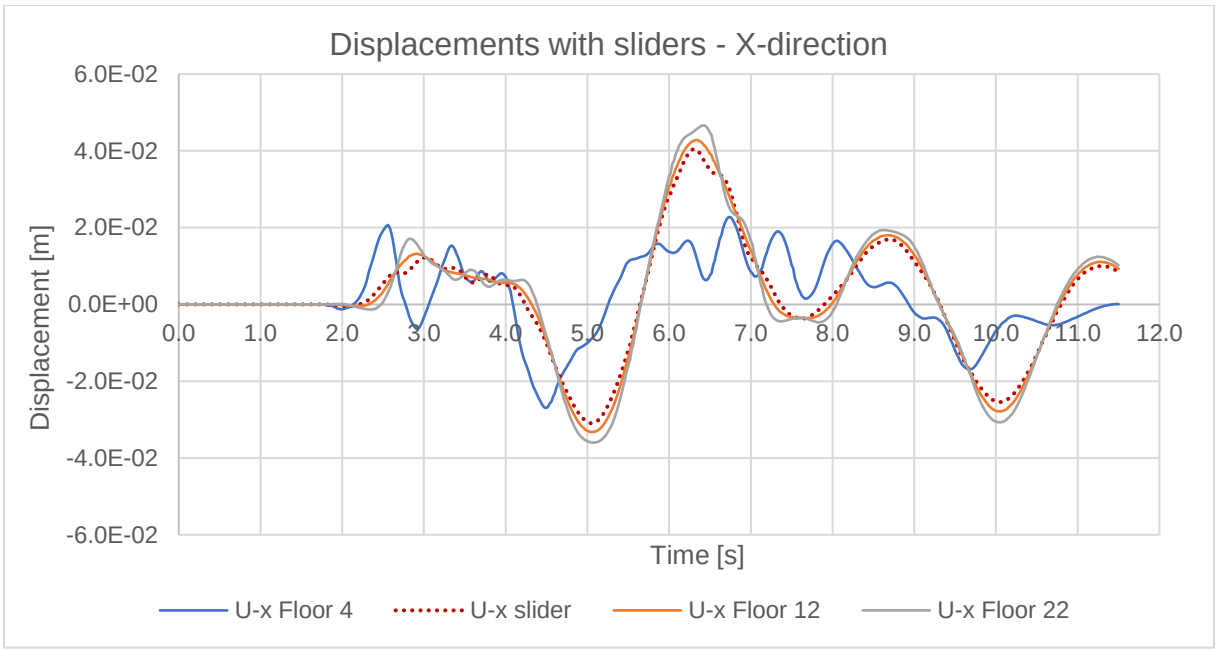

Figure 7.22: Overview of displacements in X-direction of the model with strengthening measure 3.

Table 7-6: Overview of the displacements of the existing building and the strengthened building.

Direction	Maximum displacement [m]		
	Floor 4	Floor 12	Floor 22
X (initial)	0.0238	0.0435	0.0834
X (strengthened)	0.0269	0.0428	0.0466
Drift X (initial)	0.111%	0.108%	0.137%
Drift X (strength.)	0.126%	0.014%	0.019%
Y (initial)	0.0578	0.0680	0.101
Y (strengthened)	0.0593	0.0639	0.066
Drift Y (initial)	0.280%	0.110%	0.146%
Drift Y (strength.)	0.278%	0.022%	0.029%

The graphs and table show the positive effect of the application of base isolation sliders in the building. The first graph shows that the sliders hardly influence the displacement of the fourth floor, except for some small, minor vibrations. However, the dynamic behaviour of the floors above the sliders is significantly different; the frequency is considerably smaller and also the maximum displacements are reduced significantly. Next to this, the top part moves more or less as one solid entity, since the drifts are almost negligible. This is also visible in Figure 7.22, which shows the motion of the building with the application of base isolation.
Based on the results it is expected that this measure reduces the impact of an earthquake on the building significantly. Another advantage is that it can be implemented at one floor, which makes it less drastic to implement than measure one and two.

7.4. Summary chapter 7

This chapter presented three different strengthening proposals and the analysis of the impact of these proposals on the dynamic behaviour of the building. The first and second method of strengthening measures resulted in an increase of the stiffness of the core and so the plasticity and damage will decrease. However, due to the higher stiffness, the shear forces in the building will increase; not only at the first four floors, but also in the top floors of the building and in the foundation slab and piles. Therefore, it is expected that the plasticity in the walls and floors of the top part of the building will increase due to the larger shear forces. However, this effect of increasing plasticity is smaller for the second measure, compared to the first measure. Next to this, both methods are quite drastic and costly to implement in the existing structure.

Because the lower part of the building behaves as a soft storey in the original design, the forces in the top part remain rather small. This behaviour of a soft storey is beneficial and was optimised in the third reinforcement by application of base isolation. In this measure, the first three floors were 'isolated' from the remaining part of the building. The analysis of this measure showed that the motion of the top part of the building is changed significantly due to the sliders. The frequency of the displacements of the top part is decreased, which results in a reduction of shear forces; also the maximum displacement is smaller. Overall, the third measure is expected to be the most effective and efficient solution; the damage in the first four floors will reduce together with the shear forces in the whole building and foundation. Next to this, the measure will not negatively influence the impact of the earthquake on the top floors of the building.

8. Conclusions and recommendations

The results of the research are discussed and elaborated in the previous chapters. In this chapter the conclusions of the thesis research are presented, together with recommendations for further research.

8.1. Conclusions

The objective of this thesis is defined as follows:

"Develop a reliable and efficient (3D) calculation model of an existing high-rise building under seismic loading in order to analyse the dynamic behaviour of the existing and seismic retrofitted main bearing structure"

The conclusion of the research can be divided in three parts:

1) 1D Matlab model – 3D Abaqus model;
2) 3D Modelling techniques and parameters;
3) Strengthening measures.

For each of the three parts, the main conclusions are listed and discussed below.

1D Matlab model – 3D Abaqus model

The structure of the existing high-rise building 'La Liberté' was modelled by means of a 1D and 3D model in Matlab and Abaqus respectively. The 1D model was applied for initial analysis of the building, for verification of the 3D model and for initial analysis of the strengthening measures. The 3D model was used for the nonlinear plastic analyses of the structure, in which cracking of the concrete and yielding of the reinforcement was taken into account;

The verification of the 3D model by means of the 1D model showed a similar trend in displacements for multiple floors of the building; both 1D and 3D analyses are linear elastic for verification purposes. The 3D model showed more peaks in the displacements, which can be clarified by considering the difference in the amount of elements. The 1D model consists of only three Euler-Bernoulli beam elements, while the 3D model contains over more than one million elements, which interact with each other.

Next to this, also the 'modal response spectrum analysis' results are in the same order of magnitude as the results of the NLTH analysis of the 3D model.
In conclusion, the similarities between the verification analyses results and the 3D analysis are sufficient to conclude that the 3D model in Abaqus shows reliable results.

3D modelling techniques and parameters

In Abaqus, a material model with plasticity was applied for both concrete and reinforcement steel elements. Therefore the use of the explicit solver is preferable. The implicit solver shows convergence problems once (significant) plasticity of the material occurs;

Through a process of analyses, the model in Abaqus was improved and optimised. The goal of this process was to find an optimal balance between the duration and the accuracy of the analysis. Based on this process, the following parameters are found to have a significant influence on the results:

Second order accuracy
This parameter is recommended for analyses with multiple cycles; it enables a higher order of accuracy for the element formulation. This parameter is effective for severe element distortions and (large) stress concentrations;

Beta factor of Rayleigh damping
This parameter increases the stability of the analysis significantly, especially in combination with the stiffness recovery option of the Concrete Damaged Plasticity material model. A zero beta factor was applied in the first analyses in order to reduce the duration of the analysis. However, it was found that a non-zero beta factor is required in combination with the material model properties;

Ratio of mesh dimensions
Due to a mesh refinement, the stability of the analysis was increased significantly. More cube-like elements are less sensitive to plasticity which prevents a large drop of the stable time and therefore results in a more stable analysis;

Hourglassing control
The initial analyses were performed with enhanced hourglassing, yet this mechanism gives overly stiff results once plasticity occurs; therefore, the combined hourglassing control mechanism is preferable. The combined control does not apply artificial stiffness based only on the Young's modulus, but also uses viscous hourglassing.

Although the combined mechanism gives better, more realistic results, it could be better to apply a different type of elements with multiple integration points. Those elements might not require a hourglassing mechanism and give more stability during the analysis.

Strengthening measures

Based on the results of the analysis with the final 3D model, it was found that the existing high-rise building La Liberté meets the Near Collapse criterion as defined in the NPR. Despite the fact that a large amount of plasticity and damage occurs in the walls of the core at the first four floors of the building, the structure does not collapse or closely approach collapse.

However, since the NPR states at least seven accelerograms should be applied, it might happen that the structure does not meet the NC criterion for one of these accelerograms. Therefore, three strengthening options were proposed and analysed with the 1D model in Matlab; this analysis was performed for an initial study of the effect on the dynamic behaviour. It was found that an increase of stiffness of the first four floors, in order to reduce the plasticity, has a negative influence on the behaviour of the top part of the building. The analysis also showed that the optimisation of the soft storey of the lower part of the building, by means of base isolation, has a positive impact on the dynamic behaviour of the top part of the building.

8.2. Recommendations

With the performed research, not all influences and sensitivities are investigated and assumptions are made; therefore, further research is recommended. Based on this research, it is recommended to perform further research considering the following aspects:

Type of elements

The model in this research was created with solid elements; it is recommended to investigate the possibilities of the application of different elements, for example shell elements. This might reduce/eliminate some sensitivities.

Influence of soil-building interaction

The model is modelled without the impact or interaction of the soil on the foundation and piles of the building. The mass and stiffness of the soil might have impact on the behaviour of the building.

Damping parameters

As discussed in the report (and in annex I and II), the amount of damping applied in the model has influence on the results of the analyses. Further research into the correct and optimal amount of damping is recommended.

Optimisation 1D model

The 1D Matlab model can be further developed. For example shear stiffness and the number of elements might have influence. Next to this, further research into extracting forces and accelerations from the 1D model is recommended.

Application of seven accelerograms

In this research only one accelerogram was applied, for the sake of time. Therefore, additional analyses with the different accelerograms should be executed.

Reduced integration

One of the sensitivities in the model of this research is hourglassing control; which is basically a consequence of the application of reduced integration elements. It is recommended to investigate what the advantages and disadvantages of fully integrated elements are.

Hourglassing control

During this research it was discovered that the combined option of hourglassing control is preferred instead of enhanced hourglassing control. In Abaqus, several mechanisms are available and the differences are only initially analysed. It is recommended to perform further research on the variation of control mechanisms.

Control options

In Abaqus, many different options are available and in this research most of them were defined as default; further research into these options and parameters is recommended.

Strengthening measures in Abaqus

Modelling of strengthening proposals in Abaqus in order to further investigate and analysis of impact and effectiveness is recommended.

References

Abaqus, S. . (2017). Abaqus manual 2016. *Manual for Abaqus 2016*. 3ds.

Bangash, M. (2011). *Dynamic analyses, numerical computations, codified methods, case studies and examples.* London: Springer-Verlag.

Bardakis, V., & Dritsos, S. (2007). Evaluating assumptions for seismic assessment of existing buildings. *Soil Dynamics and Earthquake Engineering*, 223-233.

Chen, X., Duan, J., Qi, H., & Li, Y. (2014). Rayleigh damping in Abaqus/explicit dynamic analysis. *Applied mechanics and materials*, vol. 627, pages. 288-294.

Christiana, F. (2013). *Seismic capacity assessment and retrofitting of reinforced concrete building - MSc Thesis.* Athens: National Technical University of Athens.

Dadayan, T., & Roudi, E. (2014). Investigations of RC shear wall-frame structures with various openings in walls under earthquake loading. *Advanced Materials Research*, vol. 1020, pages 242-247.

Deierlein, G., & Krawinkler, H. (2008). *Modeling Guidelines for Nonlinear Analysis.* Stanford: Stanford University.

Dwarshuis, K. (2017). *Informatie over aardbevingen in Groningen*. Retrieved from http://www.dwarshuis.com

Felippa, C. A. (1986). *Introduction to Finite Element Methods.* Colorado: University of Colorado.

Hoogendoorn, I. D. (2011). Wonen en werken in vrijheid. *Cement*, 4-9.

Hordijk, C. R. (1986). *Experimental determination of crack softening characteristics of normalweight and lightweight concrete.* Heron.

Huang, Y., Song, X., & Xu, F. (2011). Dynamic plastoelastic time-history analysis on a super high-rise building structure of anhui. *Advanced materials research*, Vols 163-167; pages 1955-1964.

Keijdener, C., & Jarquin-Laguna, A. (2015, Septembre). Introduction to Computational Dynamics for Offshore Structures - OE4650. *W1.L2:Solving ODES*. Delft: Delft University of Technology.

Li, F., & Xingwen, D. (2010). Mesh-dependence of material with softening behavior. *Chinese Journal of Aeronautics*, 46-53.

Louzai, A., & Abed, A. (2015). Evaluation of the seismic behavior factor of reinforced concrete frame structures based on comparative analysis between non-linear static pushover and incremental dynamic analyses. *Bull Earthquake Eng*, 1773-1793.

Martinelli, P., Martinelli, L., & Mulas, M. (2017, 4). *Modeling and analysis of the CAMUS i RC shear wall*. Retrieved from ResearchGate - share and discover research: https://www.researchgate.net/publication/274382631

Michal, S., & Andrzej, W. (2015, 8 25-29). Calibration of the CDP model parameters in Abaqus. *Advances in Structural Engineering and Mechanics - Invited paper*. Incheon, South Korea.

Nederlands Normalisatie-Instituut. (2015). *Nederlandse PraktijkRichtlijn 9998.* Delft: Nederlands Normalisatie-Instituut.

Qi, H., Li, Y., & Lu, X. (2013). Dynamic Nonlinear analysis of Shanghai Pudong Shangrila hotel extension engineering. *Applied Mechanics and Materials*, vols 438-439; pages 1510-1513.

Seo, J., & Wan Hu, J. (2016, January 26). *Sesimic response and performance evaluation of Self-centering LRB Isolators installed on the CBF building under NF ground motions.* Retrieved from MDPI - open access: http://www.mdpi.com/

Simulia Abaqus. (2005). Lecture 1 - Overview of Abaqus/explicit. *Lecture 1*.

Simulia Abaqus. (2005). Lecture 2 - Elements. *Lecture 2*.

Spijkers, J., Vrouwenvelder, A., & Klaver, E. (2005). *Structural Dynamics Part 1 - Structural Vibrations CT4140.* Delft: Delft University of Technology.

Sümer, Y., & Aktas, M. (2015). Defining parameters for concrete damage plasticity model. *Challenge journal of structural mechanics*, 149-155.

Thorenfeldt, T. (1987). *Mechanical properties of high-strength concrete and applications in design.* Norway.

Verruijt, A. (1977). *Toegepaste mechanica II.* Delft: Delftse Uitgevers Maatschappij b.v.

Wahalathantri, B., Thambiratnam, D., Chan, T., & Fawzia, S. (2011). A material model for flexural crack simulation in reinforced concrete elements using Abaqus. *eddBE2011 Proceedings - Queenslandd University of Technology*, 260-264.

Wilson, E. K. (1981). A Replacement for the SRSS Method in Seismic Analysis. *Earthquake Engineering & Structural Dynamics*, 6.

Zhang, J., & Li, J. (2012). Investigation into Lubliner yield criterion of concrete for 3D simulation. *Engineering Structures*, Vol. 44, pages 122-127.

Zonneveld ingenieurs b.v. (2016). Element Deletion for Concrete Damaged plasticity. Rotterdam.

Annex I Test with high and low Rayleigh damping in Matlab

The Rayleigh damping applied in the Matlab model is determined with the most beneficial frequencies, based on the response spectrum of the accelerograms, as discussed in chapter 3.1.2. This annex shows the sensitivity of a higher and lower damping ratio; the applied damping ratio for this test are approximately equal to 5.5% and 2% damping, as shown in the table below.

Table AI-1: Applied damping ratios and corresponding Alpha and Beta factor.

Damping ratio	Alpha factor [-]	Beta factor [-]
0.055	0.6715	0.00107
0.02	0.2442	0.00039

The following graphs show a comparison between the displacements of the building of the two analyses.

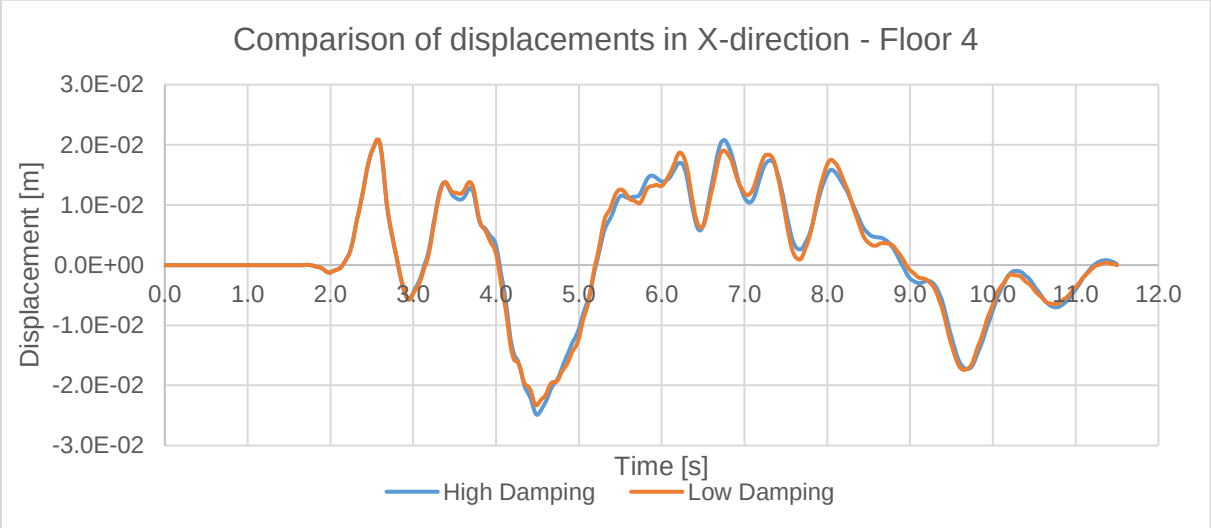

Figure AI.0.1: Displacements of floor 4 in X-direction with high (blue) and low (orange) Rayleigh damping.

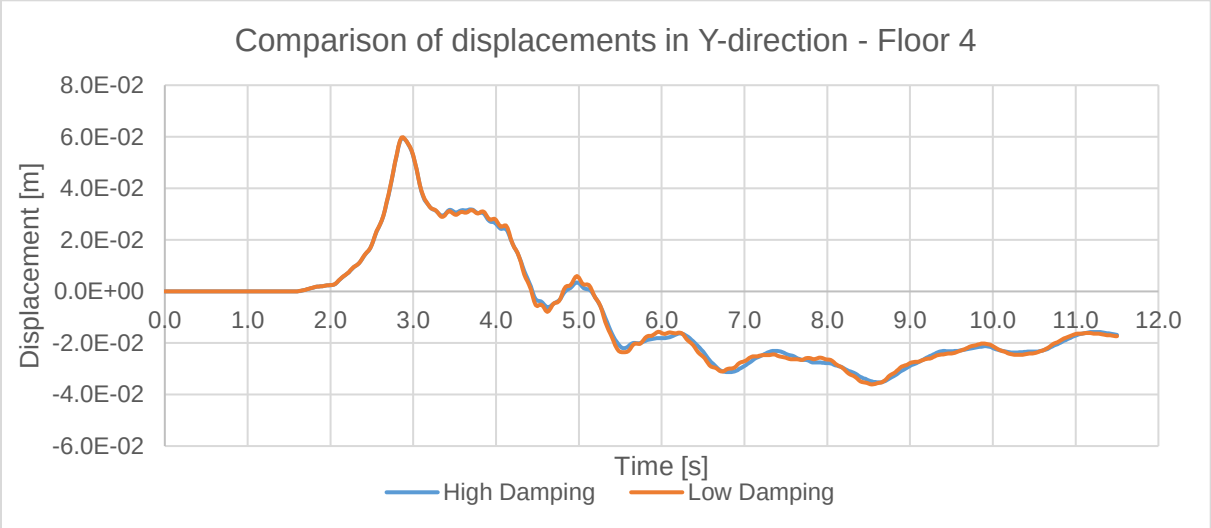

Figure AI.0.2: Displacements of floor 4 in Y-direction with high (blue) and low (orange) Rayleigh damping.

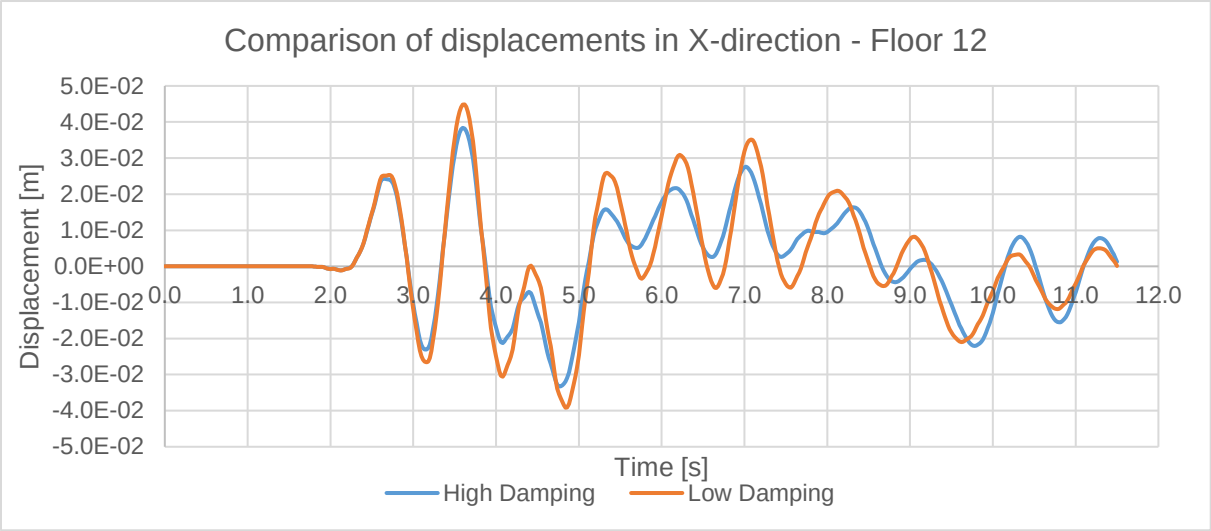

Figure AI.0.3: Displacements of floor 12 in X-direction with high (blue) and low (orange) Rayleigh damping.

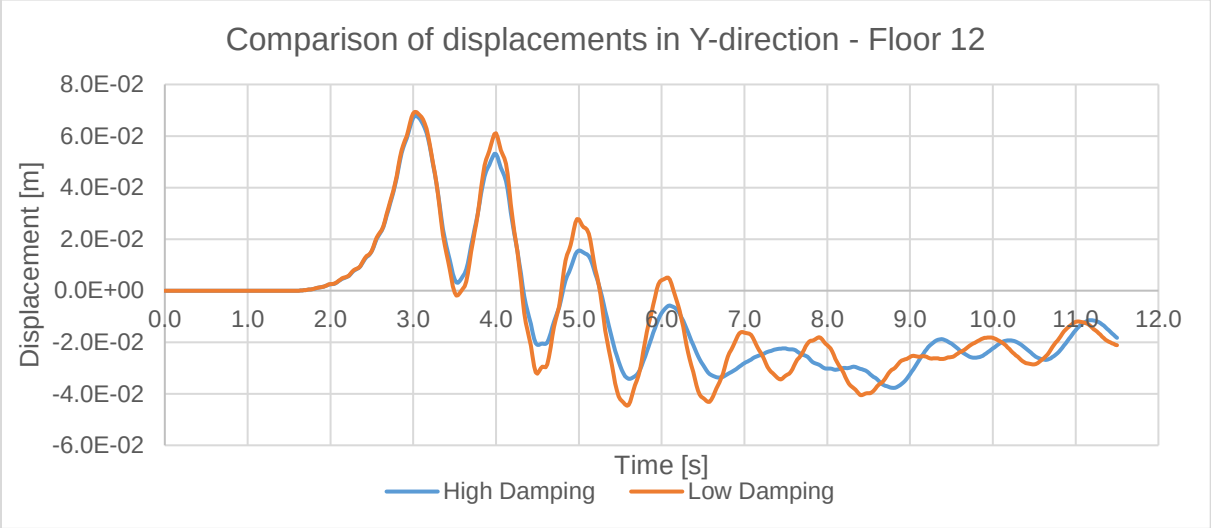

Figure AI.0.4: Displacements of floor 12 in Y-direction with high (blue) and low (orange) Rayleigh damping.

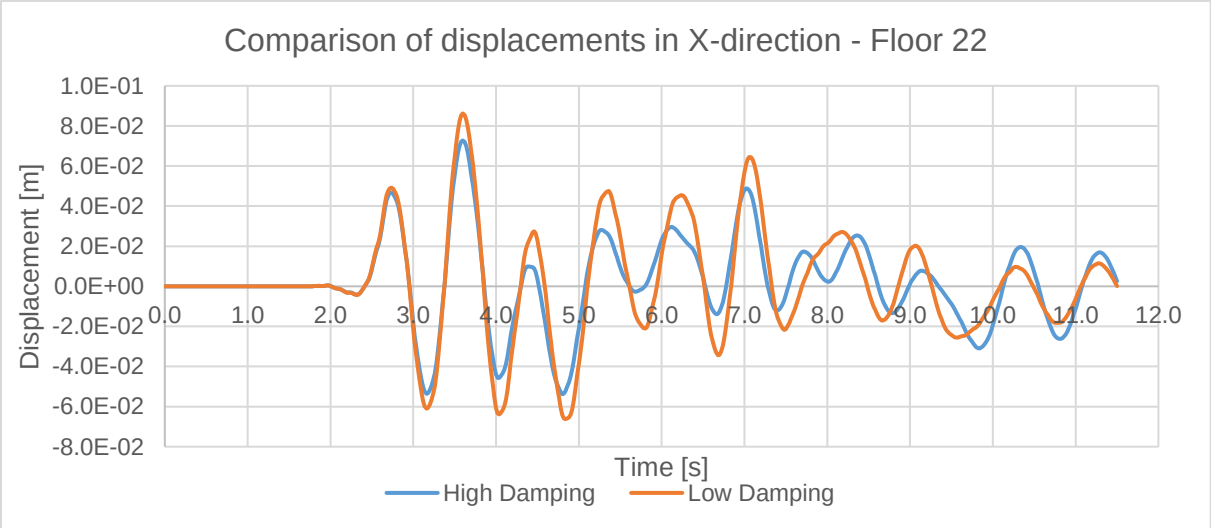

Figure AI.0.5: Displacements of floor 22 in X-direction with high (blue) and low (orange) Rayleigh damping.

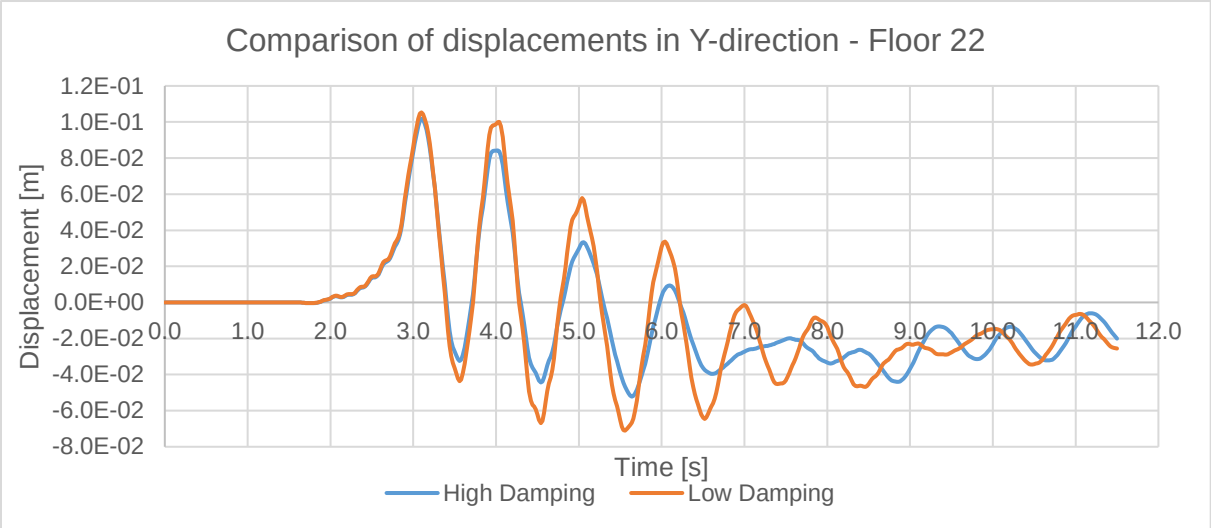

Figure AI.0.6: Displacements of floor 22 in Y-direction with high (blue) and low (orange) Rayleigh damping.

Conclusion

The results of both analyses show that the amount of damping has a significant influence on the displacements; especially on those of the higher floors of the building. The displacements of the top floors of the higher damping model are smaller and they are closer to the displacements of the base displacement. Due to the higher amount of damping, the behaviour of the building is different: it behaves stiffer.

Annex II Test with high and low beta factor in Abaqus test model

As described in chapter 5, the applied beta factor in the explicit Abaqus analysis does not correspond with the Beta factor for the recommended 2.5% damping ratio. The actual applied Beta factor is smaller in order to save time, since this Beta factor has a large negative influence on the duration of the analysis. In this annex, the sensitivity of a higher and lower Beta factor of the Rayleigh damping is discussed by means of a test.

The test object consists of a small building of 3 storeys, with columns and walls as bearing structure. The model is created with solid elements, with concrete material properties and the parameters and properties as applied in the final model of 'La Liberté'.
The test models are analysed with a same type of analysis as the model of 'La Liberté', with a shorter accelerogram of only 3 seconds. The first model is analysed with a high Beta factor of 0.00047; together with an Alpha factor of 4.282, the applied damping is approximately 5%. The second model is analysed with a low Beta factor of 0.00001; together with an Alpha factor of 4.282, the applied damping is about 3.6% for the lower frequencies and 1.47% for the higher frequencies.
The damping factors and ratios are based on the Rayleigh damping calculation, as discussed in chapter 4.2.3, and on the frequency analysis of the test model.

The results of both analyses are shown in figures of the total strains in the concrete and graphs of displacement and drifts. The first figures show the origin of cracking in the concrete, and the crack width is calculated by multiplication of the shown total strain with the mesh size (0.3 meter). The figures also show that the amount of cracks is approximately equal for both analyses, as well as the location. Yet, the width of the cracks in the model with the low Beta factor is larger.

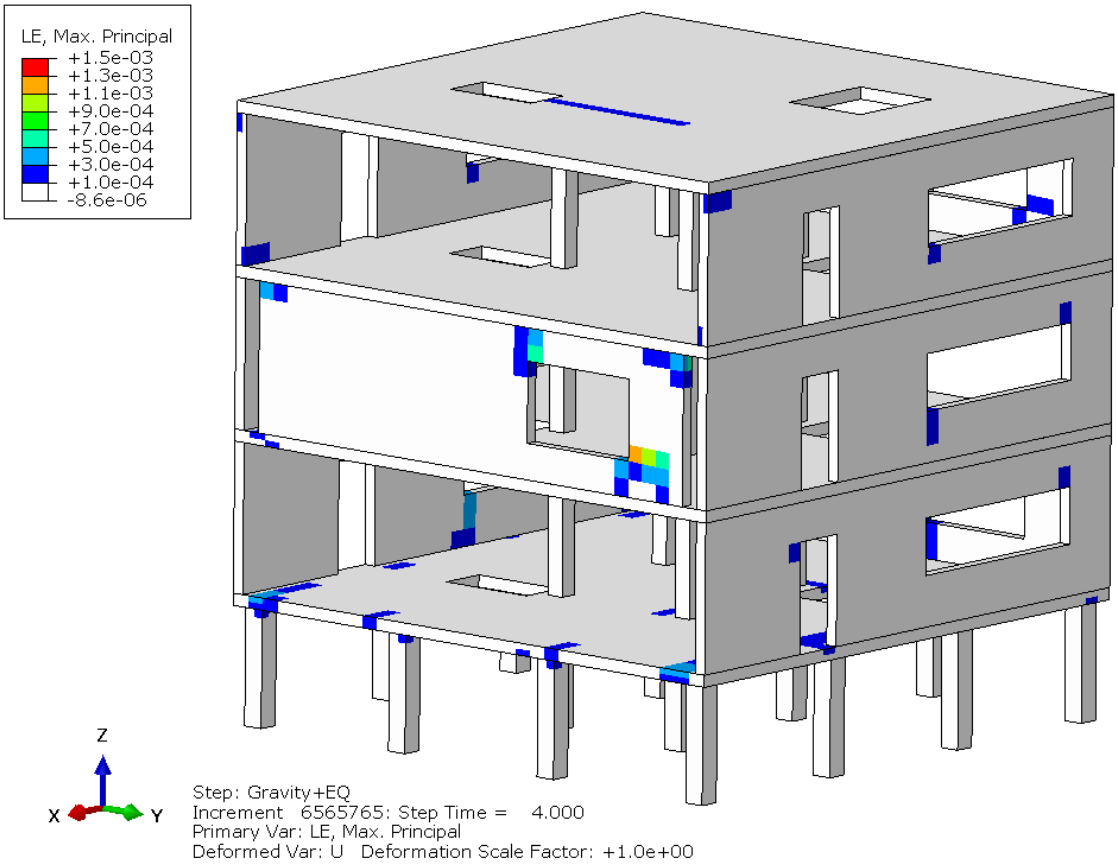

Figure AII.0.1: Total strain of the material concrete of the test model with high Beta factor.

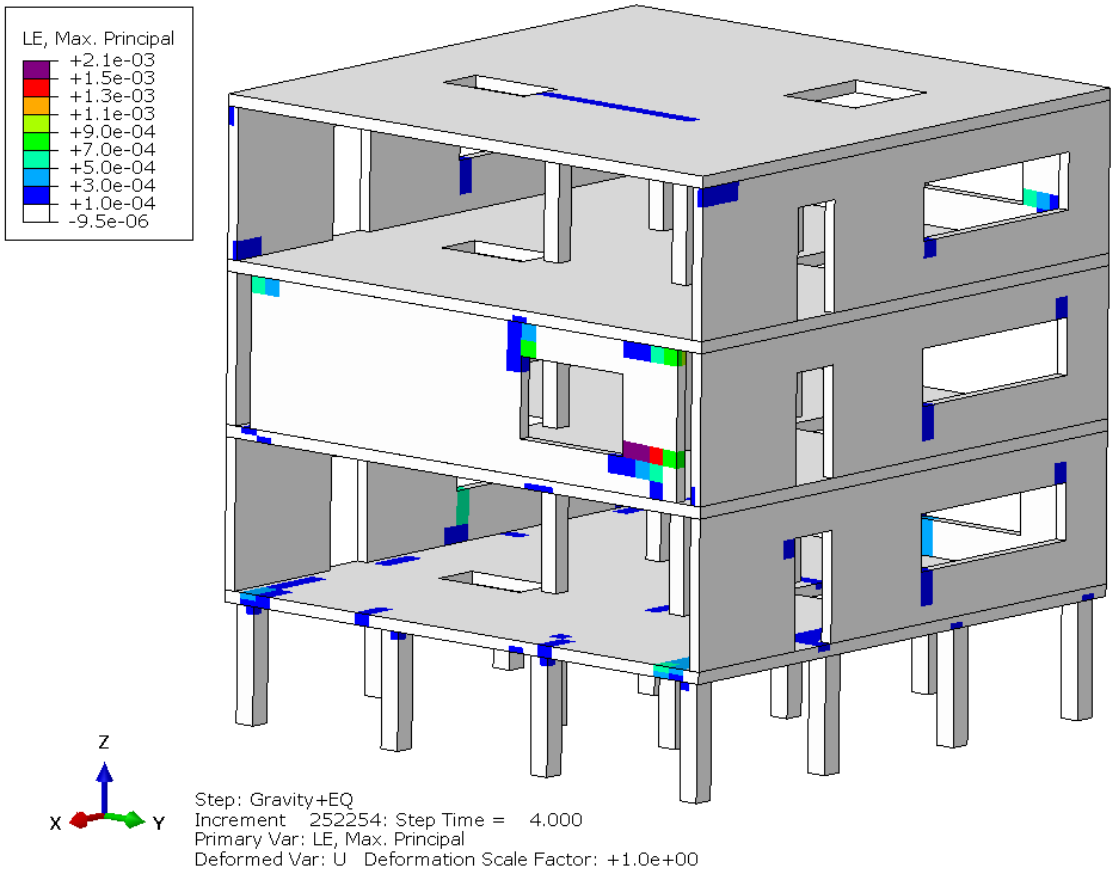

Figure AII.0.2: Total strains in the concrete of the test model with low Beta factor.

The figures show significant similarities between the results of both analyses. In The following graph the shear forces of several floors of both models are shown.

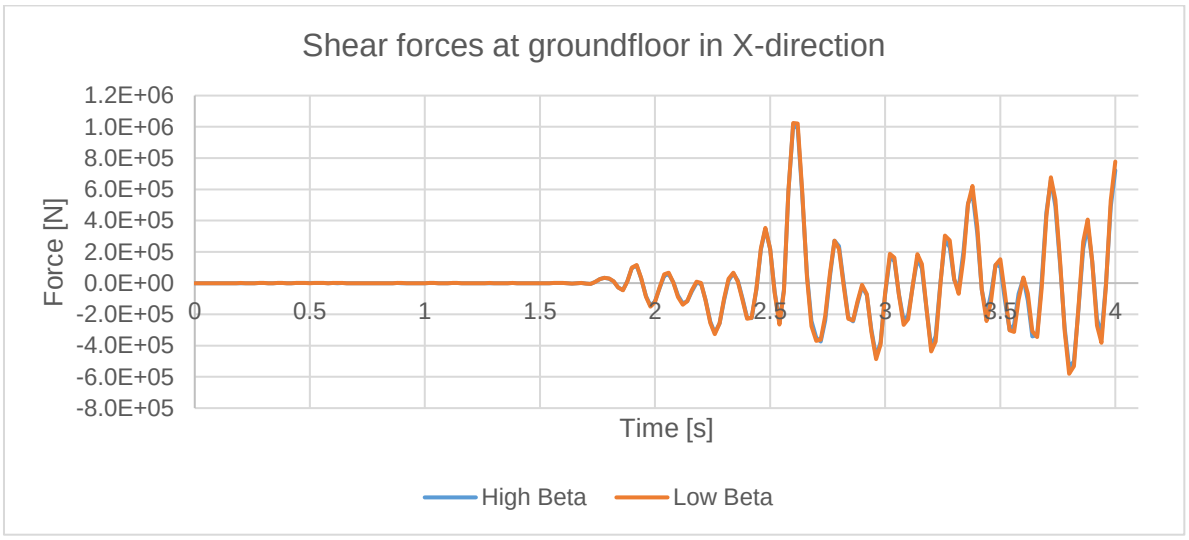

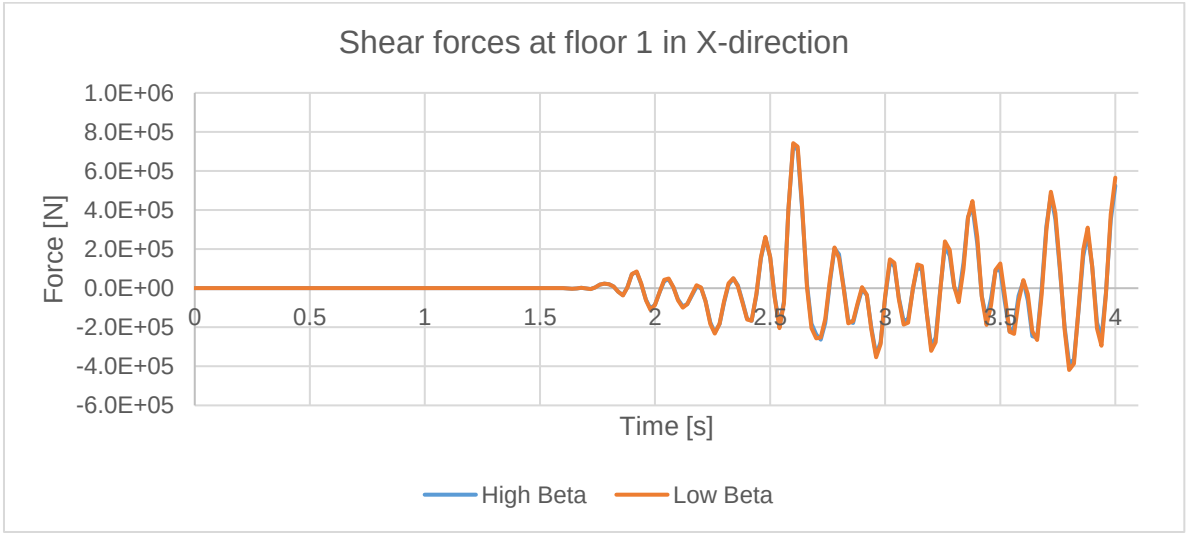

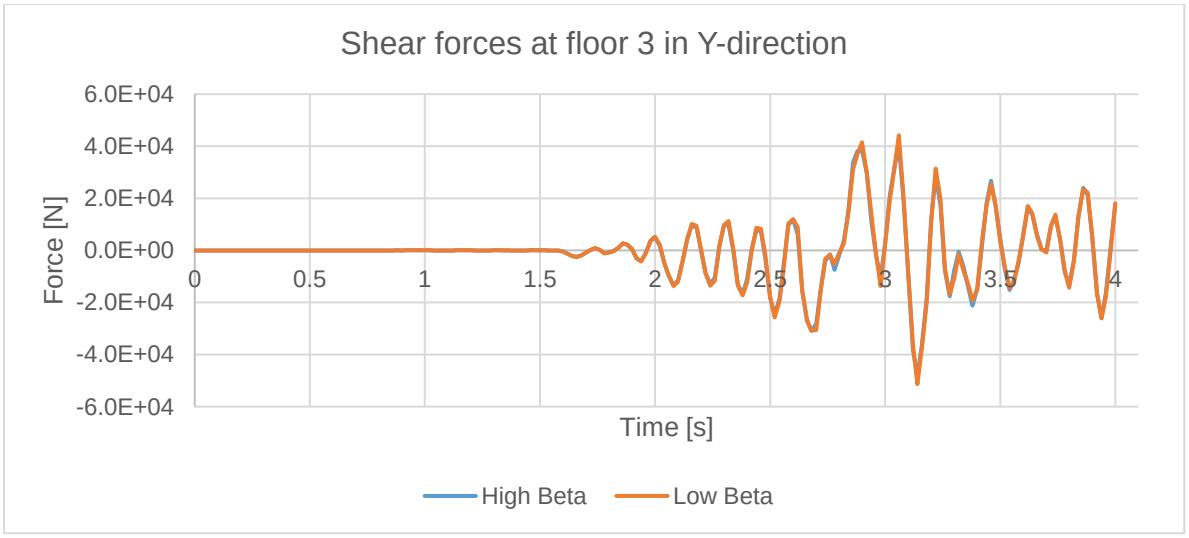

Figure AII.0.3: Three graphs with the shear forces of different storeys in X- and Y-direction.

The graphs show that the forces in both X- and Y-direction are equal, with same amplitude and frequency.

The following graph shows the dissipated energy caused by material plasticity.

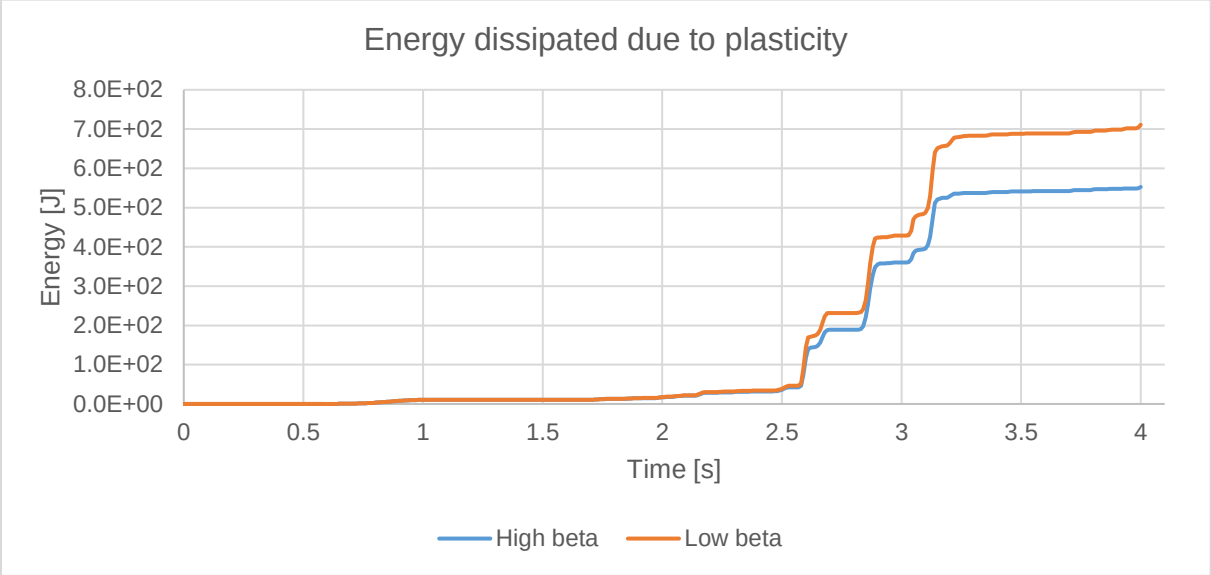

Figure AII.0.4: Energy dissipation due to plasticity of the material; cracking or crushing of concrete.

In the analysis with the low Beta factor, more energy is dissipated due to material plasticity; this corresponds to the figures above, Figure AII.0.1 and Figure AII.0.2, which showed that the crack width is larger if a smaller Beta factor is applied.

Also the interstorey drifts are larger with a smaller Beta factor, as shown in the following graphs.

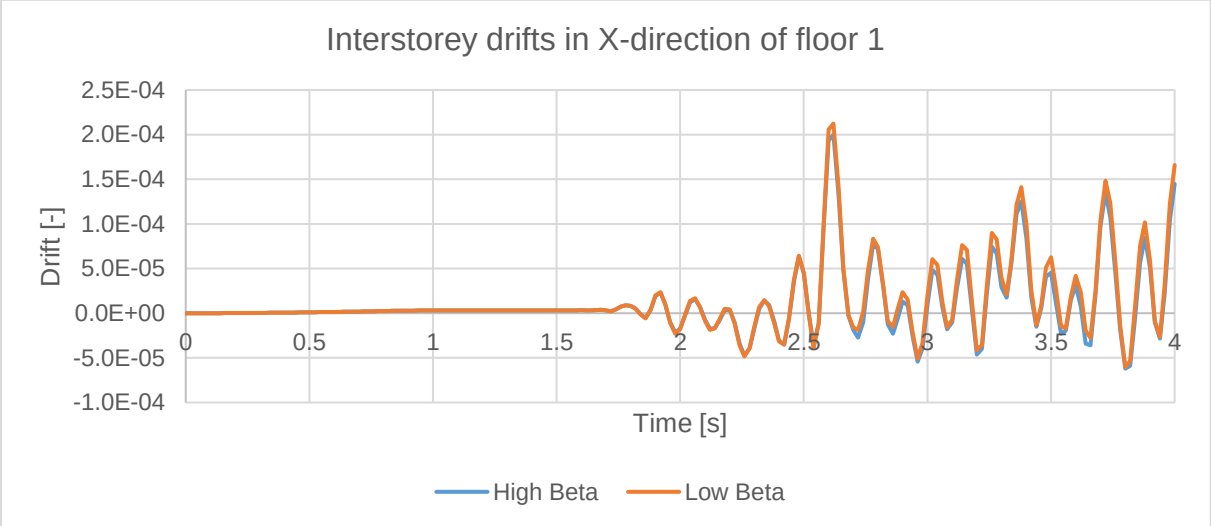

Figure AII.0.5: Interstorey drifts of the first floor in X-direction.

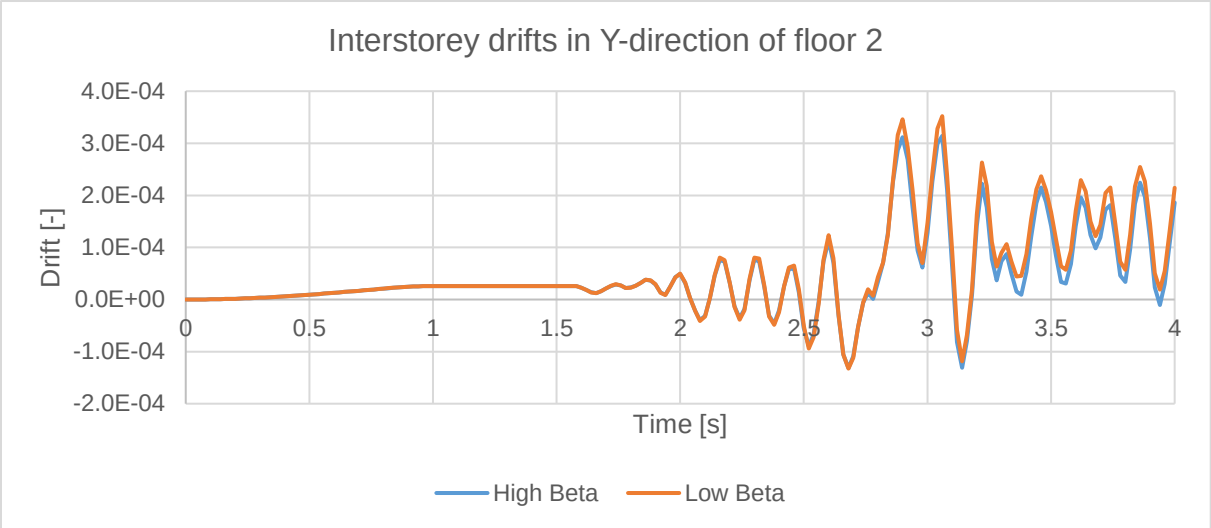

Figure AII.0.6: Interstorey drifts of the second floor in Y-direction.

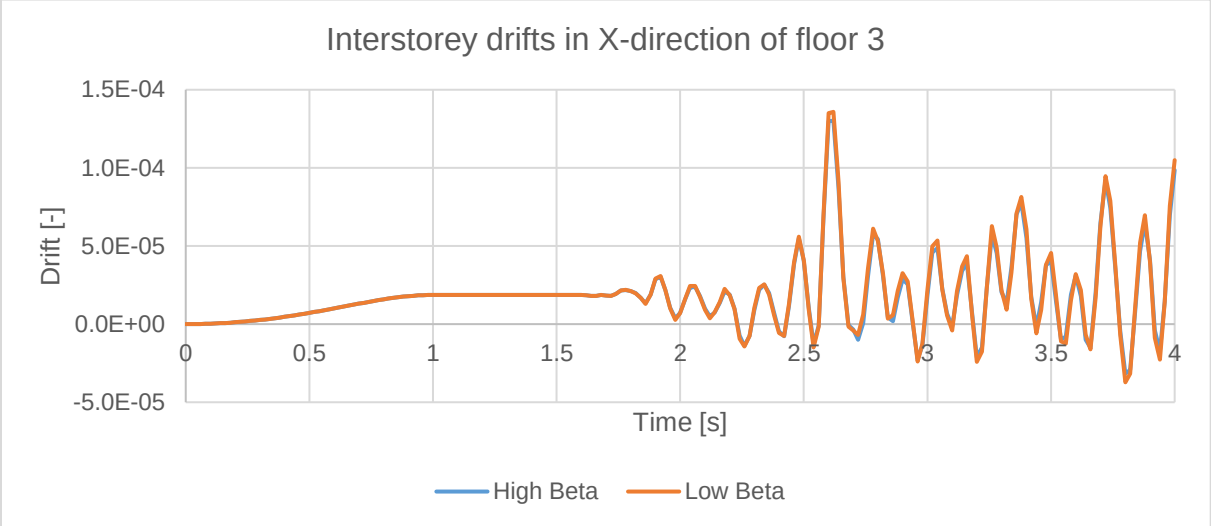

Figure AII.0.7: Interstorey drifts of floor 3 in X-direction.

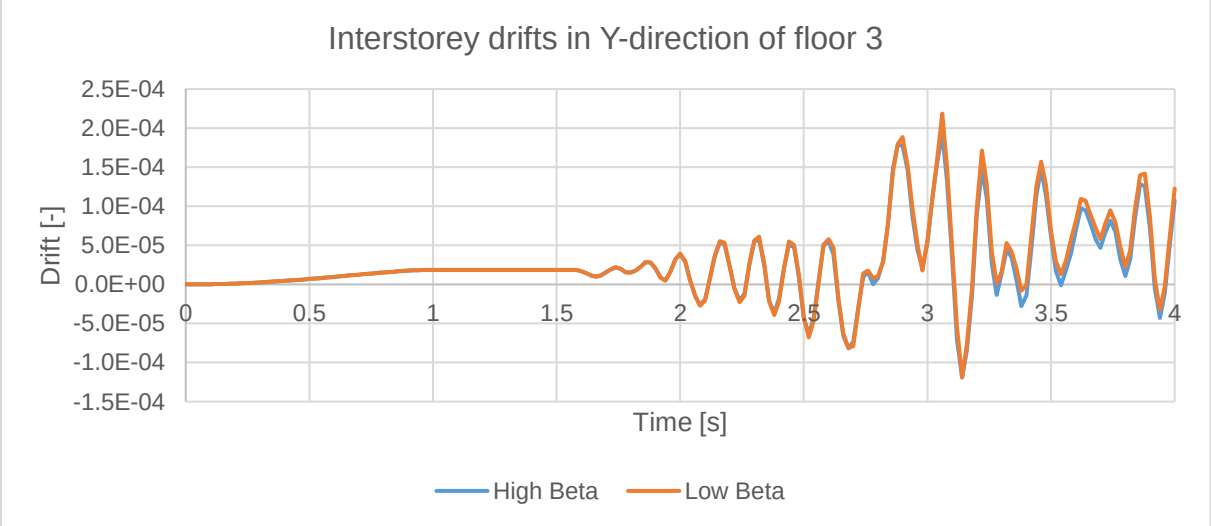

Figure AII.0.8: Interstorey drifts of floor 3 in Y-direction.

Conclusion

The results clearly show that the Beta factor of the Rayleigh damping influences the dynamic behaviour of the structure. For numerical (analysis stability) purpose, it is already recommended to apply at least a certain amount of Beta damping; yet this small test shows that the amount of Beta damping influences the dynamic behaviour. The model with a high Beta factor behaves rigid, as one stiff assembly; while the model with a relative low Beta factor shows larger drifts and so larger strains and thus more plasticity.
On the other hand, from a practical point of view, the high Beta model took more than 20 hours to finish the analysis, while the low Beta model only took approximately 1 hour. This shows the significant influence of the Beta factor on the stable time in an explicit analysis.

In conclusion, the Beta factor of the Rayleigh damping should be chosen with care; considering the *dynamic* influence on one hand and the *numerical* influence on the other hand. Next to this, the influence of the Beta factor might be of different order for larger models, as 'La Liberté'.